รายงานวิจัยฉบับสมบูรณ์

โครงการ นวัตกรรมระบบการตรวจวิเคราะห์ของไหลจุลภาคเชิงแสงและ/หรือเคมีไฟฟ้าเพื่อการเฝ้าระวัง

โดย

ศาสตราจารย์ ดร. อรวรรณ ชัยลภากุล และคณะ

กันยายน 2556

สัญญาเลขที่ BRG5380008/2553

รายงานวิจัยฉบับสมบูรณ์

โครงการ นวัตกรรมระบบการตรวจวิเคราะห์ของไหลจุลภาคเชิงแสงและ/หรือเคมีไฟฟ้าเพื่อการเฝ้าระวัง

คณะผู้วิจัย

ศาสตราจารย์ ดร.อรวรรณ ชัยลภากุล จุฬาลงกรณ์มหาวิทยาลัย

ผู้ช่วยศาสตราจารย์ ดร.วีณา เสียงเพราะ มหาวิทยาลัยศรีนครินทรวิโรฒ

สนับสนุนโดยสำนักงานกองทุนสนับสนุนการวิจัยและ

จุฬาลงกรณ์มหาวิทยาลัย

CONTENTS

PAGE

PAGE

PAGE

PAGE

PAGE

PAGE

ACKNOWLEDGEMENTS

The research team would like to express our deepest gratitude to the Thailand Research Fund (Grant Number BRG5380008/2553) and Chulalongkorn University for financial support during the project period. We would like to thank also all students and researchers for their cooperation in work.

Abstract

Project code: BRG5380008/2553

Project Title: Innovations in optical and/or electrochemical microfluidic analytical system for point-of-care testing

E-mail Address: corawon@chula.ac.th

Project period: 3 years

This research focused on the development of a new analytical system for the determination of various important compounds. Lab-on-paper was introduced as a major part for the system. In this research, there are eleven chapters that can be grouped as following. The first part is introduction that gives the inspiration, objective and scope of this research. Chapters II-V are the principle of the development of paper-based devices coupled with colorimetric detection for organic and/or inorganic determination. Chapters IV-VIII provide details of the results for the development of paper-based devices coupled with electrochemical detection for determination of organic such as dopamine and/or inorganic compound. Chapters IX-X report on the creation a system for dual electrochemical/colorimetric detection for electroanalysis of organic and/or inorganic compounds. Each chapter contains their methodology and results obtained from the use of proposed methods. Lastly, Chapter XI is the conclusion.

Keywords: Lab-on-paper, colorimetric detection, electrochemical detection, organic compound, inorganic compounds

บทคัดย่อ

Project code: BRG5380008/2553

Project Title: นวัตกรรมระบบการตรวจวิเคราะห์ของไหลจุลภาคเชิงแสงและ/หรือเคมีไฟฟ้าเพื่อการเฝ้าระวัง

E-mail Address: corawon@chula.ac.th

Project period: 3 ปี

โครงการวิจัยนี้มุ่งความสำคัญไปที่การพัฒนาระบบการวิเคราะห์แบบใหม่สำหรับการตรวจวัดสารที่มีความสำคัญในด้านต่าง ๆ โดยมุ่งเน้นและเสนอการใช้อุปกรณ์ปฏิบัติการบนกระดาษเป็นอุปกรณ์ส่วนสำคัญของการพัฒนา ในงานวิจัยนี้มีเนื้อหาของผลงานการวิจัยทั้งหมด 11 บทด้วยกัน ซึ่งสามารถแบ่งเป็นกลุ่มได้ดังนี้ บทแรก จะเป็นบทนำที่กล่าวถึงอุปกรณ์ปฏิบัติการบนกระดาษ วัตถุประสงค์ และขอบเขตของงานวิจัย บทที่ 2-5 เป็นการนำเสนอการพัฒนาระบบอุปกรณ์ปฏิบัติการบนกระดาษที่ออกแบบเพื่อการตรวจวัดเชิงสี สำหรับการหาปริมาณทั้งสารอินทรีย์หรือสารอนินทรีย์ บทที่ 6-8 เป็นการนำเสนอการออกแบบและพัฒนาระบบอุปกรณ์ปฏิบัติการบนกระดาษที่ใช้ร่วมกับตัวตรวจวัดทางเคมีไฟฟ้า และนำไปประยุกต์เพื่อการตรวจวัดปริมาณสารอินทรีย์หรือสารอนินทรีย์เช่นกัน บทที่ 9-10 เป็นการสร้างและออกแบบอุปกรณ์ปฏิบัติการบนกระดาษให้เป็นระบบสองตัวตรวจวัดคือมีทั้งการตรวจวัดเชิงสีและการตรวจวัดทางเคมีไฟฟ้า โดยที่แต่ละบทจะประกอบด้วยขั้นตอนการดำเนินดารวิจัยและผลการทดลองที่ได้ ส่วนสุดท้ายคือบทสรุปของผลการดำเนินการวิจัย

คำสำคัญ : อุปกรณ์ปฏิบัติการบนกระดาษ การตรวจวัดเชิงสี การตรวจวัดทางเคมีไฟฟ้า สารอินทรีย์ สารอนินทรีย์

Executive Summary

วัตถุประสงค์

วัตถุประสงค์ของโครงการวิจัยนี้คือการสร้างระบบการวิเคราะห์แบบใหม่เพื่อเป็นทางเลือกสำหรับการตรวจวัดสารที่มีความสำคัญชนิดต่าง ๆ เช่น สารบ่งชี้ชีวภาพ และโลหะต่าง ๆ โดยใช้อุปกรณ์ปฏิบัติการบนกระดาษร่วมกับตัวตรวจวัดเชิงสีและตัวตรวจวัดทางเคมีไฟฟ้า เมื่อได้ระบบการวิเคราะห์แบบใหม่แล้ว ระบบวิเคราะห์นั้น ๆ จะถูกนำไปประยุกต์เพื่อการหาปริมาณของสารที่สนใจในสารตัวอย่าง โดยทำการเปรียบเทียบผลการวิเคราะห์ที่ได้กับวิธีดั้งเดิมหรือวิธีมาตรฐาน

การดำเนินงานวิจัย และผลงานวิจัยที่ได้รับอย่างย่อ ๆ

จากผลการดำเนินงานเป็นระยะเวลา 3 ปี คณะผู้วิจัยประสบความสำเร็จเป็นอย่างดีในการออกแบบและสร้างระบบการตรวจวิเคราะห์ของไหลจุลภาคเชิงแสงและ/หรือเคมีไฟฟ้าเพื่อการเฝ้าระวัง การดำเนินงานได้ถูกแบ่งออกเป็น 3 ส่วนด้วยกันคือ ส่วนแรก เป็นการสร้างอุปกรณ์ปฏิบัติการบนกระดาษร่วมกับการตรวจวัดเชิงสีสำหรับการนำมาใช้วิเคราะห์หาสารประเภทต่าง ๆ ที่มีความสำคัญ ส่วนที่สอง เป็นการออกแบบและสร้างอุปกรณ์ปฏิบัติการบนกระดาษร่วมกับการตรวจวัดทางเคมีไฟฟ้า ซึ่งทำให้ได้วิธีการวิเคราะห์ที่มีประโยชน์สูงสุดต่อการตรวจวัดปริมาณสาร และสามารถแก้ไขจุดบกพร่องจากการใช้อุปกรณ์ปฏิบัติการบนกระดาษร่วมกับการตรวจวัดเชิงสีได้ดี สำหรับส่วนสุดท้ายคือ การนำทั้งระบบการตรวจวัดเชิงสีและระบบการตรวจวัดทางเคมีไฟฟ้ามาใช้ร่วมกันบนอุปกรณ์ปฏิบัติการบนกระดาษ ซึ่งมีผลทำให้การวิเคราะห์และการใช้งานระบบขยายขอบเขตได้มากขึ้น อันเนื่องจากสามารถกำจัดปัญหาจากสารรบกวนการวิเคราะห์ไปพร้อม ๆ กับการวิเคราะห์ด้วย ทำให้ได้ระบบการวิเคราะห์ที่มีความน่าเชื่อถือได้มากยิ่งขึ้น โดยวิธีที่นำเสนอใหม่ทั้งหมดนี้เป็นวิธีที่ง่าย สามารถวิเคราะห์สารได้ทั้งสารอินทรีย์และสารอนินทรีย์ รวดเร็ว ประหยัดเมื่อเปรียบเทียบกับวิธีดั้งเดิม และยังเป็นวิธีการวิเคราะห์ที่เป็นมิตรกับ

สิ่งแวดล้อมอีกด้วย จากผลการทดลองที่ได้ พบว่ามีความสอดคล้องอย่างสูงต่อวัตถุประสงค์ของโครงการวิจัยที่ได้ตั้งไว้ตั้งแต่แรกเริ่ม และแผนการวิจัยก็บรรลุตามเป้าหมายที่วางไว้ จึงสามารถกล่าวได้ว่าการดำเนินงานและผลงานวิจัยนั้นสำเร็จลุล่วงอย่างดีเยี่ยม ผลผลิตจากการนำเสนอโครงการวิจัยนี้ทำให้ได้ผลงานวิจัยที่ได้รับการตอบรับให้ตีพิมพ์ในวารสาร ระดับนานาชาติที่มี Impact factor จำนวน 9 ฉบับ ดังเอกสารแนบ

Chapter I

Introduction

1.1 Lab-on-paper

Recently, paper-based microfluidic devices, representing the next generation of paper strip test devices, have been introduced by Whitesides and coworkers. A paper-based microfluidic device combines many advantages of paper strip tests with the utility of microfluidics. They have the potential to be good alternatives for point-of-care testing over traditional paper strip tests because they are capable of simultaneous multiplex analyte detection. In addition, they are portable, easy to use, require only a small volume of sample and provide rapid analysis. For patterning channels of hydrophilic surfaces on filter paper, there are several methods such as photolithography, wax printing, wax screen-printing. Each patterning method provides the different advantages and limitation depended on the purpose of work. Photolithography was first introduced for a simple method using negative photoresist to create a small hydrophilic channel in millimeter scale on chromatography paper. Currently, wax screen-printing was introduced for the fabrication of patterned paper. This fabrication is environmentally user-friendly, inexpensive and simple method than photoresist. To create the detection method for lab-on-paper, colorimetric and electrochemical detection is an alternative detection method and has the benefits of simplicity, speed, low cost, and portability.

1.2 Research objectives

The main objective of this work is to create the novel analytical method as an alternative choices for detection of various applications using lab-on-paper. Much effort has therefore been directed towards the fabrication and development of system by coupling lab-on-paper to colorimetric and electrochemical method for creating the quantitative analysis

systems. Then, the proposed systems were used to apply for the determination of important target analysts in various kinds of samples.

In the process of developing the method, the following specific objectives of the study should therefore be described in each part of work.

1.3 Scope of research

To achieve the research objectives, the following scope was set. There are eleven chapters in this research. Chapter I is the introduction. Chapters II-V are the principle of the development of paper-based devices coupled with colorimetric detection for organic and/or inorganic determination. Chapters IV-VIII give details of the results for the development of paper-based devices coupled with electrochemical detection for determination of organic such as dopamine and/or inorganic compound. Chapters IX-X report on the creation a system for dual electrochemical/colorimetric detection for electroanalysis of organic and/or inorganic compounds. Lastly, Chapter XI is the conclusion and future perspectives.

Chapter II

The development of paper-based microfluidic devices for multiple colorimetric detection

2.1 Introduction

Point-of-care testing (POCT) has become relatively commonplace in the developed nations as a way to augment traditional medicine and increase patient compliance [1]. POCT is also needed in the developing world because it can reduce the number of clinical visits, decrease costs to the patient and healthcare system, increase patient satisfaction, improve clinical outcomes, and provide clinical services for people in low resource settings [2-5]. Paper strip tests, termed lateral-flow immunochromatographic tests, are currently used in these scenarios [6]. Paper strip tests are commercially available for pregnancy [7], diabetes [8-9], drugs of abuse [10-11], and biomarkers of pathogens test [12-13]. Most paper strip tests use visible color changes for qualitative analyte detection. In the assay, flow is directed along the paper matrix by capillary force, and the analyte is subsequently bound by the capture antibody at the test line. However, qualitative analysis is not sufficient when analyte levels are important for diagnosis or treatment. Much effort has therefore been directed towards the development of quantitative paper strip tests but these devices still required instrumentation and trained personnel for use and are limited to a single analyte [14-15].

As an alternative to traditional paper-based immunochromatographic tests, Whitesides and coworkers recently introduced paper-based microfluidics (μPAD), which represent the next generation of paper strip test devices [16-20]. This approach, which combines many advantages of paper strip tests with the utility of microfluidic devices, holds significant potential for POCT

due to its low cost, multianalyte capability, low sample volume, and inherent portability [16-20,21]. To date, μPADs have been developed for glucose, protein, lactate, uric acid, and cholesterol determination [16,21]. The results of the assay were quantified by comparing the color intensities generated by unknowns to those generated for known analyte concentrations. Matching color and intensity by eyes can be complicated by many factors, however, including different color perception, differences in lighting, and the difference between the colors of a dry printed color and those seen in wetted paper. In an effort to conduct quantitative analysis for diagnostic tests based on paper microfluidics, several authors have used cameras or scanners to record the color intensity [20]. Camera phones and portable scanners can be used by unskilled personnel in remote areas but require transmission of data from on-site to remote experts, delaying the decision making process. Moreover, the intensities of digital images from a camera are affected by the lighting.

One approach to overcome the limitations of colorimetric approaches for μPADs is to use multiple indicators for a single analyte. Greater visual discrimination is possible when more than one color is developed as opposed to different hues or intensities of a single color [22]. Hence, multiple indicators should provide more accurate results as compared to single color tests by allowing differences in hue and intensity to be averaged across multiple detection spots for the same analyte. In addition, the improved accuracy should allow for diagnosis by untrained personnel without the need to transmit the results to a central laboratory. Here, we report the development of a novel multiple-indicator approach for μPADs that allows simultaneous detection using iodide [16], the mixture of 4-aminoantipyrine and 3,5-dichloro-2-hydroxy-benzenesulfonic acid [23], *o*-dianisidine [24], acid yellow and acid black for each of the three analytes. The devices share advantages of previous μPADs, while allowing for more accurate

quantitative analysis of glucose, uric acid, and lactate without external instrumentation. The colorimetric assays in this work utilize oxidase enzymes to decompose analytes and produce hydrogen peroxide [23,25]. Hydrogen peroxide then oxidizes the indicators to generate a visible color change. Each indicator yields a different color and will also change color at different analyte concentrations, allowing a greater dynamic range to be achieved [26-28]. Here, the volume of reagent and sample spotted on the devices was first optimized. Dynamic ranges were then investigated. Our approach was successfully applied to quantify glucose (0.5-20 mM), lactate (1-25 mM), and uric acid (0.1-7 mM) in clinically relevant ranges. Finally, the devices were successfully applied to the analysis of control serum and urine samples. To demonstrate the improvements in accuracy of measurement for clinical samples, 10 random untrained individuals were asked to screen μPADs comparing single indicator versus multiple indicators. Tests using multiple indicators yielded a statistically significant improvement in accuracy of the measurement compared to tests performed with a single indicator color.

2.2 Experimental methods

2.2.1 Materials and equipments

D-(+)-glucose (99.5%), sodium L-lactate (98%), uric acid (99%), glucose oxidase (from *Aspergillus niger*, 215 U/mg), uricase (from *Candida Sp.*, 2 U/mg), peroxidase Type I (from *Horseradish*, 113 U/mg), 4-aminoantipyrine (reagent grade), 3,5-dichloro-2-hydroxy-benzenesulfonic acid (sodium salt, 99%), and *o*-dianisidine dihydrochloride (purified grade for use with peroxidase reaction) were purchased from Sigma-Aldrich (St. Louis, MO). Lactate oxidase (from *Aerococcus viridian*s, 38 U/mg) was obtained from A.G. Scientific, Inc (San Diego, CA). Potassium phosphate (ACS grade), potassium iodide (ACS grade), sodium

hydroxide (ACS grade) and acid yellow 34 (Indicator grade) were purchased from Fisher Scientific (Pittsburgh, PA). Acid Black 1 (Indicator grade) was purchased from Acros Organic (Geel, Belgium). Trehalose dehydrate (HPLC grade) was obtained from Calbiochem (Gibbstown, NJ). Acetone (AR grade) was obtained from Mallinckrodt chemicals (Phillipsburg, NJ). SU-8 3025 negative photoresist was purchased from MicroChem Corp. (Newton, MA). Whatman #1 filter paper was obtained from Cole-Parmer (Vernon Hills, IL). All chemicals were used as received without further purification. A digital camera (coolpix5000, Nikon corp.) was used to photograph results.

2.2.2 Preparation of paper-based microfluidic devices

Briefly, SU-8 3025 photoresist was poured on the center of the paper and distributed using a spin-coater (Laurell Technologies Corp., WS-400A-6NPP/LITE). The photoresist-covered paper was baked at 95 °C for ~5 min. The paper was then covered with a patterned transparency film generated using a standard laser printer and irradiated with a UV lamp at 100% intensity (400 W) for 7 s (Uvitron international, Intelli-RAY 400). After baking at 95 °C for ~3 min, unpolymerized photoresist was removed from the paper by submerging in acetone for 1 min, followed by rinsing with acetone. After that, the paper was dried under ambient conditions for approximately 1 hr. Prior to adding the reagents, the paper microfluidic devices were exposed to an air plasma (Harrick PDC-32G) at 18 W for 30 s. Areas covered with photoresist remained hydrophobic while areas without photoresist were hydrophilic.

2.2.3 Design of multiple oxidative indicators for paper-based microfluidic devices

For the current experiments, the dendritic flow channels terminating in nine detection zones (giving position number 1-4, 5-7, and 8-9 of the detection zones for glucose, lactate, and uric acid detection, respectively) connected to a central sample deposition spot were created as shown in Figure 4.8. Each detection zone was spotted with a different indicator in addition to the appropriate enzyme. The indicators used here were the mixture of 4-aminoantipyrine (AAP) and 3,5-dichloro-2-hydroxy-benzenesulfonic acid (DHBS) in the mole ratio of 1:2 abbreviated to AB, *o*-dianisidine dihydrochloride (OD), potassium iodide (KI), acid yellow 34 (Y), and acid black 1 (B). AB, OD, and KI oxidized will change from colorless to red, green-brown , and yellow-brown colors while Y and B oxidized will change from yellow and black color to colorless, respectively. For detection, sample was added to sample deposition spot and flowed outward via capillary forces to the detection zones.

2.2.4 **Effect of reagent and sample volume**

Varying volumes of red food dye (0.4, 0.5, and 0.6 μL) were dropped into the detection zone to optimize the volume of reagent. The effect of sample volumes was studied by dropping 5.0, 7.0, 9.0, and 11 μL of red food dye into the center of devices using a micropipette. The micropipette which was used to transfer and control the sample volume into device may not be available in the field. In our effort to conduct quantitative analysis for self-monitoring diagnostic tests based on paper microfluidic devices without external equipment, the assays of known volume of level 4 standard solution (11 μL) containing 5 mM glucose, 10 mM lactate, and 4.5 mM uric acid were compared with unknown volume dropped by dropper. Images of fully developed tests were captured with a digital camera for additional characterization.

2.2.5 **Preparation of multiple oxidative indicators for paper-based microfluidic devices**

For a given analyte, positions 1-4, 5-7, and 8-9 were spotted with glucose oxidase, lactate oxidase, and uricase enzyme, respectively and the different indicators. The glucose assay was prepared by spotting 0.5 μL of mixture each oxidative indicator, glucose oxidase solution (645 U/mL), *Horseradish* peroxidase (339 U/mL), and 0.3 M trehalose into the four detection areas of glucose. Trehalose is added to stabilize the enzyme according to prior reports [29]. The three lactate and two uric acid test zones were created with the different component of indicators and the same amount of *Horseradish* peroxidase and trehalose but the specific enzymes used were lactate oxidase (114 U/mL), and uricase (80 U/mL), respectively. The indicator composition of each test zone is shown in Figure 1. After spotting the reagent solution, the paper was allowed to dry at room temperature (~22°C) for 10 min. All standard and enzyme solutions were prepared in 0.1 M potassium phosphate buffer (pH 6) except for 15 mM of uric acid stock solution which prepared in 20 mM sodium hydroxide. 6 levels of standard solution containing with glucose, lactate, and uric acid and a negative control consisting of buffer were used to study the multiple indicator approach. The concentrations of glucose, lactate, and uric acid in each level of standard solution are shown in Table 1.

Table 1 Concentrations of glucose, lactate, and uric acid in each level of standard solution

Std. level	Glucose Conc. (mM)	Lactate Conc. (mM)	Uric acid Conc. (mM)
0	0	0	0
1	0.5	1	0.1
2	1.5	2.5	1
3	3	5	2.5

4	5	10	4.5
5	10	20	6
6	20	25	7

2.2.6 Human serum sample

Human control serum and urine samples (levels I and II) were obtained from Pointe Scientific (Canton, MI) and Quantimetix Corporation (Redondo Beach, CA), respectively. These complex samples are intended to mimic biological fluids and are used to validate clinical assays commercially. Analyte concentrations were provided by the supplier. All samples were analyzed using multiple oxidative indicators for paper-based microfluidic devices without pretreatment. To test the hypothesis of improved accuracy, results from urine and serum samples were interpreted by 10 randomly selected, untrained individuals who are not familiar with this assay from the varieties of faculty such as education, veterinary, science at Colorado State University for both single and multiple indicator systems.

2.2.7 Lifetime of the devices

The devices spotted with oxidase enzyme and indicators solution were kept at 8 ºC, room temperature (~22 ºC), and 40 ºC for multiple days to determine lifetime. Stored devices were tested for lifetime using the standard mixtures every four days.

2.3 Results and discussion

2.3.1 Colorimetric bioassays

The goal of this work was to test the hypothesis that multiple indicators for a single analyte would improve the accuracy of the data interpretation in colorimetric μPAD assays. Three analytes of clinical relevance (glucose, lactate, and uric acid) were tested using multiple indicators (AB, OD, KI, Y, and B) for each analyte. The device design is shown in Figure 4.8. The combination of indicators is needed for this assay because it provides the greater visual discrimination than one color. Two types of indicators were used. The first type generated a stable color on oxidation. AAP and DHBS produced a red quinone product on reaction with peroxide. In a similar fashion, green-brown and yellow-brown stable colors were generated from the reaction of H_2O_2 with OD and KI. The second type of indicator was selected to lose color when oxidized. Here, we used Y (yellow color) and B (blue color) as indicators because they are colorless when oxidized. The reactions between peroxide and these indicators were shown in below equations.

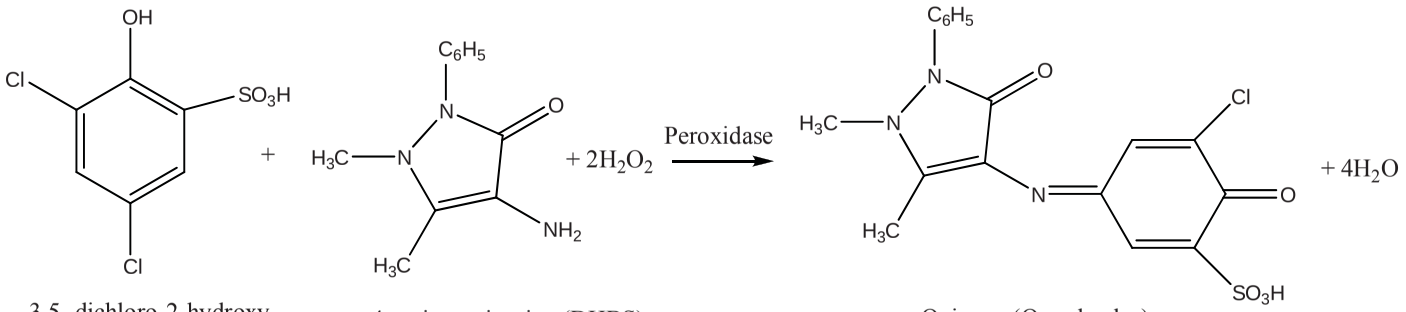

3,5 -dichloro-2-hydroxy-benzenesulfonic acid (AAP)

4-aminoantipyrine (DHBS)

Quinone (Q, red color)

(11)

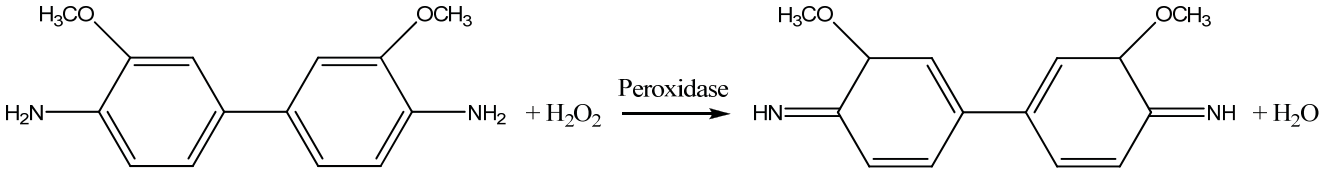

o-dianisidine (OD)

Green-brown color form

(12)

$$2I^- + H_2O_2 + 2H^+ \xrightarrow{\text{Peroxidase}} I_2 + 2H_2O$$

Yellow-brown color form

(13)

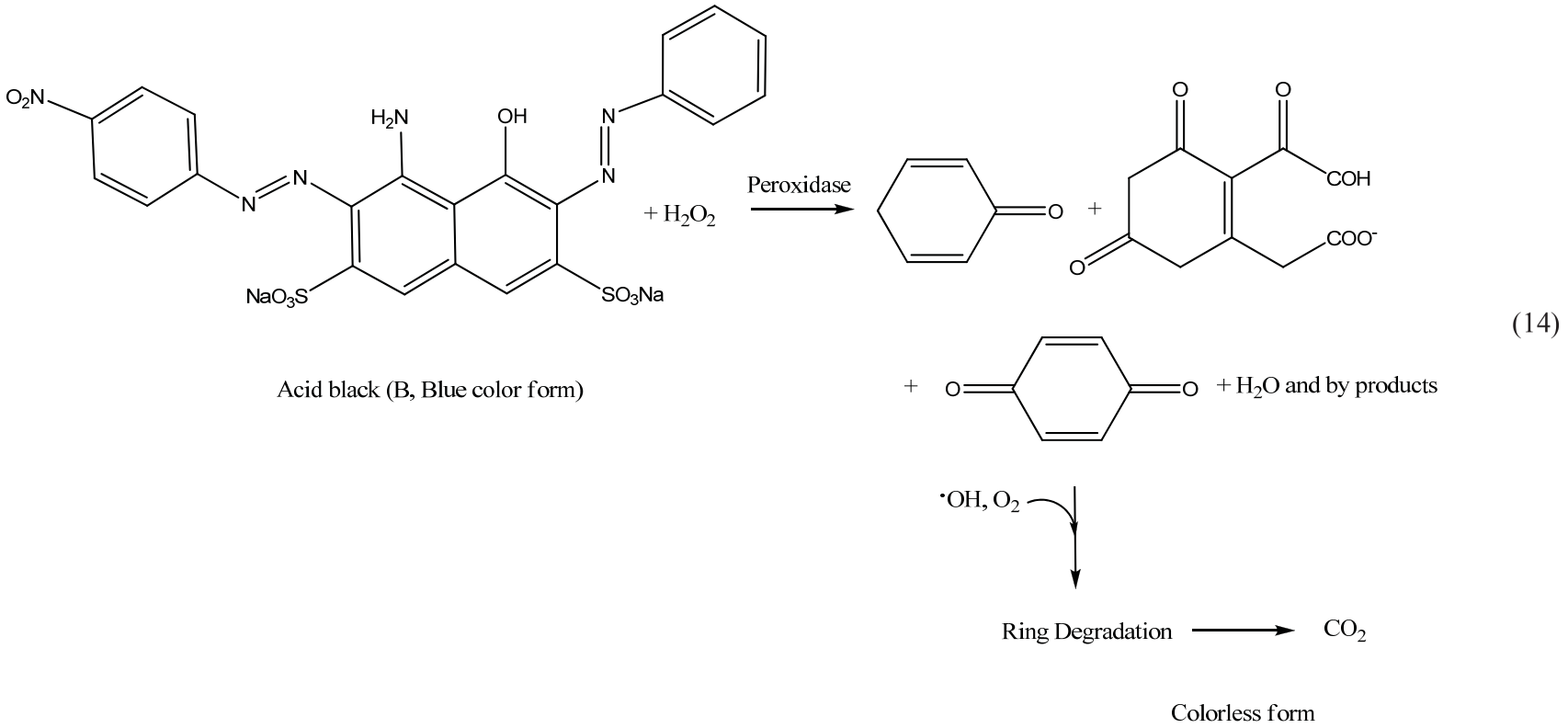
O2N
H2N
OH
N
N
N
N
NaO3S
SO3Na
+ H2O2
Peroxidase
O
O
O
COH
COO-
O
+
+
O
O
+ H2O and by products
·OH, O2
Ring Degradation
CO2
Acid black (B, Blue color form)
Colorless form

(14)

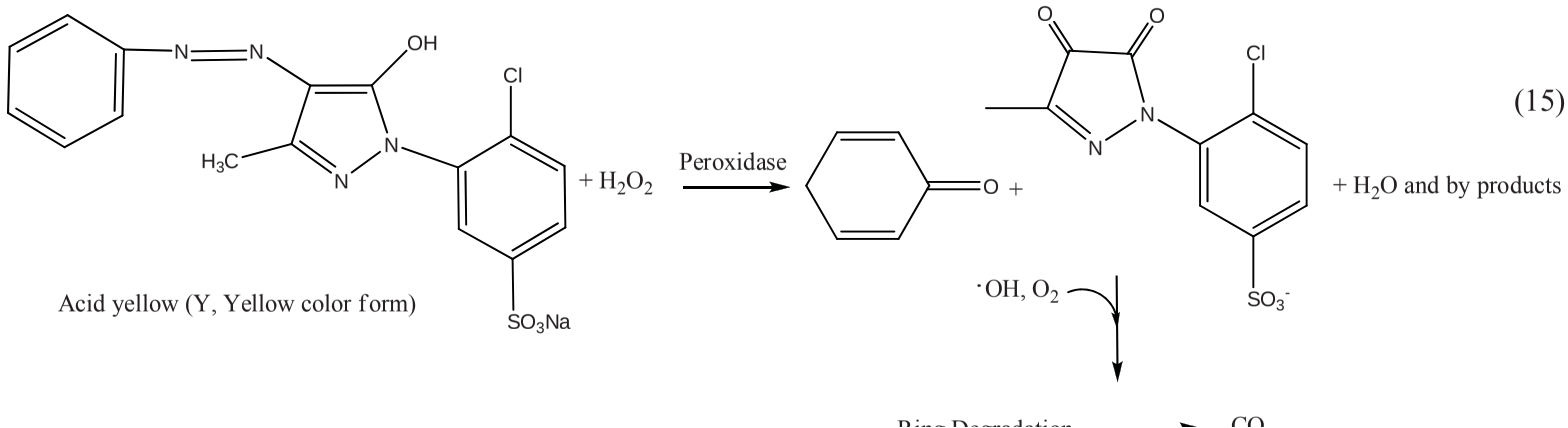
N
N
OH
Cl
H3C
N
N
+ H2O2
Peroxidase
O
O
O
Cl
N
N
+
+ H2O and by products
·OH, O2
SO3-
SO3Na
Acid yellow (Y, Yellow color form)

(15)

The first indicator shade in oxidized form will be mixed with the other indicator shade at each test zone so the gradient of shade and intensity color occurs at the different levels of analyte. For example, we used the mixture of AB as the first indictor and Y as the second indicator at position number 1 of device for the glucose test. At two levels of glucose, we will get two shades as orange (mixture of yellow and red color) and red colors whereas the previous approach using one indicator obtains only one shade at the different color intensities providing more difficult visual distinction than the indicators combination. Our proposed method was therefore expected to provide a larger difference in color hues and intensities, allowing greater visual discrimination and therefore accuracy. All case of the mixture of first and second indicator was studied to demonstrate the dynamic range between the changing of shade and glucose, lactate, and uric acid concentration but we found only 4, 3, and 2 cases of the mixture changed the shade of indicator for glucose, lactate, and uric acid assay, respectively. Therefore, our design needed 4, 3, and 2 wells for glucose, lactate, and uric acid assay as shown in Figure 1.

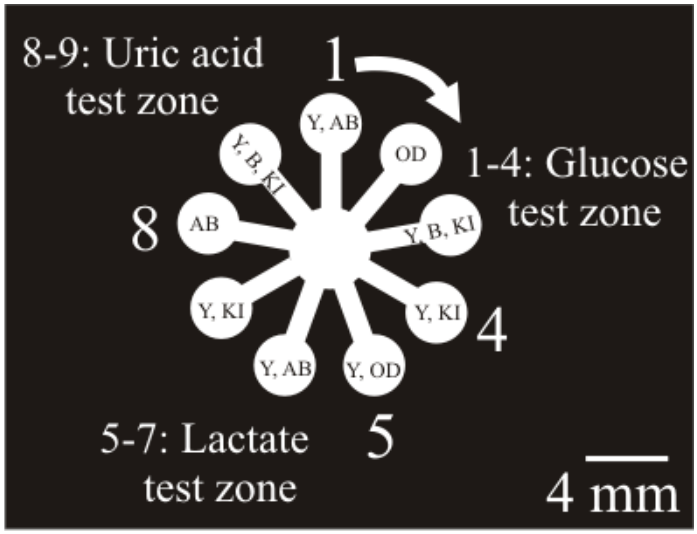

Figure 2.1 Design of multiple oxidative indicators for paper-based microfluidic devices which determine three analytes simultaneously with nine test zones. Back and white colors

refer to hydrophobic and hydrophilic area, respectively. The device size is 2 cm x 2 cm. Position numbers 1–4: glucose test zones, 5–7: lactate test zones, 8–9: uric acid test zones.

2.3.2 Effect of reagent and sample volume

The volume of reagent and sample required for analysis were first determined. In existing paper test strips, the major cost comes from reagents. Hence, we designed the reaction zones to be small (3 mm diameter) for reduced reagent consumption while still making it large enough to be visible to the naked eye. Reaction zone diameters are smaller than 3 mm were studied. Even though the reagent consumption can be reduced with a small detection zone, dispensing less than 0.2 μL is difficult with standard micropipettes. We next determined the reagent volume necessary to wet the entire detection zone by dropping red food dye in the range of 0.4 to 0.6 μL into the detection zones. As the results show in Figure 4.9A, 0.4 μL of reagent solution cannot completely wet the detection zones whereas 0.6 μL spread outside the detection zones. Therefore, we selected 0.5 μL of reagent solution for the further experiments. The minimum sample volume that can spread through the entire device was also studied by spotting red food dye into the center of the device. It was found that 11.0 μL of sample is required to fill all detection zones (Figure 2 B-E). In many situations a micropipette may not be available to apply an accurate sample volume. Hence, the effect of sample volume on the assays reaction was determined by dropping a standard solution level 4 containing 5 mM glucose, 10 mM lactate, and 4.5 mM uric acid into the center of the device with 11.0 μL. In addition, an unknown volume was dispensed with a disposable transfer pipet to simulate real field-testing. The results with controlled volumes (Figure 2F) were compared with results from unknown volumes (Figure 2G and 2H). We found that the color hue of the three indicators was the same regardless of the sample volume added, meaning tight control of sample volume was not necessary. In the field, the samples can therefore be directly dropped into our devices using simple transfer pipettes and similar spotting devices.

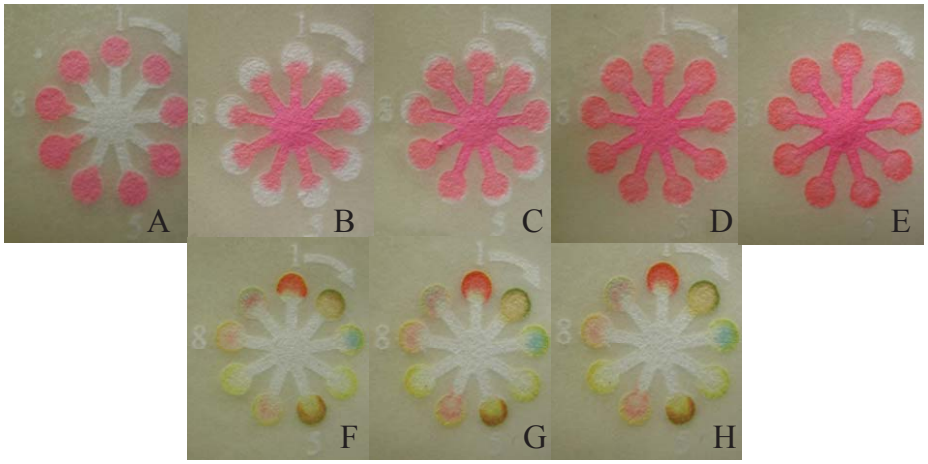

Figure 2.2 (A) Paper-based microfluidic devices after spotting red food dyes of various volumes (0.4, 0.5, and 0.6 μL into the position numbers 1–3, 4–6, and 7–9, respectively of the detection zones). (B–E) Paper-based microfluidic devices after spotting 5 (B), 7 (C), 9 (D), and 11 μL (E) of red food dye respectively into the central of devices. (F–H) Multiple oxidative indicator for paper-based microfluidic devices after spotting level 4 of standard solution including 5 mM glucose, 10 mM lactate, and 4.5 mM uric acid with 11 μL of controlled standard volume (f) and unknown of standard volume (G and H).

2.3.3. Simultaneous measurement of three analytes

The principle of our proposed method is to use the color change of each oxidative indicator and the color intensity at different analyte concentrations to improve the accuracy and extend the linear range of colorimetric μPAD assays. To demonstrate the multiple indicator systems, we studied the dynamic range of glucose, lactate, and uric acid on a single device. The results were captured with a digital camera for visualization (Figure 3). Glucose at 0.5 mM generated an orange color (position number 1). Glucose at 1.5 mM showed orange and green-brown colors, while glucose between 3 and 5 mM gave red and green-brown colors (position number 1 and 2, respectively). Glucose concentrations ≥10 mM glucose gave red, green-brown, and brown colors (position number 1-4). Moreover, the

intensity of red, green-brown increased when glucose concentrations increased. Hence, the difference of hue and intensity of multiple indicators can be used to indentify glucose concentration. The normal level of glucose is 2.5-5.3 mM in serum, and 0.1-0.8 mM in urine. Given the dynamic range of the color changes, our devices could be used in a variety of biological matrices such as serum, plasma, and urine.

Our device also gave multiple color hues for different concentrations of lactate. Lactate at 1 mM gave brown and orange colors, while lactate concentrations between 5 and 20 mM gave green-brown and red colors at positions 5 and 6, respectively. Moreover, lactate concentrations ≥25 mM showed three colors, green-brown, red, and brown at positions 5, 6, and 7, respectively. These devices are therefore sufficient for clinical diagnostics where the normal concentration of lactate is 0.5-1.7 mM in serum, and 5.5-22 mM in urine.

Uric acid detection zones also exhibited color changes as a function of concentration. Concentrations at 0.1 mM gave orange color at position number 8, while concentrations between 1 and 2.5 showed orange and red colors at position number 8 and 9, respectively. At uric acid concentrations ≥2.5 mM, both position number 8 and 9 were red. The normal level of uric acid is 0.1-0.4 mM in serum and 1.5-4.4 mM in urine [30]. These results clearly suggest the ability to visually discriminate between different concentrations using multiple indicators for a single analyte.

Std. level	0	1	2	3	4	5	6
Conc. (mM)	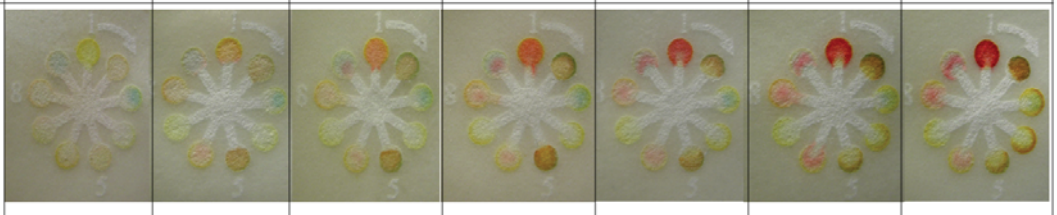						
Glucose	0	0.5	1.5	3	5	10	20
Lactate	0	1	3	5	10	20	25
Uric acid	0	0.1	1	2.5	4.5	6	7

Figure 2.3 Multiple oxidative indicators system designed on paper-based microfluidic

devices for the simultaneous semi-quantitative analysis of glucose, lactate, and uric acid. Pictures were captured after spotting varying concentration of three analytes for 10 min.

The reproducibility of our proposed method was also studied by spotting each level of standard solution into three paper devices in the same day (intra-day assay) and three different days (inter-day assay) as shown in Figure 4. At each test zone, the change in color intensity as a function of analyte concentration was obtained with high reproducibility.

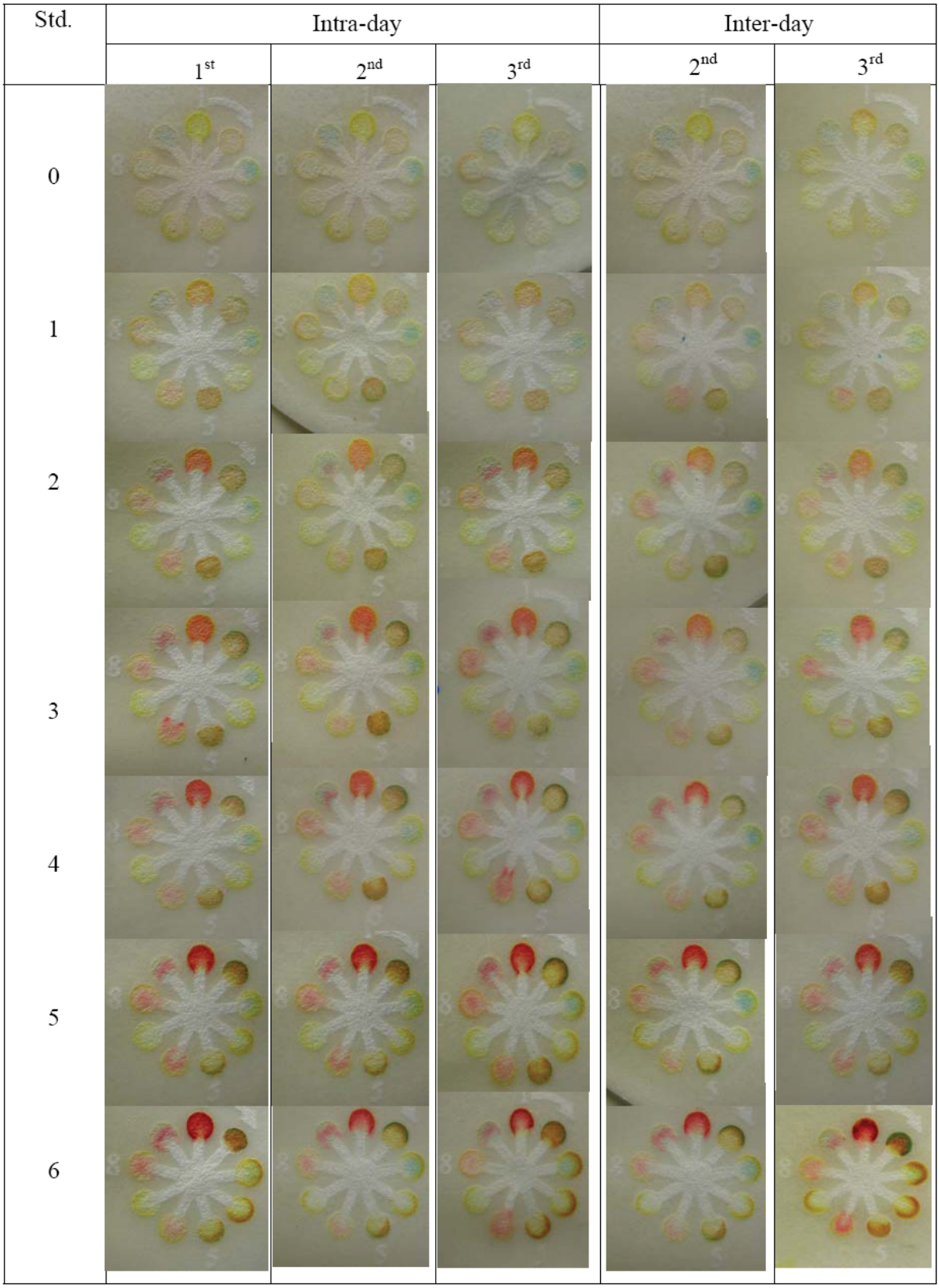

Figure 2.4 Multiple oxidative indicators system designed on paper-based microfluidic devices for the simultaneous semi-quantitative analysis of glucose, lactate, and uric acid.

Pictures were captured after spotting varying concentration of three analytes for 10 min.

2.3.4 Semi-quantitative measurement of three analytes in real samples

The multi-indicator μPAD devices were next evaluated for glucose, lactate, and uric acid analysis in clinical control samples. The control samples are used for determining the accuracy of diagnostic tests in a biologically relevant matrix without worry of blood borne pathogens. The results are shown in Figure 5. We found that level I serum and urine samples gave significantly different color patterns than the level II samples. The results indicated that glucose concentrations were between 5-10 mM in serum level I (control level: 5.6 mM), and 3-5 mM (control level: 3.3) in urine level I, whereas 20 mM glucose was determined in both serum and urine samples level II (control serum and urine level: 16.8 and 16.5 mM, respectively). For the lactate test, we obtained brown and orange colors for both serum sample levels I and II. This indicated lactate levels in both serum sample levels were between than 1-2.5 mM. Moreover, the intensities of brown color from standard lactate can be used to identify lactate concentration of 1 mM in level I (control level: 1.2 mM) and 2.5 mM (control level: 3.3 mM). In these cases, both the color intensity and hue can be used to confirm our results. Lactate test zones of both urine sample levels show insignificant difference of the color changing comparing with buffer solution (Std. level 0). Therefore, we can indicate both urine samples in the absence of lactate correlated with the certificated concentration. Uric acid concentrations in samples were determined to be 0.1 mM for level I serum and urine samples (control level: 0.2 mM in serum and 0.5 mM in urine) and 1 mM for level II serum and urine samples (control level: 0.7 mM in serum and 1.1 mM in urine) by comparing the differences in color intensity.

Samples		Certified Concentration (mM)	Our proposed method (mM)	
Serum Level I	Glucose	5.6		5-10
	Lactate	1.2		1
	Uric acid	0.2		0.1
Serum Level II	Glucose	16.8		20
	Lactate	3.3		2.5
	Uric acid	0.7		1
Urine level I	Glucose	2.9		3-5
	Lactate	Not labeled		ND
	Uric acid	0.5		0.1
Urine level II	Glucose	16.5		20
	Lactate	Not labeled		ND
	Uric acid	1.1		1

Figure 2.5 Multiple oxidative indicators system designed on paper-based microfluidic devices for the simultaneous semi-quantitative analysis of glucose, lactate, and uric acid in real biological samples.

To demonstrate our method comparing with a single indicator system in terms of accuracy, the highest sensitivity single dye indicators including Y+AB, Y+OD, and AB for the glucose, lactate, and uric acid test, respectively were selected for single indicator systems as showed in Figure 6. We also compared the percentage of correct answer obtained from 10 untrained individuals using single and multiple indicator tests (Figure 7). The results indicated that our devices were successfully applied for glucose, lactate, and uric acid screening tests by the naked eye. As can be seen in Figure 6, there is a clear difference

between the two sets of data in terms of colors generated. Furthermore, Figure 7 shows the increase in accuracy for the tests using multiple indicators. The single indicator system had an accuracy of ~70%, while the multi-indicator system had an accuracy of over 90%. The results suggest our approach provides a more accurate result when compared to a single indicator system.

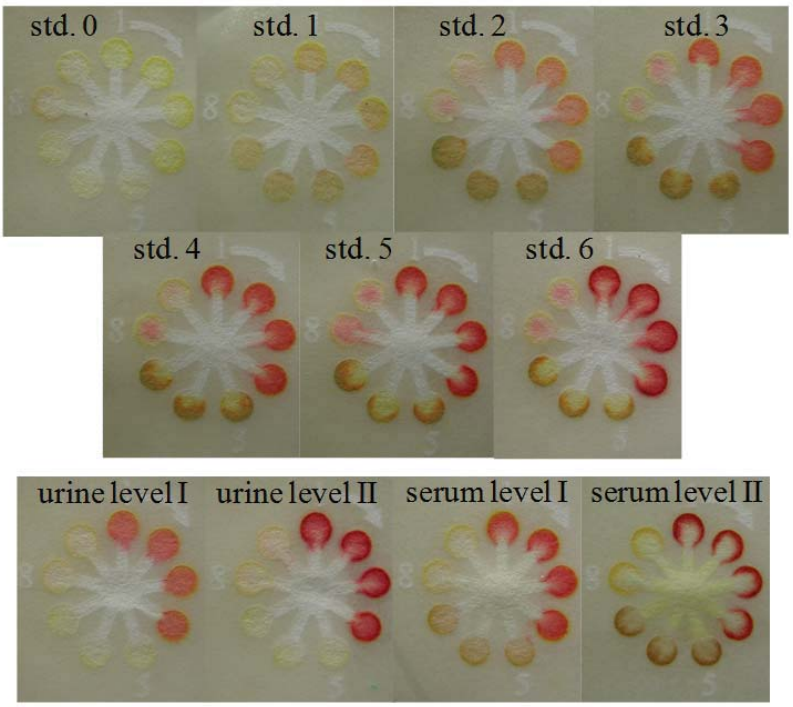

Figure 2.6 Single indicator system designed on paper-based microfluidic devices for the simultaneous semi-quantitative analysis of glucose, lactate, and numbers 1–4: glucose test zones using Y +AB indicator, 5–7: lactate test zones using Y +OD indicator, 8–9: uric acid test zones using AB indicator.

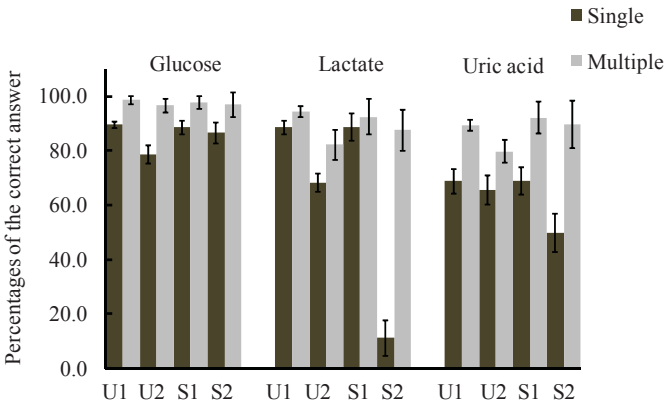

Figure 2.7 Comparison of percentages of the correct answer where a corrected answer was determined to be within ±0.5 mM of the certified concentration between single and multiple-indicator systems (n = 10). U1: level I urine human, U2: level II urine human, S1: level I serum human, S2: level II serum human, error bar: standard deviation (n = 3).

2.3.5 Lifetime of the devices

Diagnostic devices must remain stable for weeks to be useful in the field for use in developing countries. Hence, the performance of devices was studied after storing the prepared paper devices for multiple days at varying temperatures. To test stability, prepared paper devices were dried at ambient condition before storage at either 8 ºC, room temperature (~22 ºC), or 40 ºC. Oxidase enzymes can degrade, aggregate, or unfold during dry storage. Non-reducing sugars such as sucrose and trehalose, and polyols such as mannitol have been used to stabilize dried proteins during storage. Here, trehalose was added to oxidase enzymes solution during devices preparation to improve stability of the enzyme during storage. The lifetime of these devices was observed over a period of several days as shown in Figure 8. We found that multiple indicators, which were generated at all detection zones of all standard solution levels, exhibited no significant difference from day to day at all temperatures. At 12 storage days at room temperature and 40 ºC, an observable signal decrease was noted. The

results indicated the devices can be kept for 8 day without loss of activity but longer storage time requires refrigeration (Figure 9). Future work will focus on methods to increase the lifetime of these devices to allow months of storage at elevated temperatures.

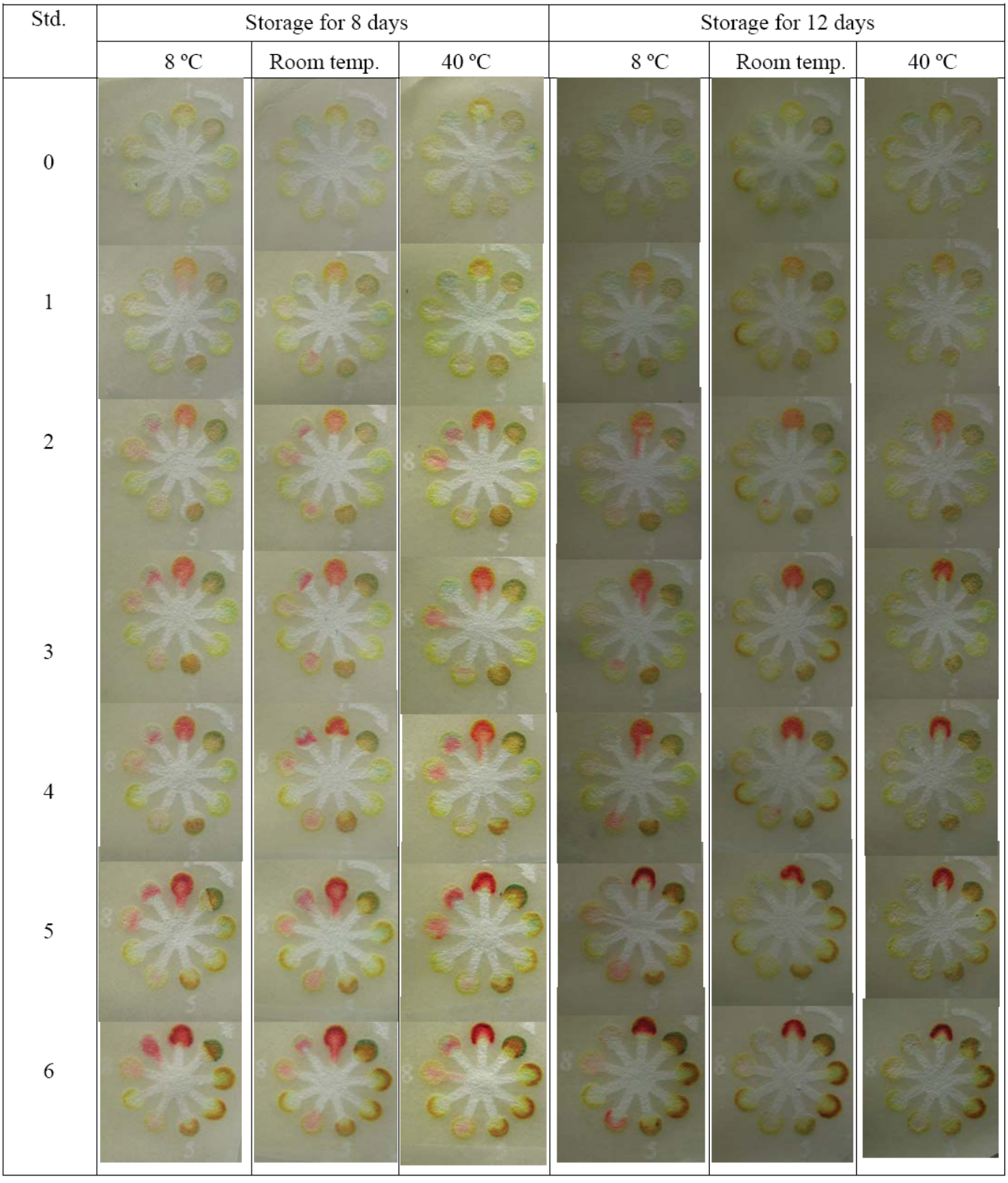

Figure 2.8 Lifetime of our devices kept at 8 ºC, room temp. (~22 ºC), and 40 ºC. Background signals were obtained by spotting 0.1 M of phosphate buffer solution while standard test signals were obtained by spotting all levels of standard solution.

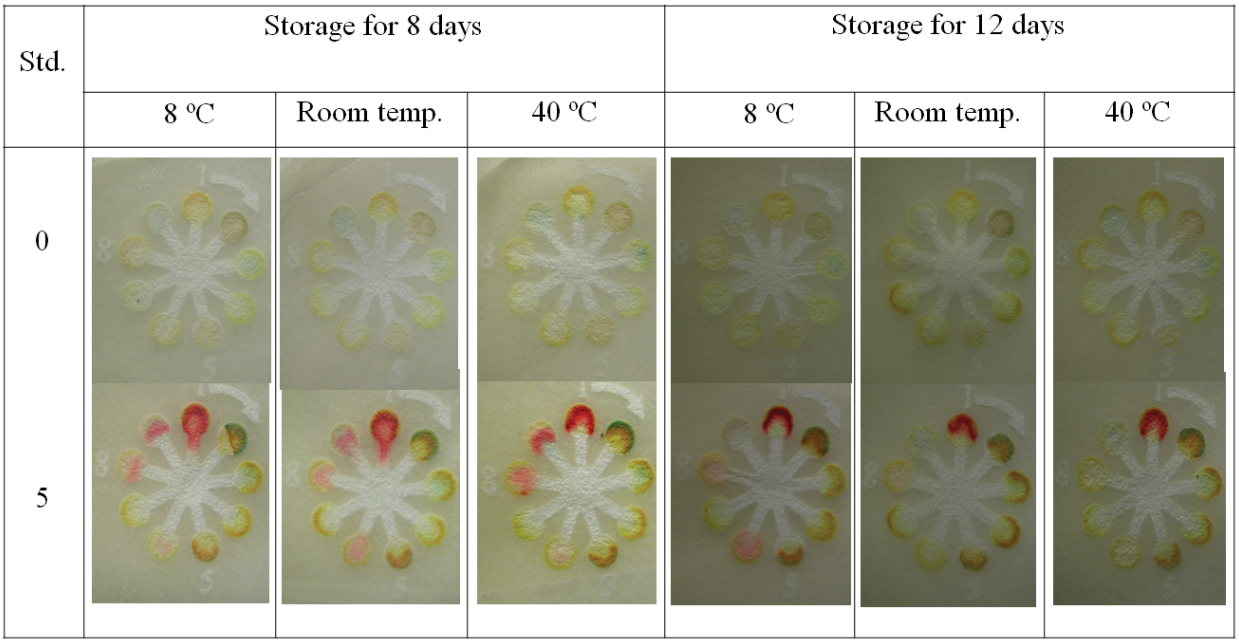

Figure 2.9 Lifetime of our devices kept at 8 ºC, room temperature (~22 ºC), and 40 ºC. Background signals were obtained by spotting 0.1 M of phosphate buffer solution while standard test signals were obtained by spotting 10 mM glucose, 20 mM lactate, and 6 mM uric acid.

2.4 Summary

This paper demonstrates the use of multiple indicators for a single analyte as part of a multianalyte μPAD. Multiple indicators improve accuracy of detection by improving the ability to visually discriminate between different concentrations. While different concentrations of the same dye could also be used to achieve a similar result, using different colors provides increase visual discrimination capability. Furthermore, different indicators generate colors at different analyte concentrations, which should provide more accuracy than different shades or intensities of a single color. Our devices were also successfully applied to the simultaneous semi-quantitative analysis of glucose, lactate, and uric acid in biologically relevant samples. These results demonstrate the feasibility of using multiple oxidative

indicators for paper-based microfluidic devices as an easy-to-use, inexpensive, and portable alternative device for point of care testing and self-monitoring diagnosis.

2.5 References

[1] Price, C. P. Point-of-care testing in diabetes mellitus. Clin. Chem. Lab. Med. 41 (2003): 1213–1219.

[2] Yager, P.; Edwards, T.; Fu, E.; Helton, K.; Nelson, K.; Tam, M. R.; Weigl, B. H. Nature. 442 (2006): 412-418.

[3] Chin, C. D.; Linder, V.; Sia, S. K. LabLab Chip. 7 (2007): 41-57.

[4] Myers, F. B.; Lee, L. P. Lab Chip. 8 (2008): 2015-2031.

[5] Sia, S. K.; Kricka, L. J.Lab Chip. 8 (2008): 1982–1983.

[6] Zhao, W.; Berg, A. V. D. Lab on a Chip. 8 (2008): 1988–1991.

[7] One Step HCG Urine Pregnancy Test (Strip), AI DE Diagnostica Co. Ltd., Shandong, China (2009).

[8] Hones, J.; Muller, P.; Surridge, N. Diabetes Technol. Ther. 10 (2008): S10–S26.

[9] Kristensen, G. B. B.; Monsen, G.; Skeie, S.; Sandberg, S. Diabetes Technol. Ther. 10 (2008): 467–477.

[10] Penttila, A.; Karhunen, P. J.; Pikkarainen, J. Forensic Sci. Int. 44 (1990): 43–48.

[11] One Step Drugs of Abuse Test, Beijing China: Core Technology Co. Ltd., 2009.

[12] Oberhofer, T. R.; Towle, D. W. J. Clin. Microbiol. 15 (1982): 196–199.

[13] Mosley, L. M.; Sharp D. S. The hydrogen sulphide (H_2S) paper strip test. SOPAC Technical Report 373 (2005).

[14] Lin, Y. Y.; Wang, J.; Liu, G.; Wu, H.; Wai, C. M.; Lin, Y. Biosens. Bioelectron. 23 (2008): 1659–1665.

[15] Mao, X.; Baloda, M.; Gurung, A. S.; Lin, Y.; Liu, G. Electrochem. Commun. 10 (2008): 1636–1640.

[16] Martinez, Andres W.; Phillips, Scott T.; Butte, Manish J.; Whitesides, George M., Angew. Chem. Int. Ed. 46 (2007): 1318-1320.

[17] Abe, K.; Suzuki, K.; Citterio, D. Anal. Chem. 80 (2008): 6928-6934.

[18] Li, X.; Tian, J.; Nguyen, T.; Shen, W. Anal. Chem. 80 (2008): 9131-9134.

[19] Martinez, A. W.; Phillips, S. T.; Wiley, B. J.; Gupta, M.; Whitesides, G. M. Lab Chip 8 (2008): 2146-2150.

[20] Martinez, A. W.; Phillips, S. T.; Carrilho, E.; Thomas, S. W.; Sindi, H.; Whitesides, G. M. Anal. Chem. 80 (2008): 3699-3707.

[21] Dungchai, W.; Chailapakul, O.; Henry, C. S. Anal. Chem. 81 (2009): 5821-5826.

[22] Fung, K.-K.; Chan, C. P.-Y.; Renneberg, R. Anal. Chim. Acta. 634 (2009): 89–95.

[23] Fossati, P.; Prencipe, L.; Berti, G. Clin. Chem. 26 (1980): 227–231.

[24] Domagk, G. F.; Schlicke, H. H. Anal. Biochem. 22 (1968): 219–224.

[25] Hamid, M.; Khalil ur, R. Food Chem. 115 (2009): 1177–1186.

[26] Ugarova, N. N.; Lebedeva, O. V.; Berezin, I. V. J. Mol. Catal. 13 (1981): 215–225.

[27] Carvalho, R. H.; Lemos, F.; Lemos, M. A. N. D. A.; Vojinovic, V.; Fonseca, L. P.; Cabral, J. M. Bioprocess. Biosyst. Eng. 29 (2006): 99–108.

[28] Björksten, F. Biochim. Biophys. Acta. 212 (1970): 396–406.

[29] Kreilgaard, L.; Frokjaer, S.; Flink, J. M.; Randolph, T. W.; Carpenter, J. F. J. Pharm. Sci. 88 (1999): 281–290.

[30] Tietz, N. W. Clinical guide to laboratory tests. PA USA: W.B. Saunders Company, 1995.

Chapter III

Selective determination of homocysteine levels in human plasma using a silver nanoparticle-based colorimetric assay

3.1 Introduction

Homocysteine (Hcy), a sulfur-containing amino acid, is an intermediate formed during the conversion of methionine into cysteine (Cys). Hcy exists in various forms in plasma, including disulfide, mixed disulfides and protein-bound homocystine, as well as the free (unattached) reduced form of Hcy. Hence, the measurement of total Hcy levels is typically completed after the chemical reduction of the disulfides. The normal concentration of Hcy in plasma ranges from 5 to 15 μM, with levels of Hcy above 15 μM defined as hyperhomocysteinemia. Hyperhomocysteinemia is categorized into three groups: moderate (15 - 30 μM), intermediate (30 - 100 μM) and severe (over 100 μM) [1]. High plasma levels of Hcy are associated with several diseases such as cardiovascular disease [2], Alzheimer's disease [3], neural tube defects [4], and osteoporosis [5].

Hcy and Cys both contain a free thiol and are structurally similar [6], and thus analytical methods for the determination of Hcy have been extensively investigated after prior separation techniques to remove the Cys, for instance, gas chromatography with mass spectrometry (GC-MS) [7], high performance liquid chromatography (HPLC) [8,9] or capillary electrophoresis (CE) [10,11] separation methods then coupled with electrochemical [12], UV-vis [13] and fluorescent [14] detection. However, these methods are rather expensive, complicated and time-consuming [15]. Recently, colorimetric assays based on nanoparticle (NP) assembly have received considerable attention for the detection of Hcy and Cys [16-20] because of their ease of operation, detection using optical methods, suitability for diagnosis, simplicity, and high sensitivity [21, 22]. Gold nanoparticles (AuNPs) have been

intensively developed as probes or sensors for the determination of aminothiols [16, 23] based on the fact that AuNPs aggregate upon the addition of aminothiols. The interparticle forces between AuNPs and aminothiols include electrostatic interactions [24], hydrogen bonding [25-28], zwitterionic forces [19, 24] and van der Waals forces [25]. The aminothiol-induced aggregation of AuNPs leads to a decrease in the plasmon resonance absorption peak and the formation of a red-shifted band [29]. The colorimetric changes of AuNPs in the presence of aminothiols such as Hcy [30-32] and Cys [33, 34], have been reported. The structurally similar Cys and Hcy molecules, which only differ by one methylene group, can be selectively detected using modified AuNPs based on the differences in their aggregation kinetics [16]. In spite of their good selectivity, these methods require a procedure involving complex surface modification. Therefore, the cost of these methods is high due to the cost of AuNPs and their chemical modification. Moreover, these methods are difficult to apply for routine analysis because of their complicated procedures. Recently, silver nanoparticles (AgNPs), which are less expensive than AuNPs, have been used as an alternative source for colorimetric sensors. AgNPs have gained in popularity owing to their chemical and physical properties [35, 36]. The advantage of AgNPs is that the molar extinction coefficient of AgNPs is approximately 100-fold greater than that for AuNPs, which leads to improved visibility based on the difference in optical brightness and increased sensitivity when using absorption spectroscopy [37]. Furthermore, AgNPs illustrate a narrower plasmon resonance band in the visible range than AuNPs do, at around 400 nm [38]. Hence, a colorimetric method based on AgNPs is a potential alternative approach for the determination of Hcy levels, but this approach has not yet been evaluated.

In this paper, we report the first use of AgNPs for the rapid, simple, and selective determination of Hcy based upon aggregation kinetics. Under optimum conditions, the red-shifted band resulting from Hcy-induced aggregation of AgNPs was observed at 525 nm,

whereas Cys gave no significant wavelength shift. Furthermore, the current AgNP-based method was successfully applied for the actual determination of Hcy levels in biological human plasma samples, where the experimentally determined levels were within the error range of the levels measured for the same samples using the traditional clinical diagnostic chemiluminescence microparticle immunoassay (CMIA).

3.2 Experimental

3.2.1 Chemicals

Hcy, glutathione (GSH), and tris(2-carboxyethyl)phosphine (TCEP) were purchased from Sigma-Aldrich (Steinheim, Germany). Cys, methionine (Met), histidine (His), and alanine (Ala) were obtained from KASEI (TCI, Tokyo, Japan). Trichloroacetic acid (TCA), sodium chloride, and disodium hydrogen phosphate were purchased from Merck (Darmstadt, Germany). Ethylenediaminetetraacetic acid (EDTA) and potassium chloride were obtained from Fluka (Buchs, Switzerland) and Univar (New South Wales, Australia), respectively. Potassium dihydrogen phosphate was acquired from BDH laboratory supplies (Poole, England). AgNPs, prepared following the reported procedure [39], were obtained from the Sensor Research Unit at the Department of Chemistry, Faculty of Science, Chulalongkorn University. All reagents were of analytical grade, and water purification was conducted using a Millipore Milli-Q purification system throughout this experiment.

3.2.2 Apparatus

AgNPs were suspended in water at 10 - 40 ppm as indicated, and the UV-vis spectra were recorded in a quartz cuvette using a UV-vis spectrophotometer (UV-vis 2401 PC, Shimadzu). Transmission electron microscopy (TEM) was performed with a JEM-2100

(JEOL, Japan) microscope operating at 200 kV. A tabletop centrifuge (4000 Kubota) was used for sample preparation.

3.2.3 Detection of Hcy levels

Aqueous solutions of each amino acid were freshly prepared before use. A stock solution of Hcy (10 mM) was prepared in 1 M phosphate buffer saline (PBS, pH 7.4), and the working solutions of Hcy were prepared by serial dilution of the stock solution with PBS. One thousand microliters of each working solution was added to 1000 µL of a suspension of AgNPs within the range of 10 - 40 ppm, from which the optimal concentration was selected (20 ppm; see results) and was used thereafter. The UV-vis absorption spectrum of each AgNP suspension was recorded as detailed above at the indicated time (range 0 - 60 min) after mixing. Consequently, the calibration standard solutions (0 -12 □M) were equilibrated for the optimum incubation time (1 min; see results). To investigate the selectivity of AgNPs for Hcy, five different amino acids (Cys, GSH, Met, Ala and His) were assayed as individual solutions. The difference in the kinetics between the Hcy/AgNPs and Cys/AgNPs interactions was observed by plotting the absorbance at 525 nm *vs.* time.

3.2.4 Characterization of Hcy-induced aggregation of AgNPs

AgNP preparations with different mean sizes were obtained from the Sensor Research Unit at the Department of Chemistry, Faculty of Science, Chulalongkorn University. The actual shapes, particle size distributions, and absorbance spectra of the AgNPs with nominal mean diameters of 10, 30, 35, 50 and 60 nm were studied using TEM (shape and size) and UV-vis spectroscopy (absorbance), respectively. For the TEM characterization of AgNP aggregation, AgNPs and Hcy were mixed at 20 ppm and 10 µM final concentrations, respectively, and after 1 min, a drop of the colloidal suspension was placed on a carbon-coated copper grid, dried at room temperature and operated as described in section 2.2.

3.2.5 Sample preparation

Fresh human blood samples (2.0 mL) to which EDTA had been added were obtained from volunteers of the local hospital and centrifuged at 4000 rpm for 10 min. The supernatant, which contained proteins and amino acids amongst other components, was used as the source of the plasma. For the reduction of disulfides, TCEP (100 g/L) was added to the plasma samples, which were then incubated for 30 min at room temperature. The interference of proteins and other substances in the plasma was removed by adding 900 μL TCA (100% (w/v)) containing 1 mM EDTA [40]. The sample was mixed immediately and centrifuged at 4000 rpm for 10 min. The supernatant, which contained Hcy and other components including other amino acids, was used for further analysis, and the unknown amount of Hcy was estimated. The CMIA was performed as a validation method.

3.3 Results and discussion

3.3.1 Aggregation of AgNPs induced by Hcy

The most attractive colorimetric sensors are based on the aggregation of metal NPs, typically AuNPs, due to the high molar absorptivity of the color changes resulting from aggregation, these molar absorptivities are several orders of magnitude greater than those of traditional organic chromophores. Metal NPs are also favored because of their simplicity and biocompatibility. AuNPs have been applied for the determination of the level of aminothiol compounds because of their strong affinity for amino and sulfur compounds.

Unfortunately, AuNPs require surface modifications to achieve selective cross-linking (and thus aggregation) between the sulfur-containing amino group (aminothiols) and the amino group. AgNPs are, therefore, an alternative source of NPs for colorimetric sensors because they do not require such surface premodification. In spite of this advantage, the practical application of AgNP aggregation for Hcy and Cys colorimetric detection remains

almost unexplored. Only one published paper has reported the selective determination of Cys using triangular AgNP aggregation without surface modification. Therefore, we first studied the effect of the size of the AgNPs on aggregation and the absorbance wavelength shift in the presence of Hcy using AgNPs with nominal diameters of 10, 30, 35, 50 and 60 nm. TEM evaluation of each AgNP preparation confirmed the different diameters of the AgNPs (Fig. 1).

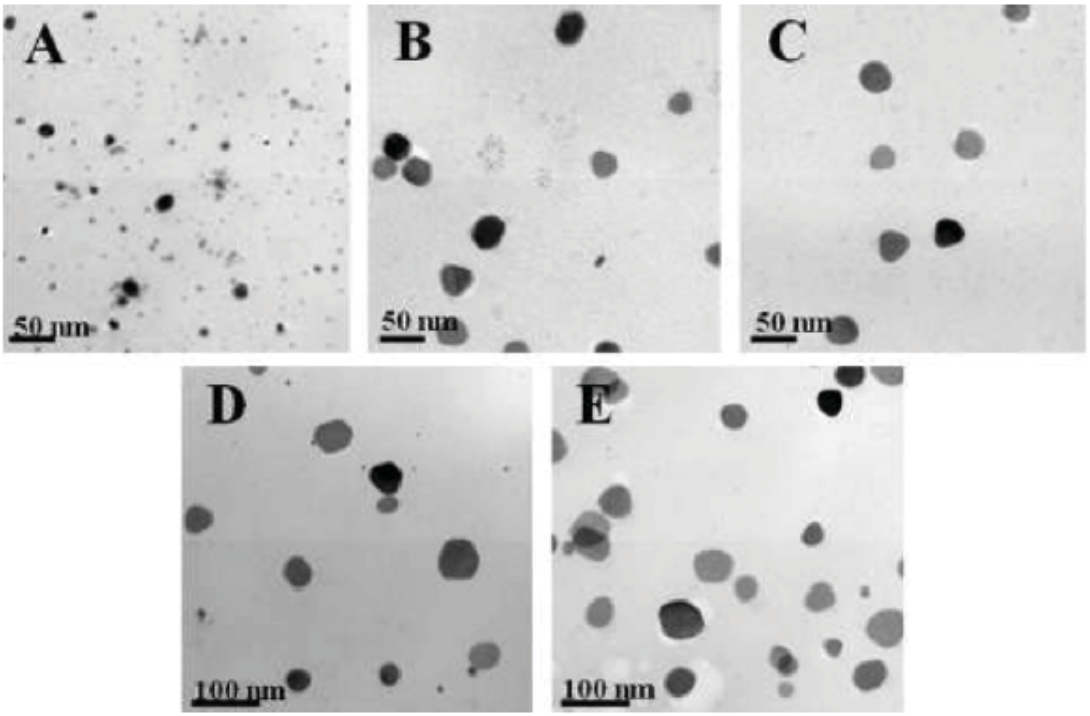

Figure 3.1 TEM images of AgNPs with nominal average diameters of (A) 10 nm, (B) 30 nm, (C) 35 nm, (D) 50 nm and (E) 60 nm.

The UV-vis spectra of the AgNPs varied with the AgNP size, with absorbance wavelength peaks at 400, 500, 520, 550 and 600 nm for 10, 30, 35, 50 and 60 nm diameter AgNPs, respectively (Fig. 2), these peaks are ascribed to the surface plasmon absorption of AgNPs. These wavelength changes were also visually detectable as color changes of the

AgNP suspensions from yellow (10 nm diameter AgNPs) through orange and purple to light blue (60 nm diameter AgNPs), as shown in Fig. 2.

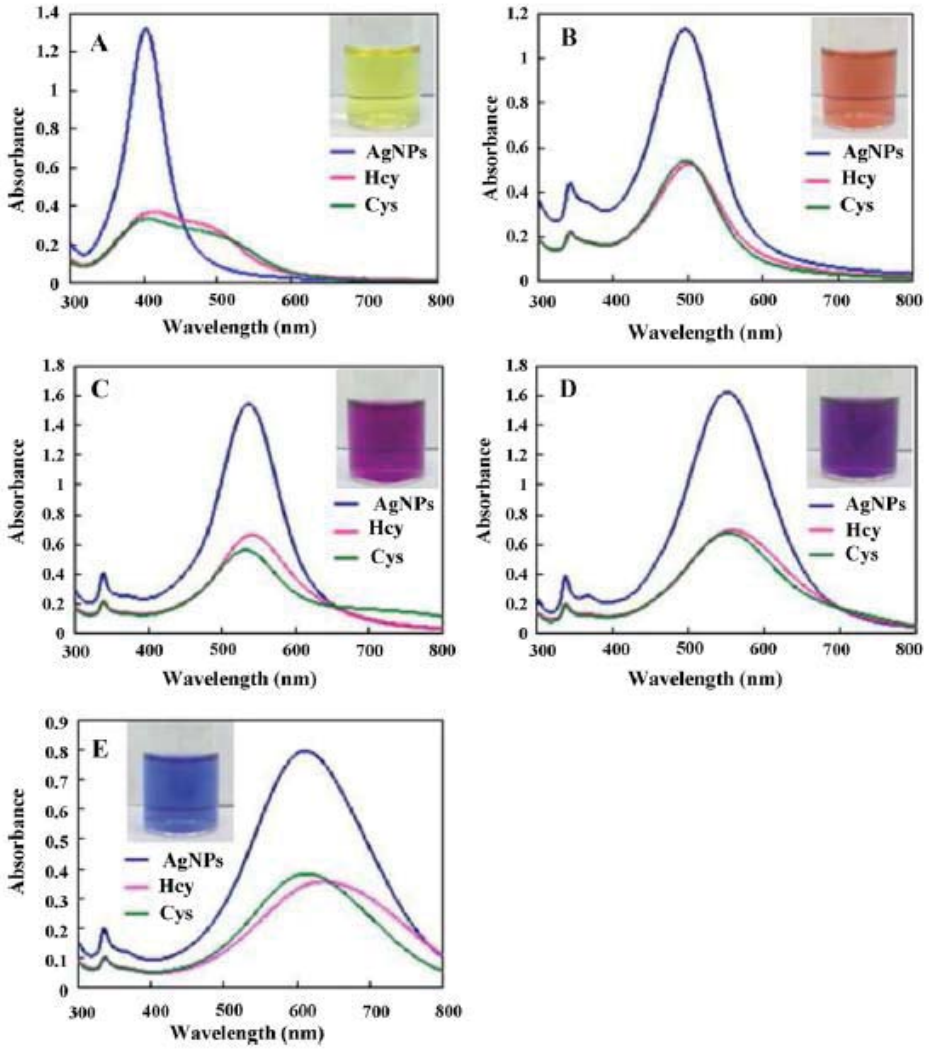

Figure 3.2 UV-vis spectra of AgNPs with nominal average diameters of (A) 10 nm, (B) 30 nm, (C) 35 nm, (D) 50 nm and (E) 60 nm, and the same sized AgNPs after incubation with 10 μM of either Hcy or Cys for 1 min. The inserts display the visible color of each AgNP suspension.

Although a new absorption peak appeared at a longer wavelength (~525 nm), and a visible color change from yellow to red occurred with the 10 nm diameter AgNPs after the addition of Hcy or Cys, no significant difference was noted with the larger-sized (30 – 60 nm diameter) AgNPs. This change in color and shift of the wavelength suggests that the average

particle size of the NPs increased, the aggregate size increased or there was shorter inter-particle spacing [41]. However, the absorption peaks of Hcy and Cys at the new peak of 525 nm were essentially indistinguishable and thus not useful for the diagnostic detection of Hcy in plasma samples. Therefore, 10 nm diameter AgNPs were selected as the optimal size and were used in further experiments to optimize the resolution of the system.

To confirm the mechanism of the interaction between Hcy and 10 nm AgNPs, the AgNPs were examined by TEM. Representative micrographs of 10 nm AgNPs in the presence of Hcy are shown in Fig. 3 and clearly show the aggregation of AgNPs in the presence of Hcy. The aggregation and change in the size and shape of AuNPs induced by Cys has been reported previously [42, 43].

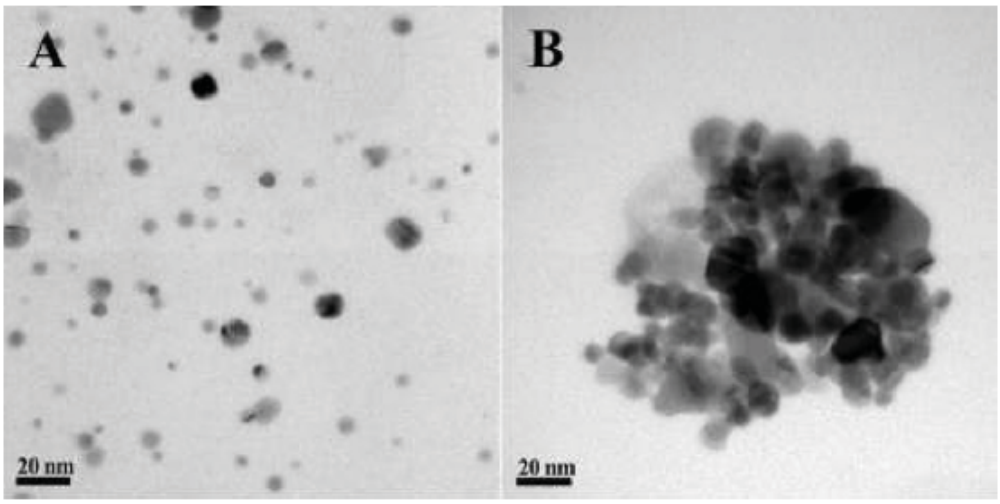

Figure 3.3 TEM images of 10 nm AgNPs after incubation for 1 min in (A) the absence or (B) the presence of 10 μM Hcy.

3.3.2 Selectivity of AgNPs for Hcy

The ability to determine Hcy levels in human plasma samples is of interest because the level of Hcy in biological samples is associated with many diseases. The selectivity of AgNP-based colorimetric sensors is directly affected by the assay conditions, such as the

concentration of the AgNPs and the reaction time. Because Cys, which is found in plasma samples, has the structure most similar to that of Hcy, the assay conditions were first optimized in terms of the AgNPs concentration and the reaction time with respect to the ability to distinguish between Hcy and Cys. The aggregation of different concentrations of AgNPs with 10 μM Hcy and Cys was investigated using absorption spectra in Fig. 4. The difference between the absorption bands at 525 nm for Hcy and Cys was insignificant at the AgNP concentration of 10 ppm (Fig. 4A). Although the absorbance at 525 nm of Hcy at 30 and 40 ppm AgNPs were higher than those of Cys, their peaks were ambiguous (Fig. 4C and 4D). The absorbance at 525 nm of 20 ppm AgNPs in the presence of Hcy was remarkably higher than that for Cys, as shown in Fig. 4B. Thus, 20 ppm AgNPs was selected as the optimum concentration for the selective detection of Hcy.

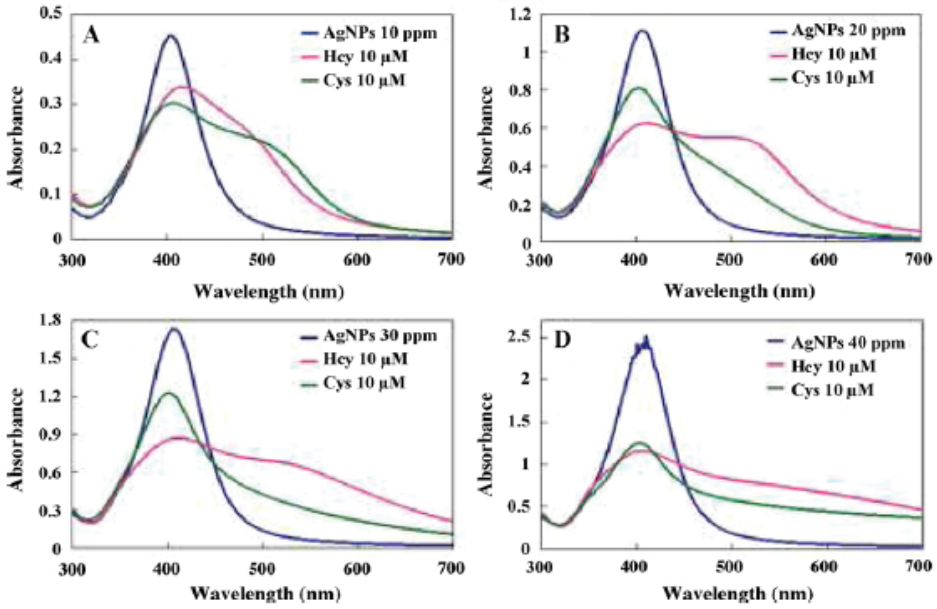

Figure 3.4 UV-vis spectra of 10 nm diameter AgNPs (yellow suspension), at AgNP concentrations of (A) 10 ppm, (B) 20 ppm, (C) 30 ppm and (D) 40 ppm, after a 1 min incubation with or without 10 μM of either Hcy or Cys.

The incubation time between AgNPs and either Hcy or Cys also lead to a different response in terms of the change in the optical spectra. The kinetic distinction between Hcy

and Cys, which is the difference in the speed of the spectral evolution between these two amino acids, was observed by plotting the absorbance at 525 nm *vs.* time (Fig. 4). The Hcy-induced aggregation of AgNPs was found to be much faster than that induced by Cys. The aggregation may involve cross-linking, where Hcy or Cys act as cross-linking agents to link AgNPs together through hydrogen bonding, electrostatic interactions [16, 41, 44], van der Waals forces [45], or a mixture of any of these forces. Regardless of the interaction mechanism, the results are in accord with those reported in the literature, which show that the cross-linking rate of AuNPs with Hcy is much faster than that with Cys [16, 45]. These results clearly show that the difference in the AgNP cross-linking rates for Hcy and Cys can be employed in the selective determination of Hcy concentrations. The absorption spectra of the 10 nm diameter AgNPs (20 ppm) in the presence of 10 μM Hcy or Cys revealed an increased absorbance at 525 nm over time, with a decreased absorbance at 400 nm over the same time scale. The aggregation of AgNPs induced by Hcy showed the new absorption peak at 525 nm after only 1 min of incubation, in contrast to that with Cys (Fig. 5). In other words, no absorption peak at 525 nm appeared after the addition of Cys to AgNPs at 1 min. The inset in Fig. 4 shows the absorbance at 525 nm of AgNPs in the presence of Hcy and Cys as a function of the incubation time, which clearly shows that the potential selectivity for the detection of Hcy over Cys is optimal at an incubation time of 1 min with AgNPs and decreases thereafter.

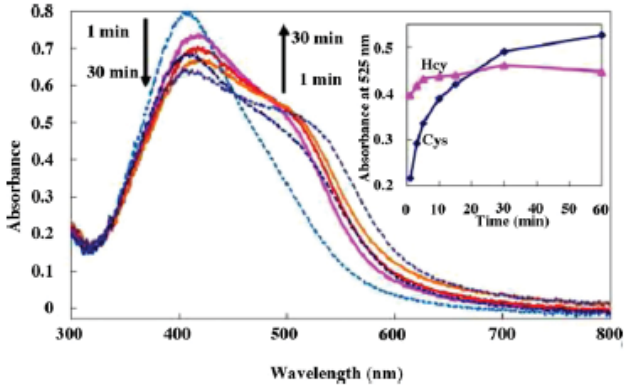

Figure 3.5 UV-vis spectra of 10 nm diameter AgNPs (20 ppm), with or without the addition of 10 μM of either Hcy (solid line) or Cys (dash line) and incubated for the indicated times (1, 10 and 30 min). Inset: the kinetics for Hcy-AgNPs and Cys-AgNPs obtained by monitoring the absorption peak at 525 nm at 1, 3, 5, 10, 15, 30 and 60 min.

To further investigate the apparent selectivity of AgNPs for Hcy, four other amino acids (Met, Ala, GSH and His), along with Cys, were evaluated by monitoring the absorbance at 525 nm in the presence of 10 nm diameter AgNPs (20 ppm). The concentration of Hcy was 10 μM, and the concentration of the other five amino acids was 10 times greater than that of Hcy (100 μM), which is far greater than the levels found in biological samples such as plasma. Upon the addition of the different amino acids to AgNPs, an absorbance shift to 525 nm occurred, but the shift for Hcy was much higher than that of the other amino acids (Fig. 6) despite the great excess molar levels of these other amino acids relative to that found in human plasma samples. This was especially relevant for Cys, as Cys is structurally similar to Hcy. Therefore, Hcy could be distinguished from the other amino acids including Cys using this method.

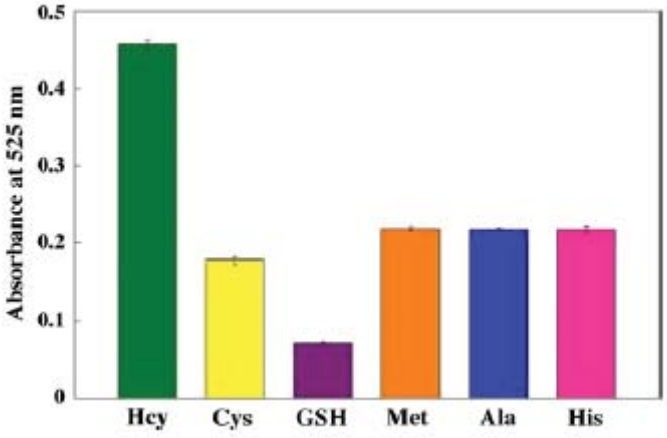

Figure 3.6 Selectivity of 10 nm diameter AgNPs (20 ppm) for 10 μM Hcy and five other amino acids, each at 100 μM. Data are shown as the mean ± SD and were derived from three replicates.

3.3.3 Analytical performance

As the previous results suggested that Hcy could induce the aggregation of 10 nm diameter AgNPs, we expected that AgNPs could be used to quantitatively determine Hcy levels, which is a biologically important analyte. The UV-vis spectra of AgNPs with different concentrations of Hcy were monitored under the optimal conditions (see above) of 1 min incubation time and 20 ppm of 10 nm diameter AgNPs. After the addition of different amounts of Hcy (2 - 12 μM) to the solution of AgNPs, the absorbance at 525 nm was plotted against the concentration of Hcy. This plot was found to be linear within the range of 2 - 12 μM (Fig. 7), with a correlation coefficient (R^2) of 0.9936. The detection and quantification limit (LOD and LOQ), that is the levels which produced the signal at three and ten times, respectively, of the standard deviation of a blank signal (n = 10), were 0.5 μM and 1.7 μM, respectively. Although both the LOD and LOQ values of this method reported here are slightly higher than those of the previously reported methods based on NP aggregation, the linear range of Hcy using this AgNP-based approach was within the range of normal levels of

Hcy found in plasma (5 - 15 μM). Furthermore, an important advantage of the system presented herein over the previously reported methods is the selective detection of Hcy without the need for complicated surface modification of the NPs. Therefore, this method should be comprehensive for the routine determination of Hcy levels in plasma samples.

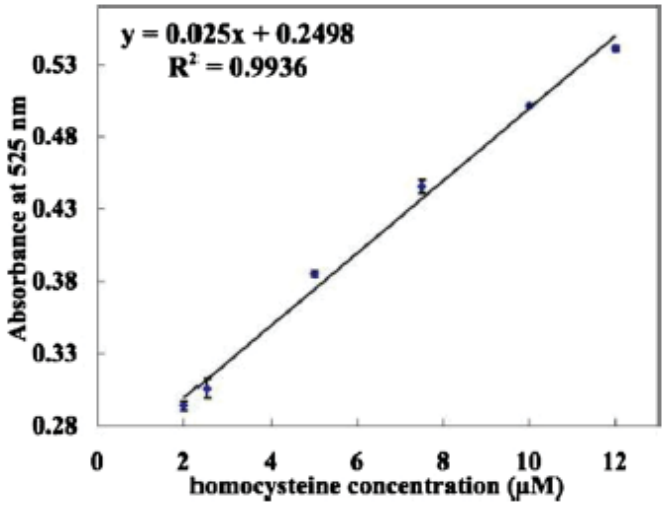

Figure 3.7 The calibration curve between the absorbance at 525 nm and the concentration of Hcy. Ten nanometer diameter AgNPs (20 ppm) were incubated for 1 min with Hcy at the indicated final concentrations before colorimetric detection. The data are shown as the mean ± S.D. and were derived from three replicates. The equation for the best fit linear line and the regression coefficient are shown.

3.3.4 Analytical application in real sample

Having evaluated the selectivity and potential application of this method with pure single analyte solutions, the proposed method was evaluated using a real biological sample, that is, in the presence of other potentially interfering components. Human plasma samples were used for this purpose. The main form of Hcy in plasma is the disulfide form bound to proteins or other thiols [1, 2, 46], which requires reduction prior to detection. After reduction with TCEP, Hcy is free in the plasma. To minimize the effect of proteins and other

substances, deproteination was then performed by standard TCA precipitation as previously described. The unknown amounts of Hcy in three different plasma samples were then determined by both the AgNP-based method reported herein and the standard CMIA method (Table 1). The data were then compared by a paired *t*-test. The levels obtained using the method described in this report were in good agreement with those from the CMIA method, falling within the 95% confidence level.

Table 1 Determination of Hcy levels in human plasma serum samples using 10 nm diameters AgNPs at 200 ppm

Sample	Concentration of Hcy (μM ± SD, $n = 3$)		Paired *t*-test
	CMIA method	Our method	
1	10.10 ± 0.40	10.15 ± 0.01	
2	10.40 ± 0.42	11.22 ± 0.01	−1.01
3	15.40 ± 0.62	15.36 ± 0.01	

Fig. 8 displays the obtained UV-vis spectra of the standard Hcy and the Hcy in human plasma at a similar concentration. The absorption spectra of Hcy in the human plasma sample was almost identical to that of the standard Hcy, showing no significant evidence of any interference from the other components in the biological plasma sample. Therefore, the AgNP-based method outlined here is potentially feasible for use in the reliable determination of Hcy in real biological samples.

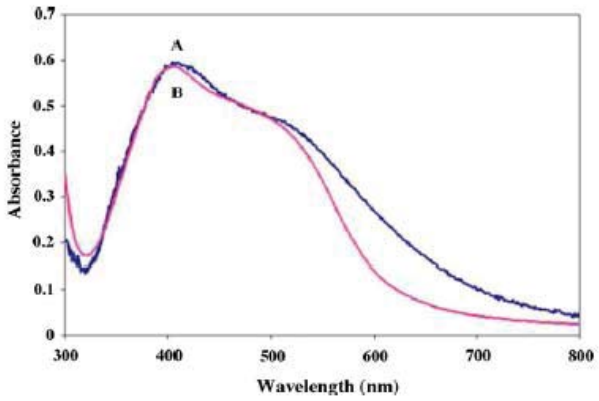

Figure 3.8 UV-vis spectra of 10 nm diameter AgNPs (20 ppm) with the addition of (A) standard 10 μM Hcy and (B) 10 μM Hcy in a normal human plasma sample.

3.4 Summary

A new straightforward approach for the determination of Hcy using AgNPs has been developed. The detection is based on the aggregation of AgNPs, which leads to a shift in the absorption spectrum. Hcy was clearly distinguishable from the other amino acids, including Cys, under the optimum conditions without the need for surface modification of the NPs, attaining good linear detection in the range of 2 - 12 μM. Furthermore, this method was successfully used for the determination of Hcy in human plasma samples and was validated using the CMIA method. This method has great potential for the inexpensive, rapid and simple determination of Hcy concentrations in real biological samples.

3.5 References

[1] H. Refsum, P.M. Ueland, O. Nygard, S.E. Vollset, Annu. Rev. Med. 49 (1998) 31-62.

[2] D. W. Jacobsen, Clin. Chem. 44 (1998) 1833-1843.

[3] S. Seshadri, A. Beiser, J. Selhub, P. F. Jacques, I. H. Rosenberg, R. B. D'Agostino, P. W. F. Wilson, N. Engl. J. Med. 346 (2002) 476-483.

[4] R. P. Steegers-Theunissen, G. H. Boers, F. J. Trijbels, T. K. Eskes, N. Engl. J. Med. 324 (1991) 199-200.

[5] J. B. J. van Meurs, R. A. M. Dhonukshe-Rutten, S. M. F. Pluijm, M. van der Klift, R. de Jonge, J. Lindemans, L. C. P. G. M. de Groot, A. Hofman, J. C. M. Witteman, J. P. T. M. van Leeuwen, M. M. B. Breteler, P. Lips, H. A. P. Pols, A. G. Uitterlinden, N. Engl. J. Med. 20 (2004) 2033-2041.

[6] O. Nekrassova, N. S. Lawrence, R. G. Compton, Talanta 60 (2003) 1085-1095.

[7] Y. F. Huang, H. T. Chang, Anal. Chem. 78 (2006) 1485-1493.

[8] X. N. Cao, J. H. Li, H. H. Xu, L. Lin, Y. Z. Xian, K. Yamamoto, L. T. Jin, Biomed. Chromatogr. 18 (2004) 564-569.

[9] C. Lu, Y. Zu, V. W. W. Yam, J. Chromatogr. A 1163 (2007) 328-332.

[10] G. Chen, L. Zhang, J. Wang, Talanta 64 (2004) 1018-1023.

[11] C. C. Shen, W. L. Tseng, M. M. Hsieh, J. Chromatogr. A 2116 (2009) 288-293.

[12] P. Houze, S. Gamra, I. Madelaine, B. Bousquet, B. Gourmel, J. Clin. Lab. Anal. 15 (2001) 144-153.

[13] K. Amarnath, V. Amarnath, K. Amarnath, H. L. Valentine, W. M. Valentine, Talanta 60 (2003) 1229-1238.

[14] I. Daskalakis, M. D. Lucock, A. Anderson, J. Wild, C. J. Schorah, M. I. Levene, Biomed. Chromatogr. 10 (1996) 205-212.

[15] J. H. Lin, C. W. Chang, W. L. Tseng, Analyst 135 (2010) 104-110.

[16] F. X. Zhang, L. Han, L. B. Israel, J. G. Daras, M. M. Maye, N. K. Ly, C. J. Zhong, Analyst 127 (2002) 462-465.

[17] S. J. Chen, H. T. Chang, Anal. Chem. 76 (2004) 3727-3734.

[18] R. Hong, J. M. Fernandez, H. Nakade, R. Arvizo, T. Emrick, V. M. Rotello, Chem. Commun. (2006) 2347-2349.

[19] I. I. Lim, W. Ip, E. Crew, P. N. Njoki, D. Mott, C. J. Zhong, Y. Pan and S. Zhou, Langmuir 23 (2007) 826-833.

[20] I. I. Lim, D. Mott, M. H. Engelhard, Y. Pan, S. Kamodia, J. Luo, P. N. Njoki, S. Zhou, L. Wang, C. J. Zhong, Anal. Chem. 81 (2009) 689-698.

[21] J. Liu, Y. Lu, Angew. Chem. Int. Ed. 45 (2006) 90–94.

[22] N.C. Tansil, Z. Gao, Nano Today 1 (2006) 28–37.

[23] P.K. Sudeep, S.T.S. Joseph, K.G. Thomas, J. Am. Chem. Soc. 127 (2005) 6516–6517.

[24] S. Zhang, X. Kou, Z. Yang, Q. Shi, G.D. Stucky, L. Sun, J. Wang, C. Yan, Chem. Commun. (2007) 1816–1818.

[25] L. Han, J. Luo, N. Kariuki, M.M. Maye, V.W. Jones, C.J. Zhong, Chem. Mater. 15 (2003) 29–37.

[26] W. Zheng, M.M. Maye, F.L. Leibowitz, C.J. Zhong, Anal. Chem. 72 (2000) 2190–2199.

[27] I.I.S. Lim, D. Mott, W. Ip, P.N. Njoki, Y. Pan, S. Zhou, C.J. Zhong, Langmuir 24 (2008) 8857–8863.

[28] Z. Y. Zhong, S. Patskovskyy, P. Bouvrette, J. H. T. Luong, A. Gedanken, J. Phys. Chem. B 108 (2004) 4046-4052.

[29] H.P. Wu, C.C. Huang, T.L. Cheng, W.L. Tseng, Talanta 76 (2008) 347–352.

[30] C. Lu, Y. Zu, V. W. Yam, Anal. Chem. 79 (2007) 666-672.

[31] C. C. Huang, W. L. Tseng, Anal Chem. 80 (2008) 347-352.

[32] J. H. Lin, C. W. Chang, W. L. Tseng, Analyst 135 (2010) 104-110.

[33] Z. Chen, S.L. Luo, C.B. Liu, Q.Y. Cai, Anal. Bioanal. Chem. 395 (2009) 489–494.

[34] X. Wei, L. Qi, J. Tan, R. Liu, F. Wang, Anal. Chim. Acta. 671 (2010) 80-84.

[35] K. Shrivas, H. F. Wu, Rapid Commun. Mass Spectrom. 22 (2008) 2863-2872.

[36] H. Li, Z. Cui, C. Han, Sensor Actuat B-Chem 143 (2009) 87-92.

[37] R. J. Stokes, A. MacAskill, P. J. Lundahl, W. E. Smith, K. Faulds, Graham, D. Small 9 (2007) 1593-1601.

[38] S. H. Choi, Y. P. Zhang, A. Gopalan, K. P. Lee, H. D. Kang, Colloids and Surfaces A: Physicochem. Eng. Aspects 256 (2005) 165–170.

[39] W. Ngeontae, W. Janrungroatsakul, P. Maneewattanapinyo, S. Ekgasit, W. Aeungmaitrepirom, T. Tuntulani, Sensor Actuat. B-Chem. 137 (2009) 320-326.

[40] B. Frick, K. Schröcksnadel, G. Neurauter, B. Wirleitner, E. Artner-Dworzak, D. Fuchs, Clin. Chim. Acta. 331 (2003) 19-23.

[41] Z. Zhong, S. Patskovskyy, P. Bouvrette, J. H. T. Luong, A. Gedanken, J. Phys. Chem. B 108 (2004) 4046-4052.

[42] Z. P. Li, X. R. Duan, C. H. Liu, B. A. Du, Anal. Biochem. 351 (2006) 18-25.

[43] T. Wu, Y. F. Li, C. Z. Huang, Chinese Chem. Lett. 20 (2009) 611-614.

[44] P. K. Sudeep, S. T. S. Joseph, K. G. Thomas, J. Am. Chem. Soc. 127 (2005) 6516-6517.

[45] C. Lu, Y. Zu, Chem. Comm. 37 (2007) 3871-3873.

[46] K. Rasmussen, J. Møller, Ann. Clin. Biochem. 37 (2000) 627-648.

Chapter IV

Simple and rapid colorimetric detection of Hg(II) by a paper-based device using silver nanoplates

4.1 Introduction

Mercury is highly toxic, and mercury exposure has severe adverse effects on human health and the environment. Environmental mercury contamination has several sources, including metal mining, industrial wastes, bleach production, agricultural pesticides, and volcanic activity. Mercury exists in the following three principal forms: elemental or metallic mercury (Hg(0)), ionic mercury salts (Hg(II)) (e.g., mercuric chloride) and organic compounds (e.g., methyl-, dimethyl- and phenyl-mercury) [1]. Because of its solubility in water, which provides a pathway for contaminating large amounts of water, Hg(II) is one of the most common and stable forms of mercury pollution. By this means, Hg(II) can accumulate in vital organs through the food chain and cause severe damage to the brain, nervous system, kidneys, heart and endocrine system [2]. Therefore, it is very important to routinely monitor Hg(II) ion levels in the environment. Due to its high toxicity, the United States Environmental Protection Agency (USEPA) limits mercury in drinking water to 0.002 mg/L [3]. Likewise, 0.005 mg/L is the maximum mercury level permitted by the industrial effluent standards set by the pollutant control department in Thailand [4]. Detection of Hg(II) has been accomplished using a variety of methods, including cold-vapor atomic absorption spectrometry [5-6], cold-vapor inductively coupled plasma mass spectroscopy [7], resonance scattering spectroscopy [8] and atomic fluorescence spectrometry [9-11]. Although these methods provide low limits of detection (LOD), they are sophisticated, time-consuming, high-cost operations that require complicated non-portable equipment and are, consequently,

not suitable for field monitoring. Thus, there is a clear need for a simple, rapid, highly sensitive and selective method for Hg(II) detection in the field.

Because paper-based device methodologies are easy to use, rapidly implemented, inexpensive, and portable [12-14], there has been considerable interest of late in using such methods for environmental and clinical analyses. This kind of paper-based device, which can be used for colorimetric assays, uses a simple fabrication method that creates a hydrophobic wall that contains and/or directs a fluid analyte into the detection area. The wax screen-printing method is a particularly attractive procedure for creating large-volume and moderate-resolution paper-based devices [15]. This method's predominant advantages are its low cost, rapid detection and ease of fabrication as well as the fact that creation of the hydrophobic wall does not require solvent or external processing steps. For these reasons, the present study used the screen-printing method.

Several recent detection studies have utilized noble metallic nanoparticles (NPs), such as gold (Au) or silver (Ag), as colorimetric sensors for the detection of Hg(II). Unfortunately, most of these methods require expensive and complicated chemical syntheses and surface modifications of the NPs using specific sensing materials, such as rhodamine B [16], aptamer [17], thymine [18] L-cysteine [19] oligonucleotides [20], thiol compounds [21] and mercaptopropionic acid [22]. Because of their lower cost compared with gold nanoparticles (AuNPs), the use of silver nanoparticles (AgNPs) in colorimetric sensors has become popular [23,24]. The molar extinction coefficient of AgNPs is also approximately 100-fold greater than that of AuNPs of the same size, resulting in improved visibility (due to the differences in optical brightness) and, therefore, increased sensitivity This work aimed to develop a colorimetric method for the simple and rapid detection of Hg(II) ion levels using AgNPs and Ag nanoplates (AgNPls) on a paper-based device.

4.2 Experimental Section

4.2.1 Chemicals and Materials

Filter paper (No. 1, 125-cm diameter) was obtained from Whatman. Silver nanoparticles (AgNPs) with a diameter of 10 nm and silver nanoplates (AgNPls) with diameters of roughly 30, 35, 45 and 50 nm were obtained from the Sensor Research Unit at the Department of Chemistry, Chulalongkorn University. Syntheses of AgNPs and AgNPls employed a facile method that used starch as the stabilizer without capping agents. Analytical-grade reagents and 18 MΩ cm^{-1} resistance deionized water (obtained from a Millipore Milli-Q purification system) were used throughout. A standard solution of 1000 ppm Hg(II) was purchased from Fluka, Switzerland, and used as the stock solution. The following chemicals were used as received: iron sulfate heptahydrate ($FeSO_4.7H_2O$) (Merck), magnesium sulfate ($MgSO_4$) (Scharlau), nickel sulfate ($NiSO_4$) (Carlo Erba), lead sulfate ($PbSO_4$) (Unilab), cadmium sulfate ($CdSO_4$) (Baker Analyzed), zinc sulfate ($ZnSO_4$) and copper sulfate ($CuSO_4$) (BDH).

4.2.2 Fabrication of Patterned Paper

Paper-based devices were made from filter paper having hydrophobic walls constructed in specific patterns. In the system used herein, the pattern was designed with Adobe Illustrator software (Adobe Systems, Inc.), and the block screen was fabricated by Chaiyaboon (Bangkok, Thailand). Each test zone was comprised of 38 circles, each with a radius of 0.6 cm, per piece of filter paper [Figure 4.1]. It is worth noting that other formats, such as linear strips and even rectangular arrays suitable for automation, can be printed and handled just as effectively. To fabricate the hydrophobic walls, solid wax (purchased from a local stationery store) was rubbed through the finely perforated screen onto the filter paper, after which the printed wax was melted on a hot plate at 100 ºC for 30 seconds to allow the

wax to be absorbed into the paper. When cooled to room temperature, this absorbed wax formed the hydrophobic barrier within the paper.

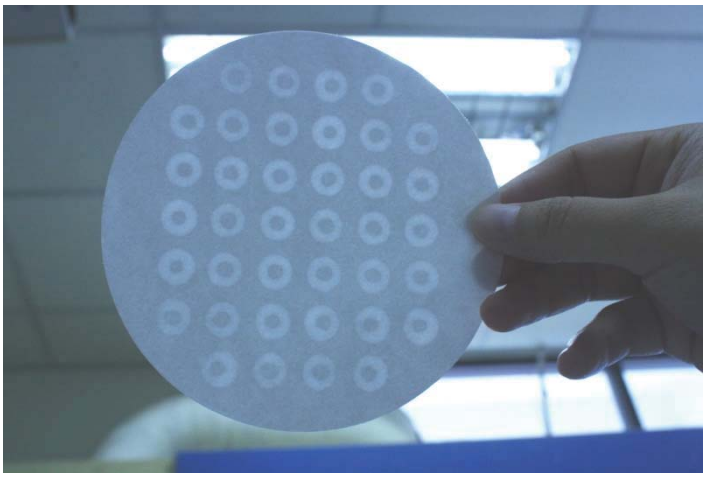

Figure 4.1 The colorimetric paper-based device created using a wax screen-printing method and shown here in a 38-test-zone disc format

4.2.3 Colorimetric measurement of Hg(II)

The absorption spectra of the AgNPs and variously sized AgNPls were obtained with a UV-vis absorption spectrometer (HP HEWLETT PACKARD 8453) following the addition of different concentrations of Hg(II).

4.2.4 Hg(II) detection utilizing the AgNP / AgNPl paper device

A 2 μL suspension of 100 ppm nanosilver (either AgNPs or AgNPls) was applied to the middle of the hydrophilic test spot on the paper-based device. After the suspension of AgNPs or AgNPls was dried, 2 μl of either the test solution or an Hg(II) standard solution (of known concentration) was applied to this test zone. The AgNPs / AgNPls clearly changed color, an observation that could be made with the naked eye, almost immediately after the addition of the Hg(II) solution. An image processing technique was subsequently adopted to

further differentiate the color changes and to improve the method's colorimetric capabilities. To this end, a picture of the paper-based device was taken by a digital camera (Cannon EOS 1000 D1, Japan) in a light control box (OPPLE 8 W daylight lamp). The image was then imported into Adobe Photoshop software, and the color signal in each test zone was measured as the mean color intensity. The readings obtained were used to generate the calibration curve. To improve the sensitivity, after the suspension of AgNPls was dried on the filter paper, various volumes (0-2 μl) of a 500 ppm $CuSO_4$ solution were applied to the test zone. The test or standard solution was then applied to the hydrophilic zone, and the reagents were allowed to react and air dry.

For quantitative analysis, standard reference solutions (with Hg(II) concentrations ranging from 0.1 to 100 ppm) were prepared and applied to the test zone, and, after 45 minutes, digital images were obtained. For each Hg(II) concentration, the signal intensity was measured and used to plot the calibration curve. The limits of detection (LOD) and quantification (LOQ) were calculated using 3 and 10 times the standard deviation of the blank measurements (n = 10), respectively.

The Hg(II) selectivity of this new lab-on-paper method was investigated by comparing the signal intensities obtained for seven other metal ions, As(III), Ni(II), Fe(III), Cu(II), Zn(II), Mg(II), Cd(II) and Pb(II), over a concentration range of 5-500 ppm.

4.2.5 Scanning electron microscopy (SEM)

The reaction between AgNPs or AgNPls and Hg(II) on the paper-based device were further characterized using scanning electron microscopy (SEM). An image was captured after applying the test or standard Hg(II) solution to the test zone. The sample was then prepared by cutting the reaction zone of the paper-based device and attaching it to conductive

adhesive tape. Finally, the prepared sample was splutter coated with gold and analyzed by SEM, and the Ag particle sizes were measured.

4.2.6 Evaluation of Hg(II)levels in real water samples

The drinking water sample (Singha, Singha Corporation) was purchased from a local supermarket, and the tap water sample was collected from a domestic drinking water supply in Bangkok after first discharging the standing tap water for 15 min and then boiling the collected sample for 10 min (to remove chlorine).

4.3 Results and Discussion

4.3.1 Colorimetric detection of Hg(II)

Maximum absorption of the AgNPs that had a mean diameter of 10 nm occurred at approximately 400 nm, whereas the maximum absorption signals of AgNPls having mean diameters of 30, 35, 45 and 50 nm occurred at approximately 500, 525, 550 and 600 nm, respectively. We first evaluated the effects of particle size (for AgNPls vs. AgNPs) on the Hg(II) detection capabilities of the paper-based device. For both AgNPs and AgNPls, the test-area color suddenly changed when Hg(II) was applied. This color change was easily observed with the naked eye for Hg(II) levels above 5 ppm for all AgNPls and AgNPs investigated (Figure 1). When the concentration of Hg(II) was increased from 1 to 25 ppm, the color of the test zone changed from yellow to light yellow for the AgNPs (~10 nm diameter) and from violet to pinkish orange, pinkish violet to pinkish yellow, dark blue to pinkish violet and blue to pinkish blue for the AgNPls with diameters of 30, 35, 45 and 50 nm diameter, respectively. In all cases, the test-area colors faded at Hg(II) levels above 25 ppm and were imperceptible when Hg(II) concentrations approached 100 ppm (Fig. 4.2).

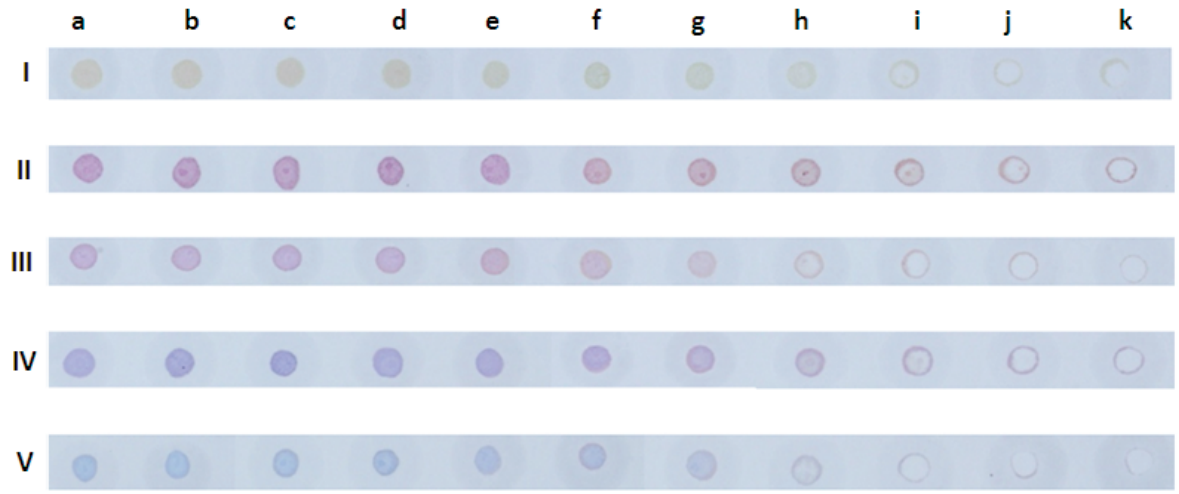

Figure 4.2. Color changes of AgNPs and AgNPls in the presence of Hg(II) at concentrations of (a) 0, (b) 0.01, (c) 0.05, (d) 0.1, (e) 0.5, (f) 1, (g) 5, (h) 10, (i) 25, (j) 50 and (k) 100 ppm with 2.00 μL of a 100 ppm solution of AgNPs (10-nm diameter) or AgNPls with diameters of (II) 30, (III) 35, (IV) 45 and (V) 50 nm. Image shown is representative of those seen in three independent repeats.

Digital images of each test zone were obtained, cropped and analyzed (using Adobe Photoshop software) to determine the mean color intensity value for each Hg(II) concentration tested. Each mean intensity value was then plotted against the concentration of Hg(II). The signal intensity increased with increasing Hg(II) concentrations from 1-100 ppm for the 10-nm AgNPs and 30-nm AgNPls and from 0.5-100 ppm for the larger AgNPls [Fig.4.3]. The curve was essentially linear in the 5-25 ppm range for the AgNPs (correlation coefficient (R^2) = 0.983). Calibration curves were essentially linear in the range of 5-25 ppm (R^2 = 0.998), 5-50 ppm (R^2 = 0.996), 5-25 ppm (R^2 = 0.997) and 5-25 ppm (R^2 = 0.980) for AgNPls with diameters of 30, 35, 45 and 50 nm, respectively.

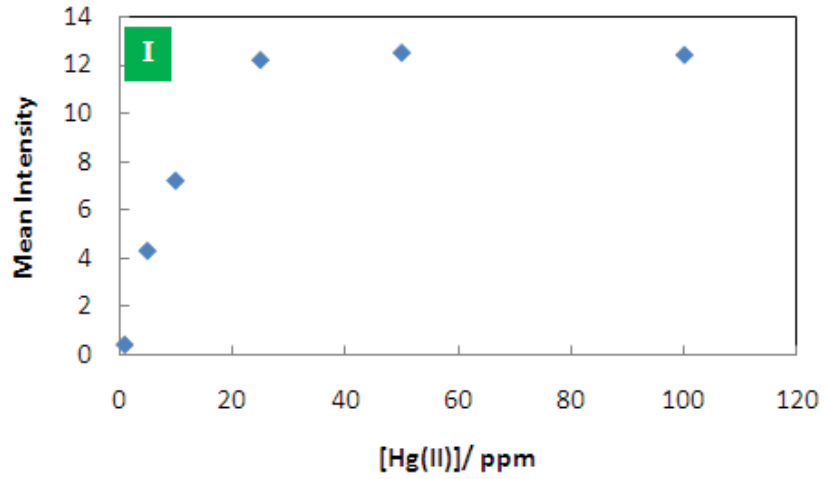
I
Mean Intensity
[Hg(II)]/ ppm
0
2
4
6
8
10
12
14
0
20
40
60
80
100
120

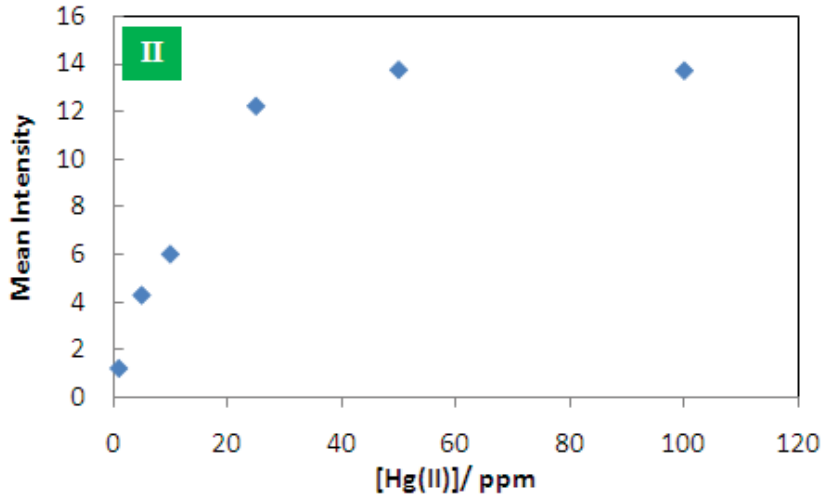
II
Mean Intensity
[Hg(II)]/ ppm
0
2
4
6
8
10
12
14
16
0
20
40
60
80
100
120

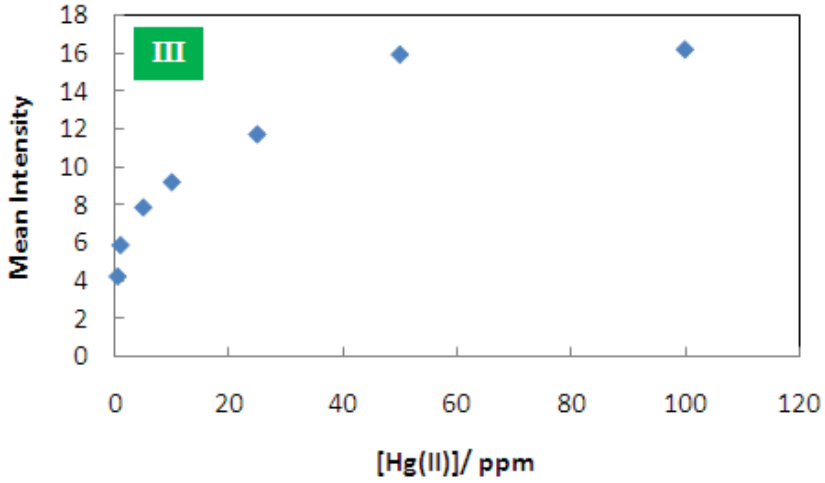
III
Mean Intensity
[Hg(II)]/ ppm
0
2
4
6
8
10
12
14
16
18
0
20
40
60
80
100
120

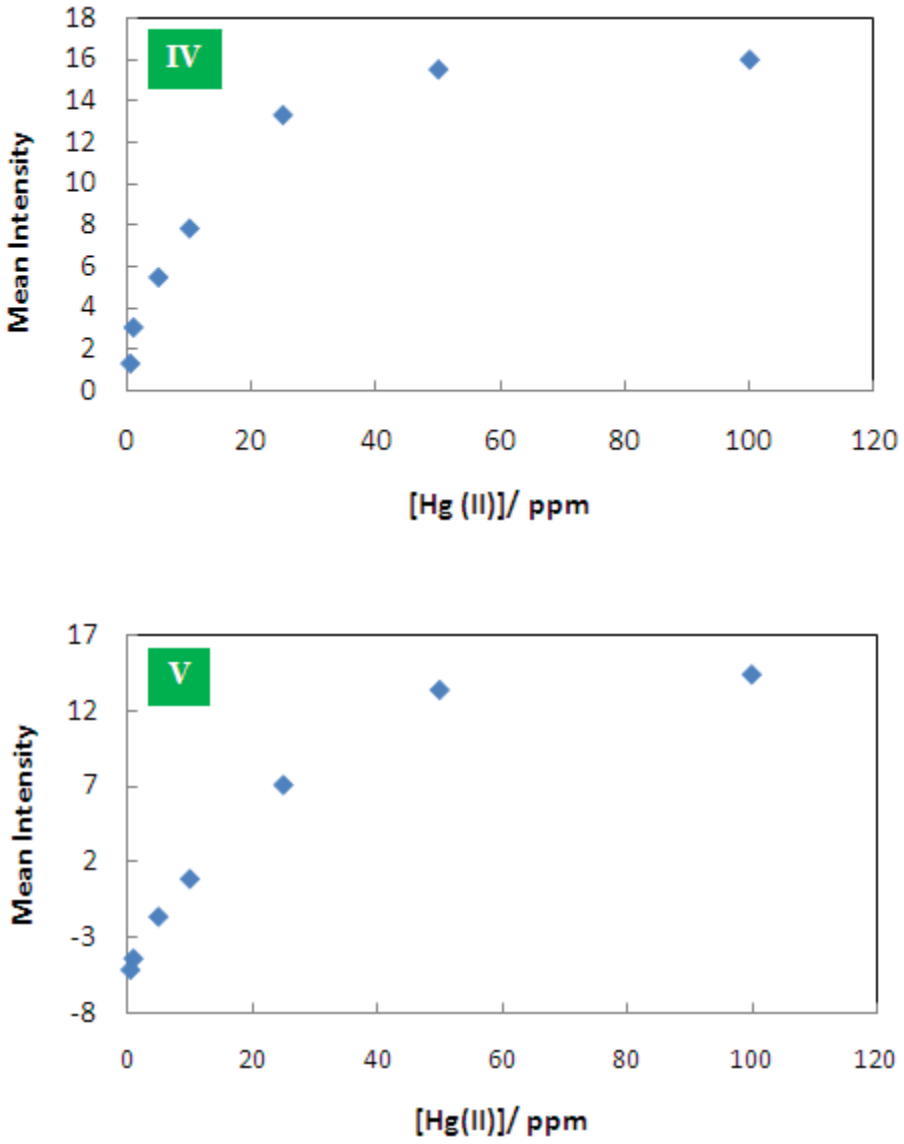

Figure 4.3 Plot of Ag color intensity for the following nanoparticle sizes: (I) 10, (II) 30, (III) 35, (IV) 45 and (V) 50 AgNPls in the presence of different Hg(II) concentrations (1-100 ppm for (I) and (II) and 0.5-100 ppm for (III)-(V)). The color intensity was derived by Adobe Photoshop analysis of digital images of the paper-device(s).

This phenomenon can be attributed to changes in the surface plasmon resonance (SPR) of the NPs / NPls, which is related to their apparent color. The 35 nm (diameter) AgNPls were selected for further evaluation because their color change (in response to Hg(II)) could be easily distinguished by the naked eye and because their Hg(II) calibration curves exhibited the widest linear concentration range.

4.3.2 Characterization of ~35-nm (diameter) AgNPls in the presence of Hg(II)

For characterization *of ~35-nm (diameter) AgNPls in the presence of Hg(II)*, there are two techniques used. The first is spectroscopy (UV-vis) that is used to characterize AgNPls in solution while SEM was used to characterize paper-based devices containing AgNPls. The maximum absorbance of these AgNPls occurred at roughly 525 nm (Fig. 4.4), which could be ascribed to the SPR absorption of the AgNPls. The absorbance of the AgNPls at 525 nm progressively decreased as the concentration of Hg(II) ions increased and was no longer visible at Hg(II) levels above 5 ppm. Concurrently, the absorption peaks continually shifted towards shorter wavelengths with increasing Hg(II) concentrations. The visible color changes and absorption wavelength shifts suggest that the average particle size of the AgNPls decreased as the Hg(II) concentration increased. Additionally, the absorption spectrum of Ag(I), which exhibited an absorption maximum at approximately 300 nm, was clearly observed when the concentration of Hg(II) was higher than 5 ppm, indicating the oxidation of Ag(0) to Ag(I).

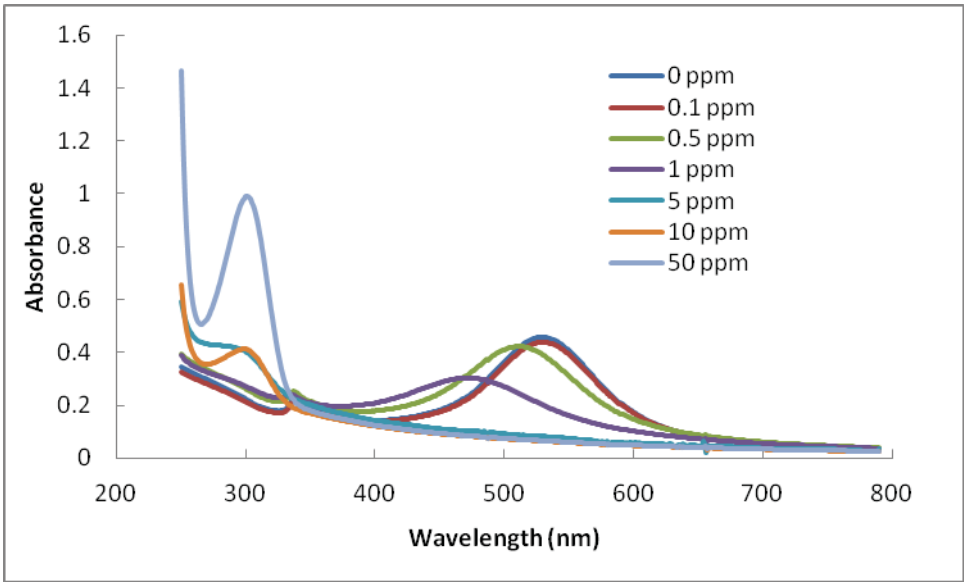

Figure 4.4 The UV-vis spectra of 35 nm diameter AgNPls at 10 ppm after the addition of Hg(II) at different final concentrations.

To verify the interaction between Hg(II) and the AgNPls, the AgNPls were examined by SEM. The resulting SEM images indicate that both the number and the average particle size of the AgNPls decreased after the addition of Hg(II) at 50 ppm (Fig. 4.5). These results are consistent with the observed visible color change(s) and absorption shift(s) reported above. Thus, these phenomena can be ascribed to a redox reaction between the Hg(II) ions and the AgNPls. It appears that the AgNPs were oxidized by Hg(II), resulting in disintegration of the AgNPls into smaller particles, which changed their shape and consequently altered their SPR extinction band(s).

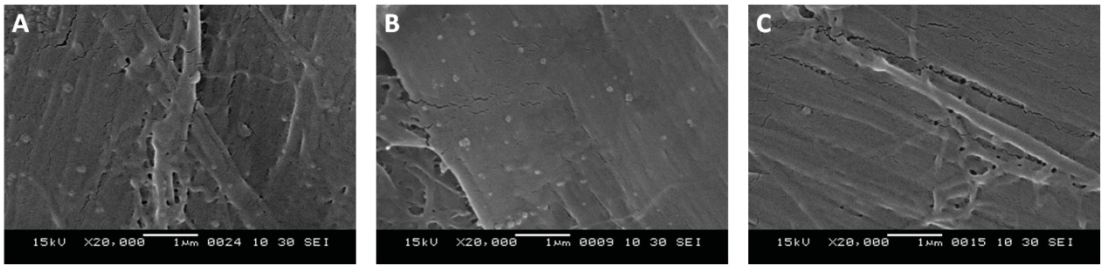

Figure 4.5 Representative SEM images (20,000 x magnification) of the 35 nm diameter AgNPls on the paper disc after exposure to (A) Milli-Q water alone or with the addition of 2 μL of (B) 50 ppm Hg(II) and (C) 50 ppm Hg(II). Micrographs shown are representative of those for at least three such fields of view per sample**.**

4.3.3 Selectivity of the 35 nm (diameter) AgNPls for Hg(II)

The selectivity of the 35 nm (diameter) AgNPls for Hg(II) ions was evaluated by individually testing potentially interfering metal ions, As(III), Ni(II), Fe(III), Cu(II), Zn(II), Mg(II), Cd(II) and Pb(II), at 5-500 ppm. Even at concentrations that were 100 times greater than that of Hg(II) (i.e., 500 ppm) all the other metal ions tested induced no obvious color changes (of the AgNPls, Fig. 4.6A). Furthermore, the more sensitive quantification method using mean color intensity values (of the AgNPls as determined by Adobe Photoshop analysis of digital images) revealed no significant detection of any of the test metal ions for concentrations up to 500 ppm (Fig. 4.6B). Only Hg(II) was found to significantly increase the AgNPl color intensity visualized with the naked eye. This finding is explained by the relatively high standard reduction potential of Hg^{2+} (E^0 $Hg^{2+/}Hg^0$ = 0.85 V) that can readily oxidize Ag^0 to Ag^+. All of the other metal ions tested have lower electrochemical potentials relative to Ag^0, thus, they have no apparent effects on the silver [26].

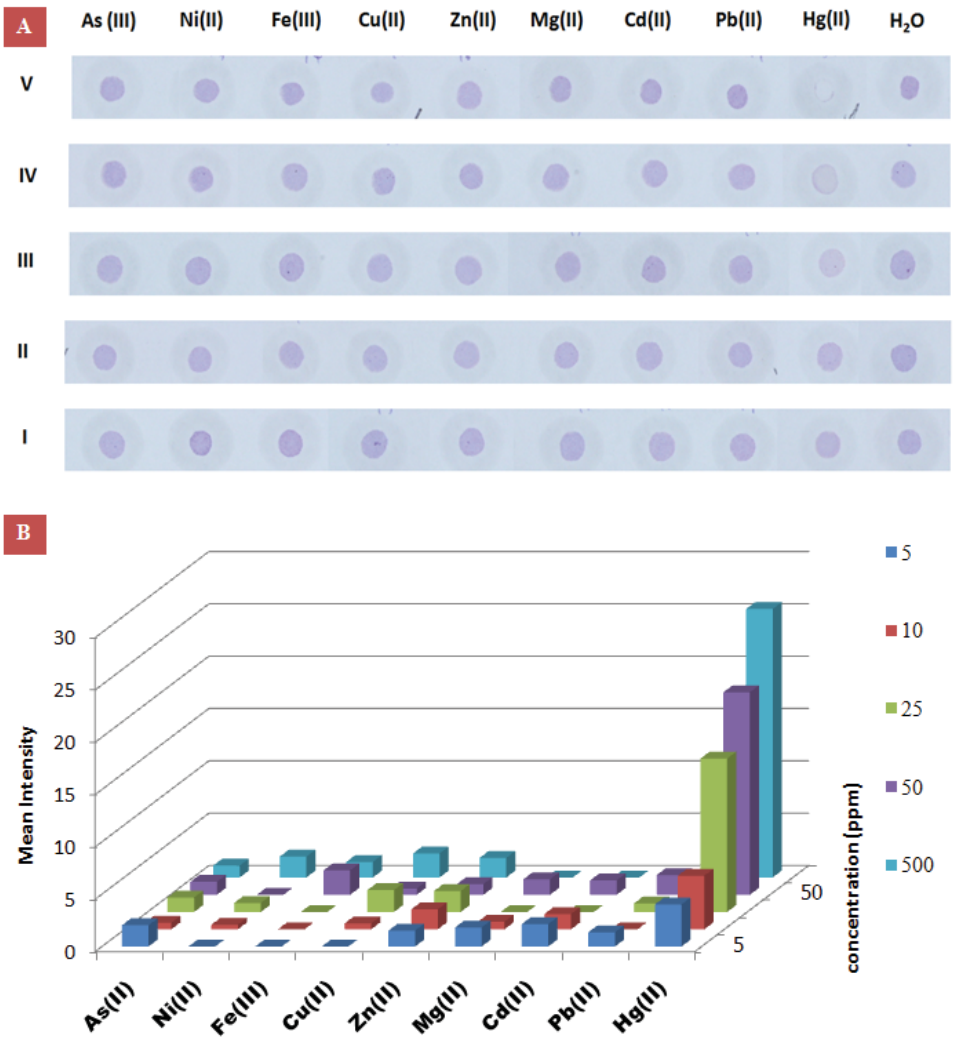

Figure 4.6 Color changes of the 35 nm diameter AgNPls in the presence of the indicated metal ions, added as 2 µL of a (I) 5, (II) 10, (III) 25, (IV) 50, (V) 500 ppm solution. **(A)** A representative visual image of the paper device **(B)** the mean intensity of the AgNPls' color determined by digital-image analysis using Adobe Photoshop.

4.3.4 Effect of copper(II) ions on the Hg(II) detection by AgNPls

It is commonly reported that Copper(II) (Cu(II)) ions interfere with the electrochemical detection of mercury [27]. Moreover, Cu(II) can bind to aminothiol, resulting in the aggregation of AgNPs, which affects the color response [28]. Thus, the effect of Cu(II)

ions on Hg(II) detection was investigated by adding varying amounts (0-2 μL) of a 500-ppm Cu(II) solution to the test zone following the deposition of AgNPls and then assaying the color and intensity of the AgNPls upon application of Hg(II) in the range of 0.1-25 ppm. The results show that, for the same amount of Hg(II) applied, the color intensity of the test zone gradually increased with increasing amounts of added Cu(II) solution up to 1 μL, after which the response remained steady [Fig. 4.7]. Thus, the addition of 1 μL of 500ppm Cu(II) was adopted for further experiments. This represents a 4.24 mole excess of Cu(II) to Ag(0) and a 9.5-190 mole excess of Cu(II) to Hg(II) for Hg(II) solutions of 5-100 ppm.

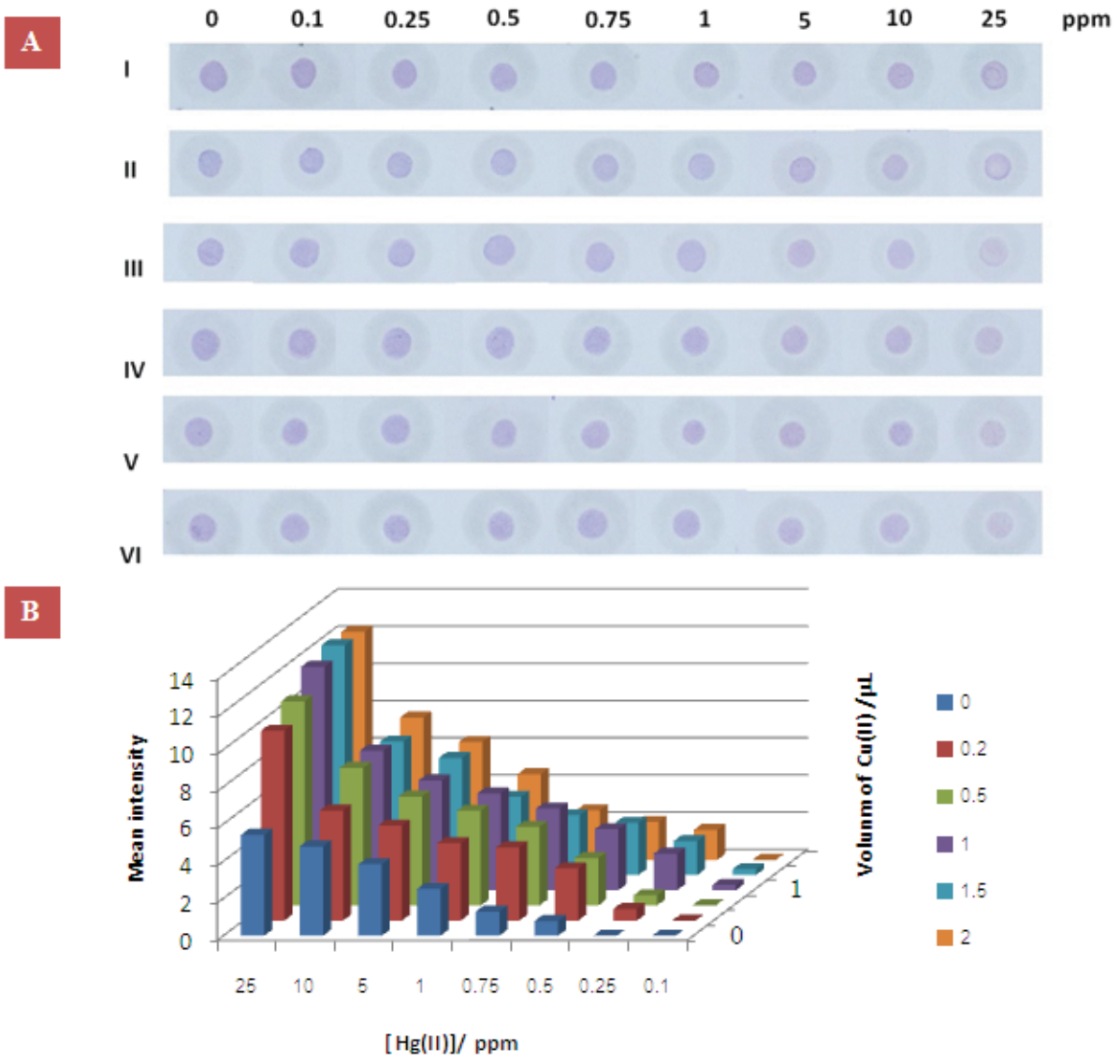

Figure 4.7 Effect of the added amount of Cu(II) (0-2 μL of a 500 ppm solution) on the signal obtained with 35 nm diameter AgNPls in the presence of the indicated Hg(II) concentrations. **(A)** A representative visual image of the paper device from three independent repeats, where the volume of added 500 ppm Cu(II) is designated as (I) 0, (II) 0.2, (III) 0.5, (IV) 1, (V) 1.5 and (VI) 2 μL; **(B)** the mean intensity of the AgNPls' color determined by digital-image analysis using Adobe Photoshop, derived from three independent repeats.

Subsequently, the effect of Hg(II) detection with or without Cu(II) (1 μL of 500 ppm) was compared. The mean color intensity of the AgNPls in the presence of Hg(II) ions was significantly greater in the presence of Cu(II) than in the absence of Cu(II), and the LOD in the presence of Cu(II) was reduced such that a 0.1ppm solution of Hg(II) could be readily detected (Figure 5). Despite the significant improvement in the analytical signal obtained in the presence of Cu(II), there were no significant changes in the color/shade of the AgNPls observed for each concentration of Hg(II) (Fig. 4.8).

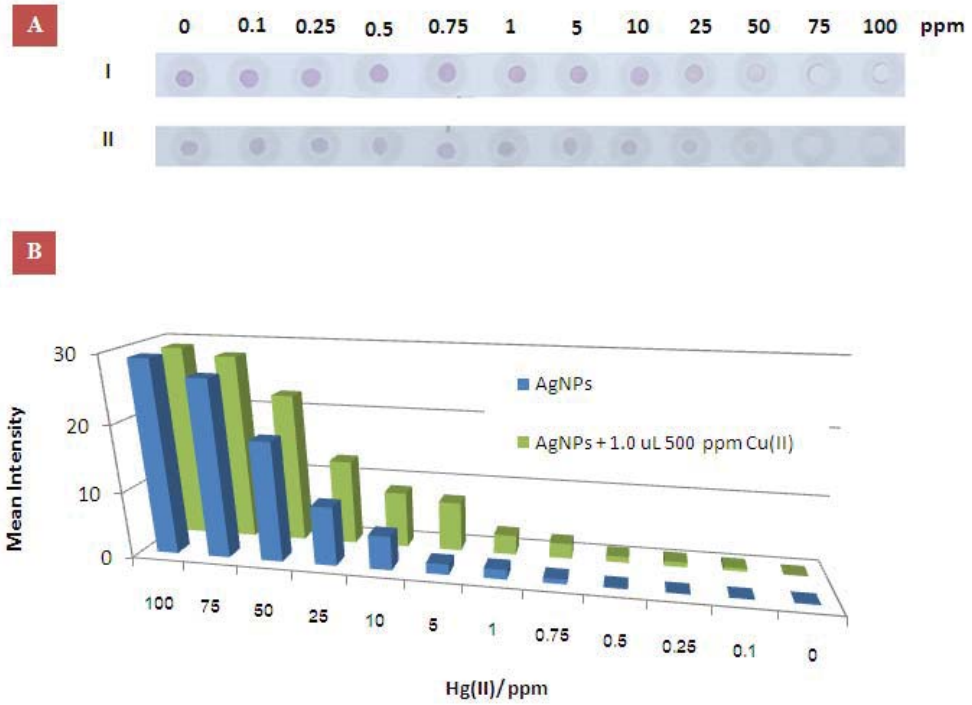

Figure 4.8 Comparison of the color change of the 35 nm diameter AgNPls after the addition of 2 μL of Hg(II) at the indicated concentrations with or without the prior addition of 1 μL of 500 ppm Cu(II). **(A)** A representative visual image of the paper device (I) with or (II) without the addition of Cu(II)**(B)** the mean intensity of the AgNPls' color determined by digital-image analysis using Adobe Photoshop.

The effect of Cu(II) on the AgNPs-Hg(II) interaction was evaluated by SEM, which revealed that the particle size (mean diameter) of the AgNPls in the presence of Cu(II) was similar to that seen in the absence of Cu(II) [Fig. 4.9]. However, in the presence of Cu(II), the average particle size of the AgNPls decreased upon addition of Hg(II), and the number of AgNPls was reduced to a greater extent (compared with results obtained in the absence of Cu(II)). Enhancement of the color signal may be due to the catalytic effect of Cu(II) on the redox reaction of Hg(II) with AgNPls to form Ag(I).

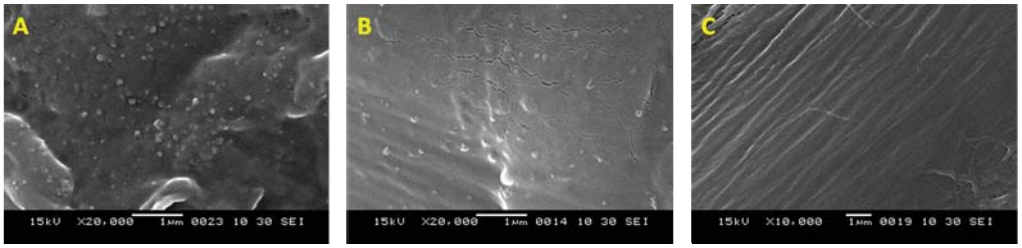

Figure 4.9 Representative SEM images (20,000 X magnification) of the 35 nm diameter AgNPls in Milli-Q water with **(A)** 0.1 μL of 500 ppm Cu(II), **(B)** 0.1 μL of 500 ppm Cu(II) plus 2 μL of a 50 ppm solution of Hg(II) and **(C)** 2 μL of a 50 ppm solution of Hg(II). Micrographs shown are representative of those seen in at least three such fields of view per sample.

4.3.5 Calibration curve of Hg(II) detection by the 35-nm (diameter) AgNPls

A calibration curve was obtained by plotting the mean color intensity values (recorded from the Adobe Photoshop software analysis) versus the standard Hg(II) concentrations in the range of 0-100 ppm (Fig. 4.10). Reasonable linearity was obtained in the range of 5-75 ppm (R^2 = 0.991), with a LOD and LOQ of 0.12 ppm and 3.9 ppm, respectively. Clearly, the LOD requires enhancement for Hg(II) detection in real samples.

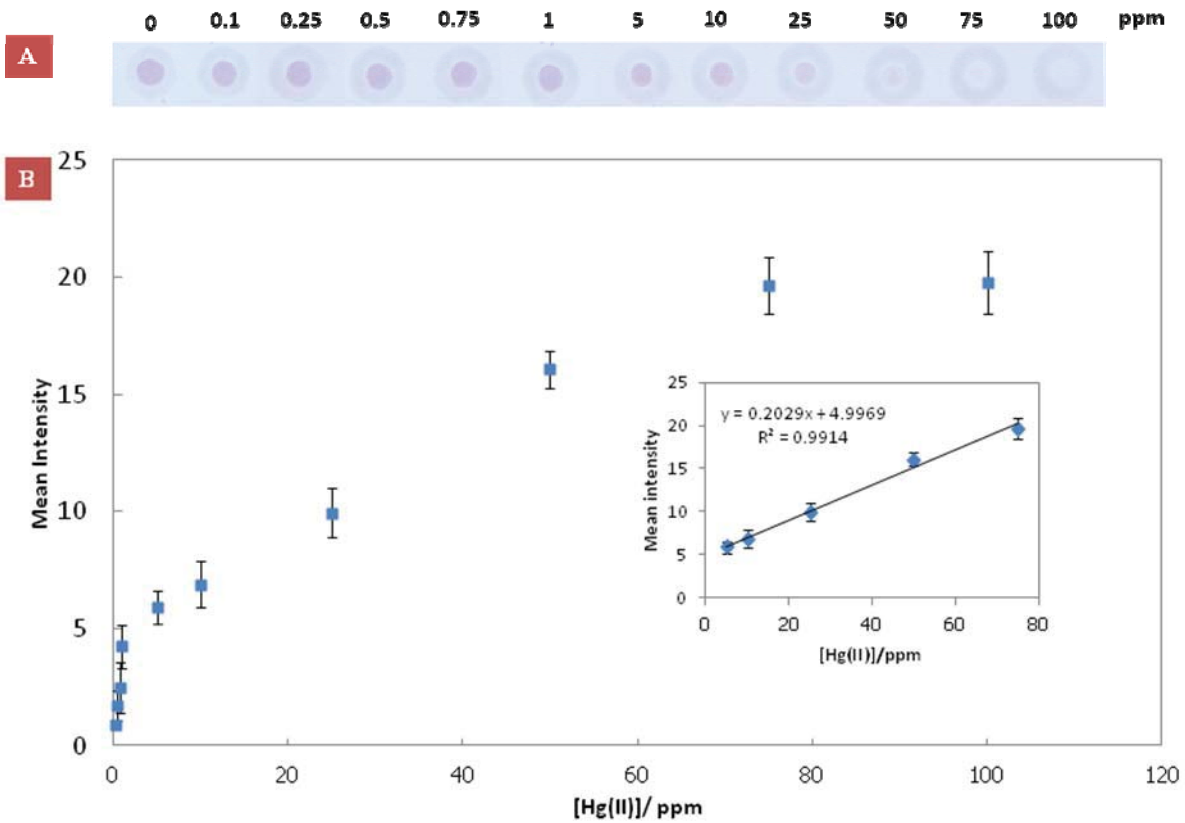

Figure 4.10 Detection of Hg(II) in the range of 0-100 ppm in the presence of 1 μL of 500 ppm Cu(II) (applied in the preparation step). **(A)** A representative visual image of the paper device from three independent repeats; **(B)** the mean intensity of the AgNPls' color determined by digital-image analysis using Adobe Photoshop, plotted as an Hg(II) calibration curve. (Inset) Linear regression analysis and best fit line in the 5-75-ppm Hg(II) concentration range.

4.3.6 Pre-concentration of samples (multiple applications)

One advantage of lab-on-paper devices is that analyte pre-concentration, which enhances the signal intensity, can be easily obtained via multiple applications of the analyte sample to the test zone. Solutions containing less than 0.5 ppm Hg(II) can be readily determined using this pre-concentration scheme. For example, the method used in this study is clearly able to detect 50, 5 and 2 applications of 2 µL of 0.2, 2 and 5 ppm Hg(II) solutions, all of which resulted in signal intensities more or less equivalent to that obtained with a single 2µL application of 10ppm Hg(II) solution [Fig. 4.11]. The pre-concentration results show a percent recovery in the range of 95 to 114% and a reduction in the LOD to 0.2 ppb Hg(II), which makes the technique more applicable to real samples and use in the field of environmental science.

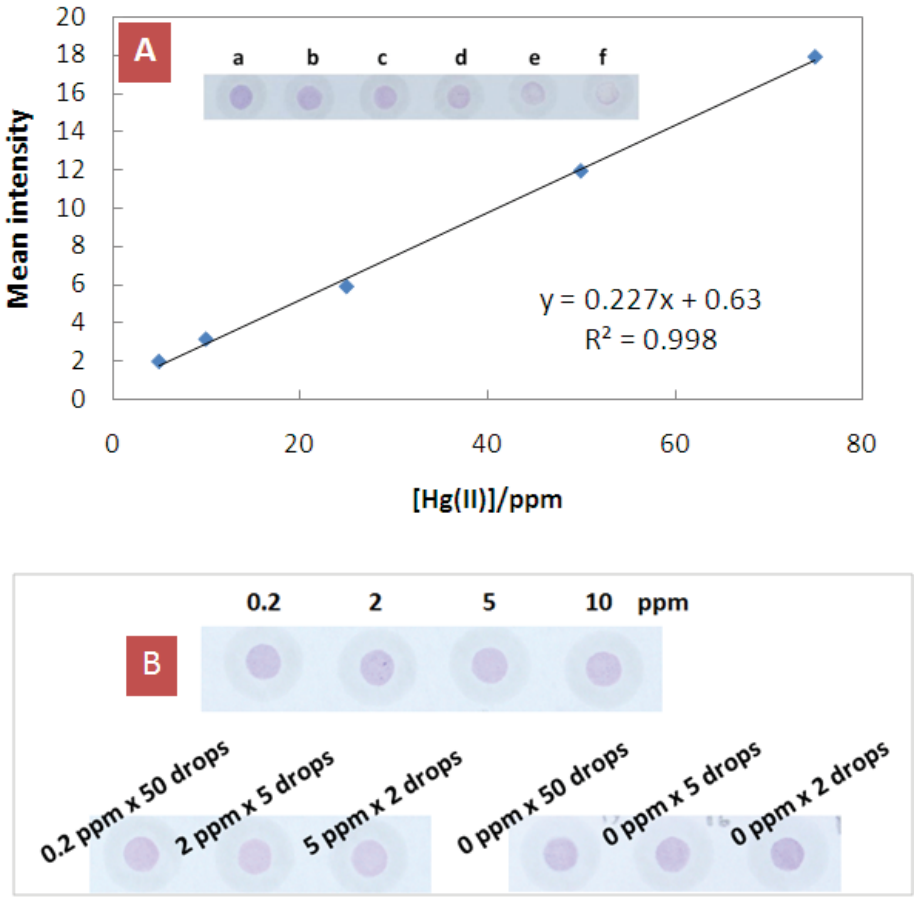

Figure 4.11 (A) The calibration curve obtained using mean color intensity values of the 35-nm diameter AgNPls and the concentrations of the added Hg(II) solutions determined by digital-image analysis using Adobe Photoshop; (inset) a representative visual image. **(B)** A representative visual comparison of the results obtained for the molar equivalent of 50, 5 and 2 applications of 2 μL of a 0.2, 2 and 5 ppm Hg(II) solution from three independent repeats, and comparison with that of a single 2 μL application of a 0.2, 2, 5 or 10 ppm solution of Hg (II).

The minimum numbers of 2 μL applications of Hg(II) solution in which color changes are visually discernible were determined for five different Hg(II) concentrations in the 0.02 to 0.2 ppm range (Fig. 4.12). The color change was visibly distinguishable after 15, 30 and 30 applications of 2 μL of the 0.2, 0.1 and 0.075 ppm Hg(II) solutions, respectively. Using digital images and Adobe Photoshop analysis, a concentration of 0.1 ppm Hg(II) could be detected with only five 2-μL applications. For sample concentrations of less than 0.1 ppm, the number of applications could be increased to obtain a sufficient signal (Fig. 7B). Accordingly, the proposed method can be used to detect Hg(II) concentrations as low as 2 ppb, although this concentration requires 70 applications. Thus, pre-concentration (via repeated applications of the test sample onto the same test zone) successfully improved the LOD of this system.

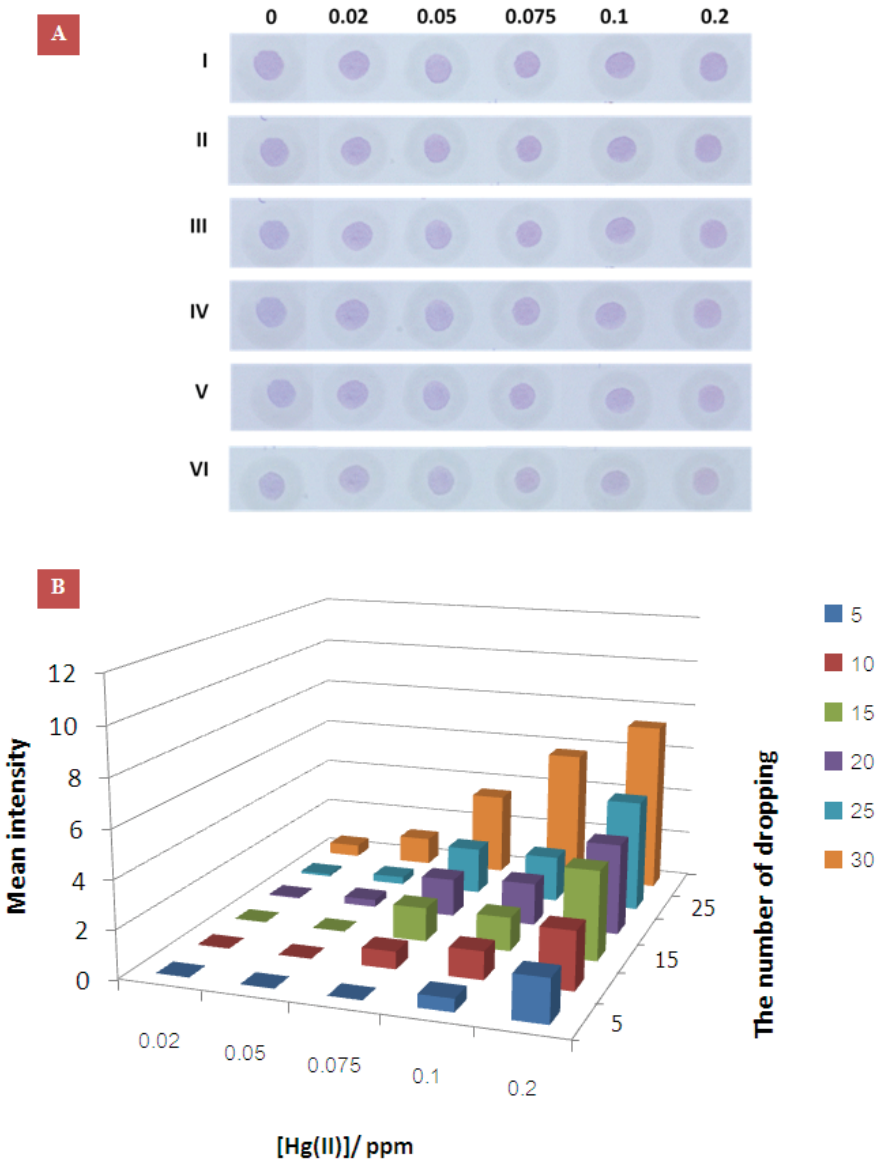

Figure 4.12 Decreased LODs for Hg(II) levels obtained via *in situ* pre-concentration of the test sample (repeat 2 μL applications on the test zone) using the 35 nm AgNPls and the indicated Hg(II) concentrations. **(A)** A representative visual image of the paper device, from three independent repeats, showing (I) 5, (II) 10, (III) 15, (IV) 20, (V) 25 and (VI) 30 applications of 2 μL of the indicated Hg(II) concentration and **(B)** the mean intensity of the AgNPls' color determined by digital-image analysis using Adobe Photoshop.

4.3.7 Application of AgNPls on paper to detect Hg(II) levels in real water samples

The proposed paper-AgNPls/Cu(II) device for determination of Hg(II) ion levels was evaluated with two real water samples, one from commercially bottled drinking water and another from domestic tap water. Neither sample induced any visible color change in the AgNPls, indicating that the Hg(II) contents of these water samples were below 5 ppm. No color change was observed even after pre-concentration with 70 applications of the sample. Therefore, it can be concluded that the Hg(II) concentrations in these samples were below 2 ppb. The declared ICP-OES (a model iCAP 6000 series) analysis (detection limit of 2 ppb), also detected no Hg(II). When these water samples were spiked with different Hg(II) concentrations, the analytical recoveries were in the acceptable range of 96-103% and 90 to 113% for the bottled and tap water, respectively, and exhibited precisions (% RSD) in the range of 3.2 to 4.9 % and 3.3 to 8.6 %, respectively. The agreement between the detected and expected values suggests that it is likely that the Hg(II) levels in the two water samples are less than 2 ppb and that they have not been masked by their matrices. These findings thereby validate the detection method employed and demonstrate the potential of the method developed herein for the detection of Hg(II) in real water samples.

4.4 Summary

A colorimetric Hg(II) detection method using 35 nm diameter AgNPls on a paper-based device has been developed. The paper-based device is easily constructed using wax-screen printing, and Hg(II) can be easily detected with the naked eye via the resulting color change of the AgNPls (on the paper-based device) after a 2μL application of the Hg(II) test solution. Digital imaging of the paper device and analysis using Adobe Photoshop software improves the sensitivity of the method from 5 ppm (obtained by the naked eye) to 0.1 ppm (LOD). The method has demonstrated good selectivity for Hg(II) against other metal ions,

and the signal can be further enhanced with the addition of Cu(II). A significant reduction in the Hg(II) LOD (to as low as 2 ppb) is achieved by *in situ* pre-concentration (multiple applications of the test sample). Finally, the method developed herein has been successfully used to determine Hg(II) levels in real water samples.

4.5 References

[1] http://www.chem.unep.ch/mercury/report/Final%20report/final-assessment-report-25nov02.pdf

[2] Z. Gu, M. Zhao, Y. Sheng, L.A. Bentolila and Y. Tang, Anal. Chem. 83 (2011) 2324-2329.

[3] http://water.epa.gov/drink/contaminants/basicinformation/mercury.cfm

[4] http://www.pcd.go.th/info_serv/en_reg_std_water04.html.

[5] Y. Zhang and S.B. Adeloju, Talanta 74 (2008) 951-957

[6] K. Edyta, P. Krystyna, G. Slawomir and B. Ewa, Anal. Sci. 16 (2000) 1309-1312.

[7] J.L. Mann, S.E. Long and W.R. Kelly, J. Anal. At. Spec. 18 (2003) 1293-1296.

[8] G. Wen, A. Liang, Z. Jiang, X. Liao, J. Li and H. Jiang, Luminescence 25 (2010) 373-377.

[9] Q.Q. Zhang, J.F. Ge, Q.F. Xu, X.Bo. Yang, X.Q. Cao, N.J. Li and J. Lu, Tetrahedron Lett. 52 (2011) 595-597.

[10] K. Leopold, M. Foulkes and P.J. Worsfold, Anal. Chem. 81 (2009) 3421-3428.

[11] M.J. Bloxham, S.J. Hill and P.J. Worsfold, J. Anal. At. Spec. 11 (1996) 511-514.

[12] W.A. Zhao and A. van den Berg, Lab Chip. 8 (2008) 1988–1991.

[13] W. Dungchai, O. Chailapakul and C.S. Henry, Anal. Chem. 81 (2009) 5821–5826.

[14] A. Apilux, W. Dungchai, W. Siangproh, N. Praphairaksit, C.S. Henry and O. Chailapakul, Anal. Chem. 82 (2010) 1727-1732.

[15] W. Dungchai, O. Chailapakul and C.S. Henry, Analyst, 136 (2011)77-82.

[16] C.C. Huang and H.T. Chang, Anal. Chem. 78 (2006) 8332-8338.

[17] L. Li, B. Li, Y. Qi and Y. Jin, Anal. Bioanal. Chem. 393 (2009) 2051-2057.

[18] X. Liu, X. Cheng, T. Bing, C. Fang and D. Shangguan., Anal. Sci. 26 (2010) 1169-1172.

[19] F. Chai, C.G. Wang, T.T. Wang, Z.F. Ma and Z.M. Su, Nanotechnology 21 (2010) 025501-025507.

[20] Y. Wang, F. Yang and X. Yang, ACS Appl. Mater. Inter. 2 (2010) 339-342.

[21] Y.J. Du, J.L. Yan, M. Ni and B.A. Du, J. Iran. Chem. Res. 4 (2011) 87-91.

[22] C.C.Huang and H.T. Chang. Chem. Commun. 12 (2007) 1215-1217.

[23] W. Leesutthiphonchai, W. Dungchai, W. Siangproh, N. Ngamrojnavanich and O. Chailapakul, Talanta 85 (2011) 870-876.

[24] H. Li, Z. Cui and C. Han, Sens. Actuators B 143 (2009) 87–92.

[25] P.D. Selid, H. Xu and E.M. Collins. Face-Collins, M.S., Zhao, J.X, Sensors, 9 (2009) 5446-5459.

[26] E. Sumesh, M.S. Bootharaju and A.T. Pradeep. J. Hazard. Mater, 189 (2011) 450−457.

[27] F. Okcu, F.N. Ertas, H.I. Gokcel and H. Tural, Turk. J. Chem. 29 (2005) 355 -366.

[28] L. Li and B. Li, Analyst 134 (2009)1361-1365.

Chapter V

A microfluidic paper-based analytical device for rapid quantification of particulate chromium

5.1 Introduction

There are many industrial uses of Cr, including pigment dyes, plastics, protective coatings, ferrochromium alloys, chromate production, tannery facilities, and steel alloys [1]. Chromium exists primarily in one of two oxidation states, trivalent (Cr(III)) and hexavalent (Cr(VI)). Trivalent chromium has an LD_{50} of 200-600 mg/kg and is suggested to play an important role in insulin action and glucose regulation in the human body [2-5]. Cr(VI) has an LD_{50} of 50-150 mg/kg and effects respiratory, gastrointestinal, immunological, hematological, reproductive, and developmental systems [6, 7]. In addition, Cr(VI) is a potent carcinogen [8]. Airborne exposure to both forms of chromates in dye pigments, anticorrosive agents, surface coatings, and welding is linked with lung, nasal, and stomach cancers [9]. The legal limit for airborne exposure to total Cr in U.S. workplaces is 0.05 $\mu g/m^3$, set by The Occupational Safety and Health Administration (OSHA) in 2012.

At present, occupational exposure to metals in particulate matter (PM) requires sampling onto filters, which are then transported to a centralized analytical laboratory for analysis. Many instrumental techniques have been used to measure Cr, including UV-Visible spectrophotometry [10], ion chromatography [11], inductively couple plasma-mass spectrometry [12], atomic absorption spectroscopy [13], and X-ray techniques [14]. Although highly sensitive, these approaches are time-consuming (approximately two weeks for assessment), expensive (over $100 per sample), and require trained operators. Consequently, there is a need for simple, sensitive methods for Cr analysis to enable more frequent assessment of exposures of ‘at-risk’ workers.

Paper-based microfluidic devices (μPADs) have emerged as a low-cost alternative for quantitative chemical measurement. Relative to traditional assays, μPADs are easy to operate, consume small reagent volumes, and provide rapid results (typically in min) [15-19]. μPADs represent a new generation of lateral-flow chemical assays utilizing hydrophobic barriers printed on paper. These barriers direct flow so that specific chemical assays may be conducted rapidly and efficiently [20]. Paper substrates are easy to use because flow is generated via capillary action. Reagents impregnated in 'detection zones' on the μPAD allow analytes to be quantified by visual assessment using an external optical reader (i.e. camera, scanner) [21-23]. The utility of this technology has been demonstrated for applications in point-of-care [24-26], food safety [27-29], and environmental monitoring [30-33]. Several reports have focused on quantifying metals using μPADs. Hossain and Brennan used the enzymatic activity of *β*-galactosidase and silver nanoparticle aggregation to detect metals in water [31]. Yang and Wang developed a method for determining Ag and Cu via an autocatalytic reaction with *o*-phenylenediamine followed by detection with fluorescence [34]. Ratnarathorn et al. used silver nanoparticles to detect Cu ions in water [35]. Our group demonstrated the use of μPADs for determination of Fe, Cu, and Ni in aerosolized incineration ash as a first step towards monitoring occupational exposure, with detection limits of 1 – 1.5 μg [30].

Here, a μPAD was developed for total Cr determination using tetravalent cerium Ce(IV) and 1,5-diphenylcarbazide (1,5-DPC) as oxidizing [36] and colorimetric [37] reagents, respectively. The μPAD approach is different from previous reports because it includes sample pretreatment on the device as well as addition of stabilizing agents to give the device long-term shelf life. Furthermore, the device includes four separate detection zones to provide an estimate of analytic precision and to ensure (statistical) reproducibility.

Tetravalent cerium oxidizes all forms of soluble Cr to Cr(VI) for reaction with 1,5-DPC. We chose Ce(IV) over hydrogen peroxide [38], perchloric acid [39], and bromine [40] because these latter chemicals typically require multiple reagent additions, time-consuming steps, and precise temperature control. Alternatively, Ce(IV) does not require precise temperature control, is easy to use, and can be stored on paper. For colorimetric detection of Cr(VI), many published methods have been reported including the use of gold and silver nanoparticles [41, 42] and nanoparticle derivatives [43]. 1,5-diphenylcarbazide has been used as a selective Cr(VI) reagent for decades [44]. 1,5-DPC reduces Cr(VI) to Cr(III) and is itself oxidized to diphenylcarbazone (DPCO). DPCO complexes with the generated Cr(III) to form an intensely purple-colored complex [37]. Phthalic anhydride stabilizes 1,5-DPC on the μPADs [45]. Method viability was established using standardized metal-containing baghouse dust samples. Dust collected on cellulose filters was digested using microwave-assisted wet digestion, followed by μPAD analysis. Quantitative evaluation showed good correlation with known Cr levels.

5.2 Experimental

5.2.1 Materials and equipment

Ammonium dichromate (VI), lead(II) nitrate, cadmium(II) nitrate tetrahydrate, iron(III) chloride hexahydrate, nickel(II) sulfate hexahydrate, barium(II) chloride, manganese(II) chloride tetrahydrate, zinc(II) nitrate hexahydrate, vanadium(III) chloride, silver(II) nitrate, cobalt(II) chloride, aluminum(III) sulfate hydrate, copper(II) sulfate pentahydrate, phthalic anhydride, cerium (IV) ammonium nitrate, 1,5-diphenylcarbazide, and polydiallyldimethylammonium chloride (medium molecular weight) were obtained from Sigma-Aldrich (St. Louis, MO). Sodium acetate and glacial acetic acid were obtained from Fisher Scientific (Pittsburgh, PA). Metal-containing certified industrial incineration ash

samples (RTC-CRM012) and pre-validated baghouse dust (RTC-CRM014) were purchased from LGC Standards (Teddington, UK). Milli-Q water from Millipore ($R \geq 18.2$ MΩ cm^{-1}) was used for all experiments. All chemicals were used as received.

5.2.2 Device design and fabrication

The μPADs described here were fabricated using wax printing [20]. Hydrophobic barriers were printed using a commercial wax printer (Xerox Phaser 8860, VWR) onto Whatman grade one filter paper, as described previously [20, 27]. The μPAD design shown in Figure 5.1 was generated using graphics software (CorelDRAW). The RGB values 248-195-0 were selected as the barrier color, providing a high contrast background for subsequent image analysis. Printed wax was melted at 200 °C for 120 s on a hot plate. One side of the paper substrate was then covered with packing tape to prevent leakage of eluent through the bottom of the μPAD.

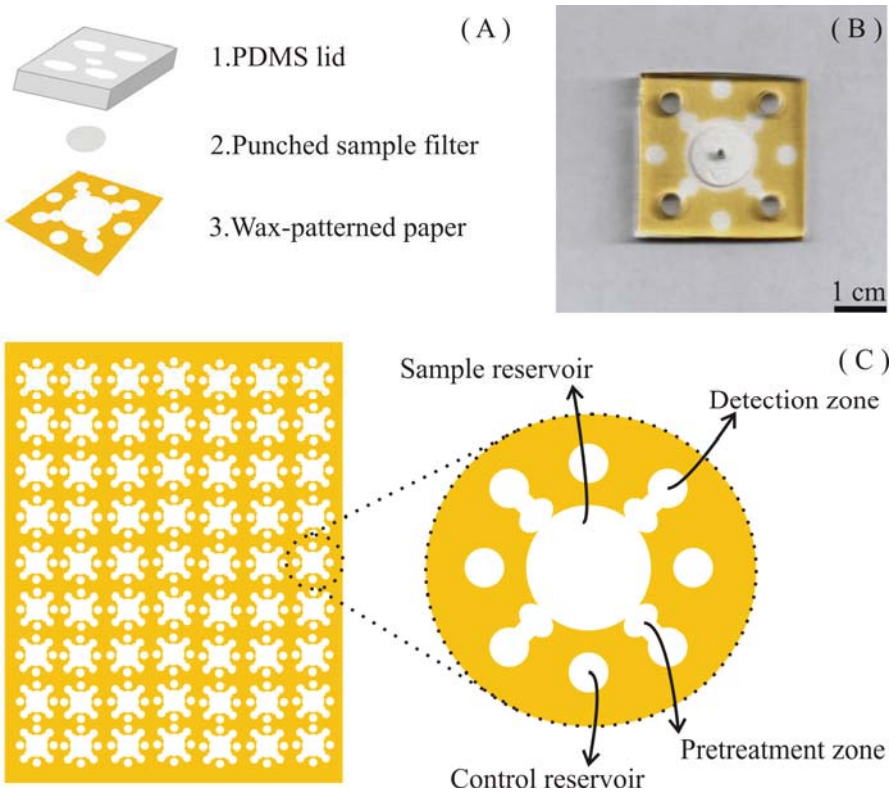

Figure 5.1. (A) Schematic of a μPAD, consisting of a PDMS lid for applying equal pressure across the paper surface, a 10 mm filter punch containing PM from baghouse dust, and a patterned filter paper treated with reagents for colorimetric analysis of total Cr. (B) The combined device. (C) Analytical devices can be mass-produced on a single sheet of filter paper (the figure shows 63 individual devices).

5.2.3 Colorimetric detection of total chromium

For Cr detection, a solution containing 1.5 g of 1,5-diphenylcarbazide (1,5-DPC) and 4.0 g of phthalic anhydride was dissolved in 100 mL of acetone. The μPAD was prepared by adding 0.5 μL of ceric(IV) ammonium nitrate (0.35 mM) twice onto the pretreatment zone, followed by 0.5 μL of polydiallyldimethylammonium chloride (PDDA) (5% w/v). PDDA was added to stabilize the reaction product between Cr and 1,5-DPC and to prevent the

complex from flowing to the edges of the hydrophilic channels [30]. Two 0.25 μL aliquots of the detection reagent solution (1,5-DPC and phthalic anhydride) were then added to the detection zone. The device was allowed to dry completely between each reagent addition.

5.2.4 Experimental procedure

An overview of the experimental procedure is shown in Figure 5.2. For measurements, a 10 mm (diameter) circular punch was taken from an air sampling filter (described below). Calibration plots were generated by adding standard solutions to one 10 mm punch. When dry, the punch was placed on the μPAD sample reservoir. For method validation, a sample of baghouse PM was resuspended in the laboratory and onto mixed cellulose ester (MCE) filters. After sample collection, 20 μL of SDS was added to each 10 mm punch to enhance the elution of metal ions from the relatively hydrophobic MCE filter. Microwave-assisted acid digestion on the filter samples was performed by adding 5 μL of concentrated nitric acid, followed by 30 μL of water to the filter punch. The punch was then placed in a household microwave (1100 W) for a total of 30 s (two 15 s intervals). Between each 15 s interval, 30 μL of deionized water was added to each punch to wet the filter. After digestion, 10 μL of sodium bicarbonate (0.5 M, pH 9.5) was added to neutralize the acid. To accelerate neutralization, the μPAD was heated in the microwave for an additional 15 s. Finally, a polydimethylsiloxane (PDMS) lid with holes punched over the sample reservoir (2 mm diameter) and detection zone (5 mm diameter) was placed on top of the μPAD. Acetate buffer (40 μL, 0.1 M, pH 4.5) was added to the center hole of the PDMS lid, eluting the digested metals from the filter through the pretreatment zones to the detection zones. A 300 g weight (a water filled Erlenmeyer flask) was placed on the PDMS lid to distribute pressure evenly across the device. Color formation was complete in less than 10 min. The device was allowed to dry before color intensity was measured.

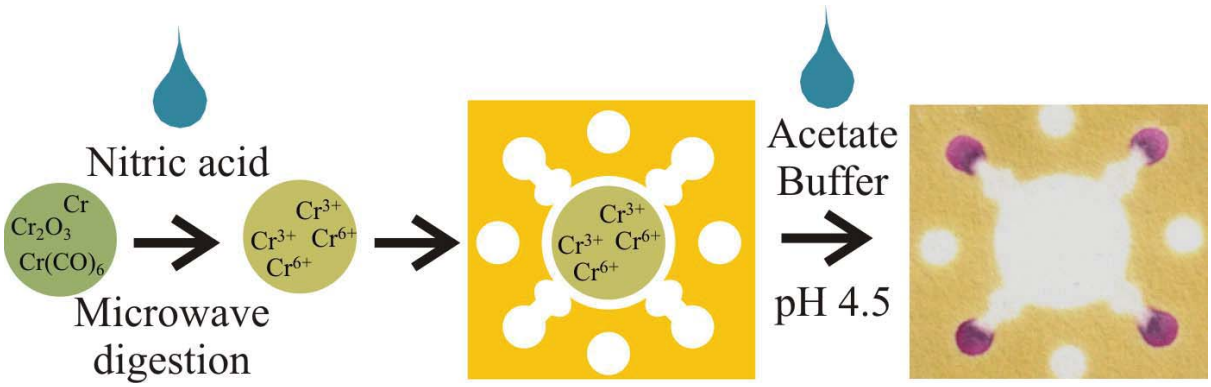

Figure 5.2. Acid digestion procedure for measuring total soluble Cr. HNO_3 is deposited on a 10 mm filter punch and digested using a commercial microwave. The digested punch is placed on the μPAD and acetate buffer (pH 4.5) is added to the paper substrate through the PDMS lid. The buffer elutes Cr ions from the MCE filter to the detection zones.

5.2.5 Quantitative image processing

Color intensity was measured using a desktop scanner (XEROX DocuMate 3220). To quantify intensity, a color threshold window was applied to the Cr(III)-1,5-diphenylcarbazone product (0-180) using NIH ImageJ software, effectively removing all unwanted color channels. This method passes only the purple of the Cr(III)-1,5-DPC complex, and removes the wax background. After thresholding, images were converted to gray scale and inverted, yielding higher intensity values for darker (more concentrated) Cr samples [30]. For background measurements, color intensities for blank samples were measured using the same protocol described above. The background values were used to determine the baseline intensity for detection limit calculations.

5.2.6 Particulate metal collection and digestion

A suspension of 0.1% (w/v %) incineration ash in deionized water was prepared and nebulized into a 0.8 m^3 plexiglass chamber. The average PM concentration in the chamber was 0.73 mg/m^3 as measured using an aerosol photometer (TSI, Model 8250). Relative humidity was not controlled but was monitored and remained below 50% throughout all experiments. Resuspended dust was sampled onto Pallflex and mixed cellulose ester (MCE) filters (37 mm diameter) at a flow rate of 10 L/min for 4 hrs. Sampled PM mass was quantified using a Mettler-Toledo analytical microbalance (model MX5). These filters collected approximately 1.16 μg ash per mm^2 of exposed filter area (or 91.14 μg per punch). After sample collection, 10 mm diameter punches were taken from the filter, extracted, and prepared according to the procedure described above.

5.3 Results and discussion

We first evaluated the ability to measure total Cr using the combination of Ce(IV) oxidation followed by colorimetric detection with 1,5-DPC. After the reaction was complete, the purple 1,5-DPCO product was readily visible in the detection zone. A log-linear calibration curve was obtained from standard chromium solutions added to 10 mm MCE punches (Figure 5.3). Intensities were linear with respect to total chromium mass (log scale) from 0.23-3.75 μg with a detection limit of 0.12 μg and a pooled relative standard deviation (RSD) for all measurements (n = 7 measures for each Cr level) of 4.9%. The detection limit was determined by the lowest Cr mass with an intensity three standard deviations above the background standard deviation. Above 3.75 μg, the paper surface saturated and no additional increase in intensity was measured. Although the overall linear range covers only one order of magnitude, this range should be sufficient for hazard evaluation, since higher exposures (once detected) will likely require further investigation. Analysis of smaller punch sizes can

also be employed. The linear range of the assay is extendable by increasing the surface area of the detection zone; larger detection zones facilitate analysis of greater chromium mass. The minimum detectable levels of Cr using the μPAD were compared to the permissible exposure limit (PEL), stipulated by the OSHA. For method validation, minimum detectable limits were measured as a TWA, collected at sampling rate of 4 L/min. At the detection limit of 0.12 μg Cr, we calculated a minimum detectable level as a TWA of 0.72 $\mu g/m^3$. Although this level exceeds the PEL for Cr, stacking MCE punches and analyzing multiple filters simultaneously can be used to further decrease detection sensitivity. As a result, this proposed method should be sufficient for monitoring occupational exposure to particulate Cr.

We found, from prior work in our laboratory, that the metal complex should be homogenously distributed over the detection zone to maximize accuracy and detection sensitivity [30]. If the reaction product migrates to the detection zone edge, quantification (via color intensity integration) is more challenging. The final Cr complex generated here was highly mobile on paper, and as a result, the reaction product flowed to the detection zone edge, reducing measurement accuracy and sensitivity (Figure 5.4A). Tricapylmethyl ammonium chloride has been used previously to prevent the Cr-DPCO complex from spreading on spot tests [46]. Unfortunately, this surfactant must be dissolved in acetone. When applied to the device, the acetone caused dissolution of the wax and leaking of subsequent aqueous solutions. As a result, polydiallyldimethylammonium chloride (PDDA) was used to produce the same effect (Figure 5.4) [30]. The intensities of blank samples (0.1 M acetate buffer, pH 4.5) in the presence and absence of PDDA were measured to be 2.4 ± 1.1 and 10.8 ± 1.7 (n=7). The use of PDDA achieved a two-fold increase in signal strength; intensities of 3.75 μg Cr with and without PDDA were measured to be 121.4 ± 4.4 and 65.1 ± 1.1, respectively.

We next investigated potential interferences from other metals. Cr(III) was added to the μPAD in the presence of Mg, Mn, Zn, Al, Ba, V, Co, Cu, Fe, and Ni (Figure 5) in metal:Cr ratios of 1:1 and 4:1. The measured levels of Cr were found to be 0.5 ± 0.1 and 1.8 ± 0.2 (n=7) μg in the two samples. A paired t-Test confirmed that the presence of other metals did not significantly impact measurement.

For method validation, a baghouse sample certified for Cd, Cr, and Pb, and containing unmeasured levels of Al, Sb, As, Ba, B, Be, Ca, Co, Cu, Fe, Mg, Mn, Hg, Mo, Ni, P, K, Ag, Se, Na, Sr, Tl, Sn, Ti, V, and Zn, was aerosolized and collected on filters. Total Cr mass was measured using combinations of two and three punches stacked over the sample zone (Figure 5.5). The measured Cr intensities were 31.8 ± 0.9 and 44.6 ± 2.1 (n=7), respectively. Gravimetric analysis was also performed on the filter punches to verify the Cr mass present. For two punches, the actual and measured Cr levels were 0.41 and 0.4 ± 0.1 (n=7) μg, respectively. For three punches, the absolute and measured Cr levels were 0.61 μg and 0.6 ± 0.1 (n=7) μg, respectively. These results suggest we can measure Cr concentrations from complex PM samples. Furthermore, detection limits and method sensitivity can be improved using multiple sample punches analyzed simultaneously on a single device.

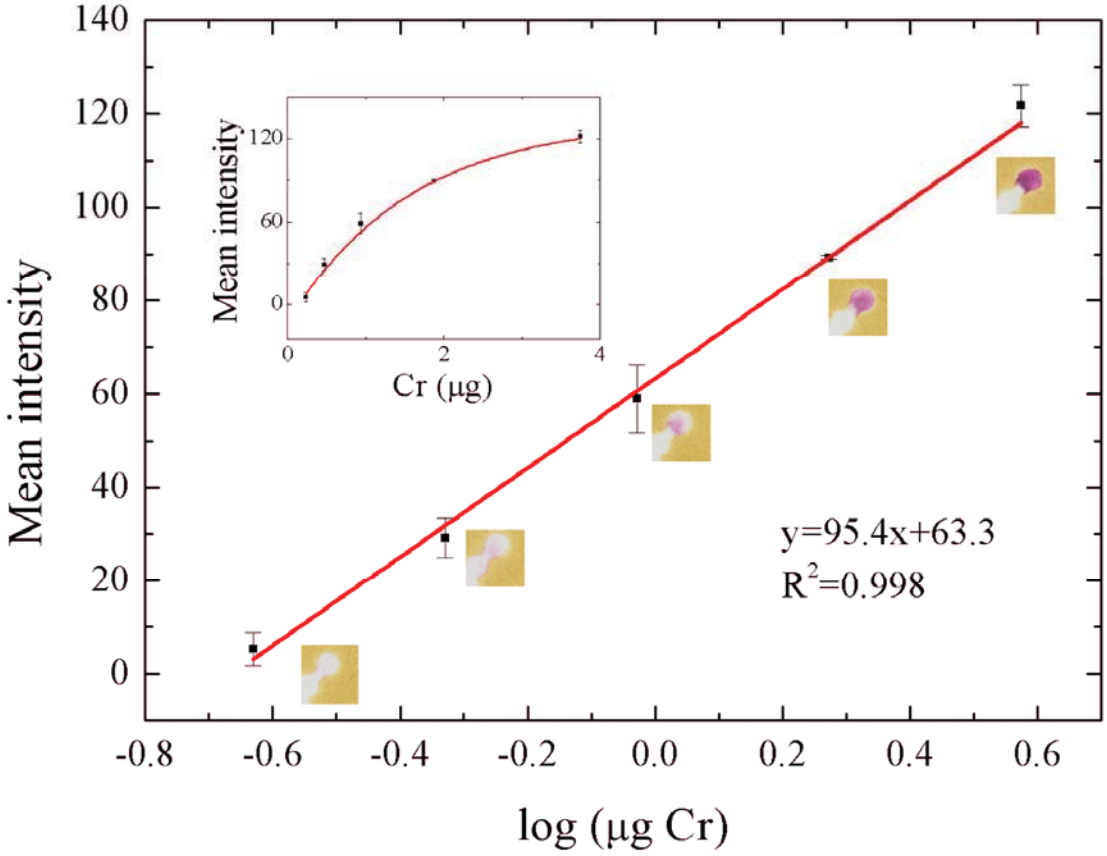

Figure 5.3. Colorimetric intensity as a function of log Cr mass added to the µPAD. The working range was 0.23-3.75 µg and is log-linear with measured intensity. The inset shows the same data plotted on a linear mass scale (n = 3).

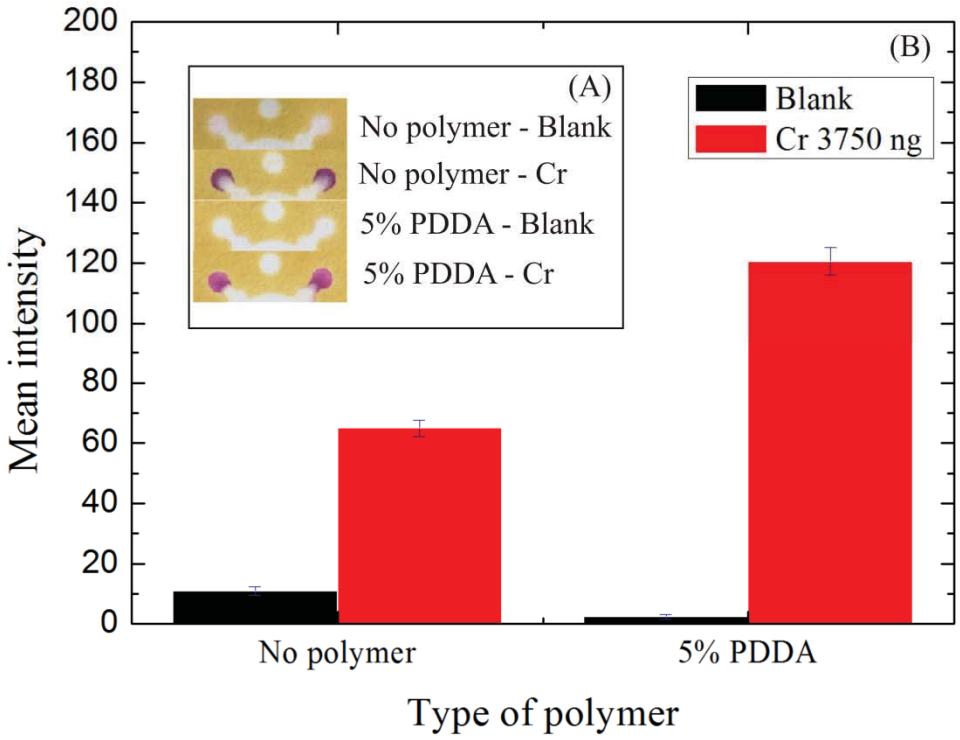

Figure 5.4. PDDA was investigated as a compound for retaining Cr the detection zone. (A) The devices were photographed, and (B) mean color intensity was measured in the presence and absence of PDDA in the detection zone.

We also investigated the effects of long-term storage on device performance. A series of μPADs were stored at 4 and 22 ± 2°C for 2, 3, 7, 14, 21, and 28 days. Colorimetric intensities as a function of storage time are shown in Figure 5.6 for samples with 0.0, 0.94, and 3.75 μg Cr. In the absence of Cr and phthalic anhydride, the indicator (1,5-DPC) changed color after two days, regardless of temperature. In the presence of phthalic anhydride, color formation was observed after three days only at 22°C. In the presence of phthalic anhydride, no significant color developed after 28 days when the device was covered and stored at 4°C. These results show that when storing the device it is important to cover and keep in a cold environment.

Punch	Actual level (µg)[a]	Color product on the device	Measured level(µg)[b]
2 punches	0.41		0.4±0.1
3 punches	0.61		0.6±0.1

Figure 5.5. Detection of Cr from baghouse dust containing the Al, Sb, As, Ba, B, Be, Ca, Co, Cu, Fe, Mg, Mn, Hg, Mo, Ni, P, K, Ag, Se, Na, Sr, Tl, Sn, Ti, V, and Zn. Measured levels are shown in which multiple 10 mm punches were taken and stacked for simultaneous analysis to enhance the mean intensity of the colored product.

[a]The actual mass of Cr was calculated from gravimetric analysis of the filters after collection of baghouse dust.

[b]The measured mass of Cr was obtained from the paper-based colorimetric assay.

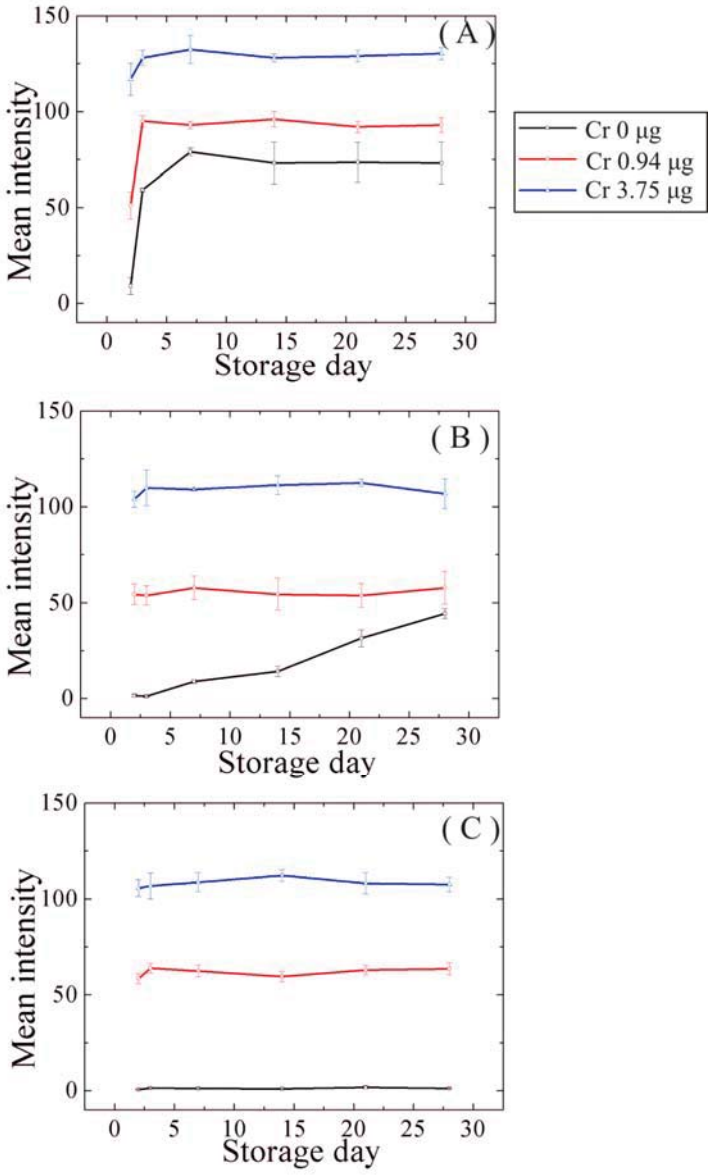

Figure 5.6. Effect of storage on µPAD performance in the presence and absence of pretreatment reagents**.** Cr masses of 0, 0.94, and 3.75 µg were measured using the µPAD with the following conditions: (A) devices stored at 4^{o}C without phthalic anhydride(B) devices stored at 25°C with phthalic anhydride(C) devices stored at 4^{o}C with phthalic anhydride. The µPADs were stored for 2, 3, 7, 14, 21, and 28 days.

5.4 Summary

A μPAD was developed for quantifying levels of particulate Cr. Colorimetric μPADs provide a simple, portable approach for measuring particulate Cr relative to traditional methods. Using our system, total Cr mass can be quantified using devices that are inexpensive (<$0.05/test) and easy to use. Ultimately, the goal of this work is to provide a system whereby the analysis is performed at the point of use to avoid transportation costs. Rapid sample analysis will lead to more effective risk communication, improved assessment, and a lower exposure to occupational aerosol hazards.

5.5 References

[1] H. Abdolmohammad-Zadeh, G.H. Sadeghi, Talanta, 94 (2012) 201.

[2] Z. Han, L. Qi, G. Shen, W. Liu, Y. Chen, Analytical Chemistry, 79 (2007) 5862.

[3] H.A. Schroeder, J.J. Balassa, I.H. Tipton, Journal of Chronic Diseases, 15 (1962) 941.

[4] L. Zhao, Y. Jin, Z. Yan, Y. Liu, H. Zhu, Analytica Chimica Acta, 731 (2012) 75.

[5] S.A. Katz, H. Salem, J. Appl. Toxicol., 13 (1993) 217.

[6] S.K. Tandon, D.K. Saxena, J.S. Gaur, S.V. Chandra, Environ. Res., 15 (1978) 90.

[7] S.A. Katz, H. Salem, J. Appl. Toxicol., 13 (1993) 217.

[8] R.M. Sedman, J. Beaumont, T.A. McDonald, S. Reynolds, G. Krowech, R. Howd, Journal of environmental science and health. Part C, Environmental carcinogenesis & ecotoxicology reviews, 24 (2006) 155.

[9] R.B. Hayes, Cancer Causes Control, 8 (1997) 371.

[10] J. Wang, K. Ashley, E.R. Kennedy, C. Neumeister, Analyst, 122 (1997) 1307.

[11] S.M. Talebi, Environ. Res., 92 (2003) 54.

[12] M.J. Powell, D.W. Boomer, D.R. Wiederin, Analytical Chemistry, 67 (1995) 2474.

[13] Y.L. Huang, I.C. Chuang, C.H. Pan, C. Hsiech, T.S. Shi, T.H. Lin, Atom. Spectrosc., 21 (2000) 10.

[14] I. Tsuyumoto, Y. Maruyama, Analytical Chemistry, 83 (2011) 7566.

[15] A.W. Martinez, S.T. Phillips, G.M. Whitesides, E. Carrilho, Analytical Chemistry, 82 (2010) 3.

[16] C. Parolo, A. Merkoci, Chem. Soc. Rev., 42 (2013) 450.

[17] X. Li, D.R. Ballerini, W. Shen, Biomicrofluidics, 6 (2012).

[18] D.R. Ballerini, X. Li, W. Shen, Microfluid. Nanofluid., 13 (2012) 769.

[19] D.D. Liana, B. Raguse, J.J. Gooding, E. Chow, Sensors, 12 (2012) 11505.

[20] E. Carrilho, A.W. Martinez, G.M. Whitesides, Analytical Chemistry, 81 (2009) 7091.

[21] A.W. Martinez, S.T. Phillips, B.J. Wiley, M. Gupta, G.M. Whitesides, Lab on a Chip, 8 (2008) 2146.

[22] A.W. Martinez, S.T. Phillips, M.J. Butte, G.M. Whitesides, Angew Chem Int Ed Engl, 46 (2007) 1318.

[23] L. Shen, J.A. Hagen, I. Papautsky, Lab Chip, 12 (2012) 4240.

[24] W. Dungchai, O. Chailapakul, C.S. Henry, Analytica Chimica Acta, 674 (2010) 227.

[25] S.J. Vella, P. Beattie, R. Cademartiri, A. Laromaine, A.W. Martinez, S.T. Phillips, K.A. Mirica, G.M. Whitesides, Analytical Chemistry, 84 (2012) 2883.

[26] L. Ge, J.X. Yan, X.R. Song, M. Yan, S.G. Ge, J.H. Yu, Biomaterials, 33 (2012) 1024.

[27] J.C. Jokerst, J.A. Adkins, B. Bisha, M.M. Mentele, L.D. Goodridge, C.S. Henry, Analytical Chemistry, 84 (2012) 2900.

[28] S.M.Z. Hossain, R.E. Luckham, M.J. McFadden, J.D. Brennan, Analytical Chemistry, 81 (2009) 9055.

[29] S.M.Z. Hossain, C. Ozimok, C. Sicard, S.D. Aguirre, M.M. Ali, Y.F. Li, J.D. Brennan, Anal. Bioanal. Chem., 403 (2012) 1567.

[30] M.M. Mentele, J. Cunningham, K. Koehler, J. Volckens, C.S. Henry, Anal Chem, 84 (2012) 4474.

[31] S.M.Z. Hossain, J.D. Brennan, Analytical Chemistry, 83 (2011) 8772.

[32] A. Apilux, W. Siangproh, N. Praphairaksit, O. Chailapakul, Talanta, 97 (2012) 388.

[33] N. Ratnarathorn, O. Chailapakul, C.S. Henry, W. Dungchai, Talanta, 99 (2012) 552.

[34] X. Yang, E.K. Wang, Analytical Chemistry, 83 (2011) 5005.

[35] N. Ratnarathorn, O. Chailapakul, C.S. Henry, W. Dungchai, Talanta, 99 (2012) 552.

[36] M.J. Whitaker, Analytica Chimica Acta, 174 (1985) 375.

[37] F.G. Kong, Y.H. Ni, BioResources, 4 (2009) 1088.

[38] J.E.T. Andersen, Analytica Chimica Acta, 361 (1998) 125.

[39] J.J. Lichtin, Ind. Eng. Chem.-Anal. Edition, 2 (1930) 0126.

[40] N. Balasubramanian, V. Maheswari, J. AOAC Int., 79 (1996) 989.

[41] A. Ravindran, M. Elavarasi, T.C. Prathna, A.M. Raichur, N. Chandrasekaran, A. Mukherjee, Sens. Actuator B-Chem., 166 (2012) 365.

[42] L. Zhao, Y. Jin, Z.W. Yan, Y.Y. Liu, H.J. Zhu, Analytica Chimica Acta, 731 (2012) 75.

[43] Y.J. Lai, W.L. Tseng, Analyst, 136 (2011) 2712.

[44] N.M. Stover, J. Am. Chem. Soc., 50 (1928) 2363.

[45] J.F. Ege, L. Silverman, Analytical Chemistry, 19 (1947) 693.

[46] B. Saha, R.J. Gill, D.G. Bailey, N. Kabay, M. Arda, React. Funct. Polym., 60 (2004) 223.

Chapter VI

Electrochemical Detection for Paper-Based Microfluidics

6.1 Introduction

The development of microfluidic devices has been spurred at least in part by the desire to produce low-cost point-of-care diagnostics and environmental monitoring devices [1,2]. For point-of-care applications, the goal is to provide a total answer where a sample is introduced to the device and data is generated that can be used to make an informed decision. A variety of devices meeting these requirements have been demonstrated. The most common example, by far, has been for DNA analysis where complex functions such as DNA capture, amplification, and separation on a single device have been demonstrated [3-7]. The Burns group has successfully generated a device with integrated microchannels, heaters, temperature sensors, and fluorescence detectors used to analyze nanoliter-size DNA samples on a single glass and silicon substrate. The device is capable of mixing the solution together, amplifying or digesting the DNA, then separating and detecting those DNA [3-7]. In another example from the Landers group, a two-stage microfluidic device consisting of C_{18} reversed-phase monolithic column for DNA extraction efficiency on a single glass slide (3 x 2.5 cm) was coupled with a device that was able of performing polymerase chain reactions (PCR) and DNA separations [6]. While these examples show the power of microfluidic devices and their potential for solving complex problems, a significant portion of the world's population could never afford the cost of such advanced devices. To this end, there is a growing push to generate microfluidic devices that are extremely low cost (<$1 US) and require minimal external instrumentation for obtaining quantitative information.

Among the least expensive of the microfluidic devices are the recently introduced paper microfluidic devices. Paper-based microfluidic devices have the potential to be good alternatives for point-of-care testing over traditional glass and polymer based devices because they are easy to use, inexpensive, require small volumes of reagents and sample, provide rapid analysis, are disposable, can be made from renewable substrate materials, and are portable [8-13]. These devices have been used for the simultaneous determination of glucose and protein on a single piece of patterned paper [8]. The results of the assay were quantified by visually comparing the color intensity of the reaction spots with the developed color intensity. Matching color and color intensity by the naked eye is complicated by many factors including different visual perception of color from one person to another, lighting, and the difference between the colors of a dry printed color on label stock and the colors seen in a reacted (i.e., wetted) paper. In an effort to conduct quantitative analysis for diagnostic tests based on paper microfluidics, several authors have used cameras or scanners to record the color intensity. Using this approach, glucose, pH, and protein levels were simultaneously determined by paper-based microfluidic devices [13]. Camera phones and portable scanners are an attractive format because they can be used by unskilled personnel and provide more accurate results as compared to visual inspection. However, the transmission of data from on-site to experts is still required to analyze the data. Moreover, the intensities of digital images from the camera are affected by lighting conditions and a calibration curve using standards of known color and intensity is necessary for processing data of each imaging device. Finally, camera phones and portable scanners lack the sensitivity and selectivity of traditional analytical instrumentation. Therefore, a detector with high sensitivity and selectivity is still needed for determination of low levels of analytes in biological samples and complex sample matrixes such as blood and plasma.

Electrochemical detection (ECD) is an attractive alternative detection scheme for paper-based microfluidics due to its small size, portability, low cost, high sensitivity, and high selectivity by proper choice of detection potential and/or electrode material [14-19]. An additional advantage of ECD is simplicity of the instrumentation resulting in low electrical power requirements for in-field use [19]. These advantages have led to the almost universal use of electrochemical detection in handheld glucometers for monitoring diabetes. Finally, screen-printed carbon electrodes have many attractive advantages for ECD including low cost, disposability, flexibility in design, ease of chemical modification, and ability to produce with minimal outside technology [20-22]. Here, we present electrochemical based detection for paper-based microfluidic devices for simultaneous determination of glucose, lactate, and uric acid in biological samples. Electrodes modified with Prussian Blue (PB) for improved selectivity for H_2O_2 detection were characterized to show the viability of the combined approach. Electrodes were subsequently modified with appropriate enzymes for the detection of small molecule markers in urine and blood samples. Experimentally determined levels measured using the paper microfluidic devices were within error of the levels measured for the same samples done using traditional clinical diagnostic assays.

6.2 Experimental Methods

6.2.1 Materials and equipment

D-(+)-glucose, sodium L-lactate, uric acid, glucose oxidase (from *Aspergillus niger*, 215 U/mg) and uricase (from *Bacillus fastidiosus*, 9 U/mg) were purchased from Sigma-Aldrich (St. Louis, MO). Lactate oxidase (from *Aerococcus viridians*, 38 U/mg) was obtained from A.G. scientific, INC (San Diego, CA). Potassium phosphate was purchased from Fisher Scientific

(Pittsburgh, PA). Acetone was obtained from Mallinckrodt chemicals (Phillipsburg, NJ). SU-8 3025 negative photoresist was purchased from MicroChem Corp. (Newton, MA). Whatman filter paper 1 was obtained from Cole-parmer (Vernon Hills, Illinois). Carbon ink mediated with Prussian blue (C2070424D2) was purchased from Gwent group (Torfaen, United Kingdom). Silver chloride ink (Electrodag 7019) was obtained from Acheson colloids company (Port Huron, MI). All chemicals were used as received without further purification. Electrochemical measurements were made using a potentiostat (CHI 1207A, CH Instruments, Austin, TX) at room temperature (22 ±1°C).

6.2.2 Preparation of paper-based microfluidic devices

Photolithography was used to pattern Whatman filter paper 1 according to previously reported methods [8-12]. Briefly, SU-8 3025 photoresist was poured on the center of the paper and spread over the paper using a spin-coater. The photoresist-covered paper was baked at 95 °C for ~10 min. The paper was then covered with transparency film photomask generated using a standard laser printer and irradiated with a UV lamp. After baking at 95 °C for 1-3 min, unpolymerized photoresist was removed from the paper by submerging the paper in acetone for 1 min, and by rinsing the paper with acetone. Next, the paper was dried under ambient conditions for 1 hr. Prior to use, paper microfluidic devices were exposed to air plasma (Harrick PDC-32G) for 30 s. Areas covered with photoresist remained hydrophobic while areas without photoresist were hydrophilic.

6.2.3 Design and preparation of electrochemical detector for paper-based microfluidic devices

The electrodes were screen-printed in house using carbon ink containing PB as the working (WE) and counter electrode (CE) and silver/silver chloride ink as the reference electrode (RE) and conductive pads. The screen-printing emulsion was designed with Corel Draw 9 software and generated by Chaiyaboon Co. (Bangkok, Thailand). The electrode design is shown in Figure 6.1. The working electrode was designed to be as close as possible to the reference electrode to minimize the effect of uncompensated resistance between the WE and RE (spacing about 0.15 mm). The counter electrode (geometric area about 7.5 mm^2) was designed to be larger than the working (geometric area 1.3 mm^2) and reference electrodes (geometric area 1.2 mm^2) to allow unlimited current transfer in the circuit. All electrodes were designed with the working portion of the electrode on the hydrophilic portion of the paper and the contact pads on the hydrophilic portion of the paper. The screen printing process consisted of two layers. The first layer was applied with the silver/silver chloride ink and served as the reference electrode and conductive pads. Next, carbon ink containing PB was screened on the paper. Both layers were subsequently cured for 30 min at 65 °C and allowed to cool at room temperature.

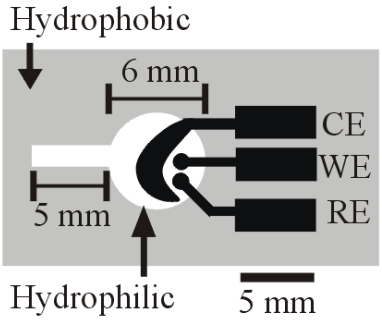

Figure 6.1 Basic design of the electrochemical detection cell for paper-based microfluidic devices. WE: working electrode, RE: reference electrode, CE: counter electrode.

6.2.4 Design and preparation of paper-based microfluidic devices for multianalyte determination

The characterization of electrochemical detection for paper-based microfluidic devices was firstly studied by dropping 5 μL of 0.1 M potassium phosphate buffer solution (pH 6) on the end of the paper at the detection zone. The solution flowed directly through the electrode zone and cyclic voltammetry was performed using a CH Instruments 1207A potentiostat. The scan rate dependence was studied at the carbon electrode containing PB. In addition to single analyte devices, multianalyte systems were fabricated using the method described above. A photograph showing the design is shown in Figure 6.2. Each reaction area was spotted with different enzymes for the specific analytes of interest. The glucose, lactate, and uric acid test zones were prepared by spotting 0.3 μL of glucose oxidase solution (645 U/mL), lactate oxidase (114 U/mL), and uricase solution (27 U/mL), respectively into the respective test zones. The paper was allowed to dry at room temperature for 10 min. All standard and enzyme solutions were prepared in 0.1 M potassium phosphate buffer (pH 6). For analysis, 5 μL of standard or sample solution was dropped on the center of paper and subsequently flowed to each test zone. Direct current chronoamperometry were then used for analysis at the screen-printed carbon PB-mediated electrode. The sampling rate for all chronoamperometric analyses was 10 Hz.

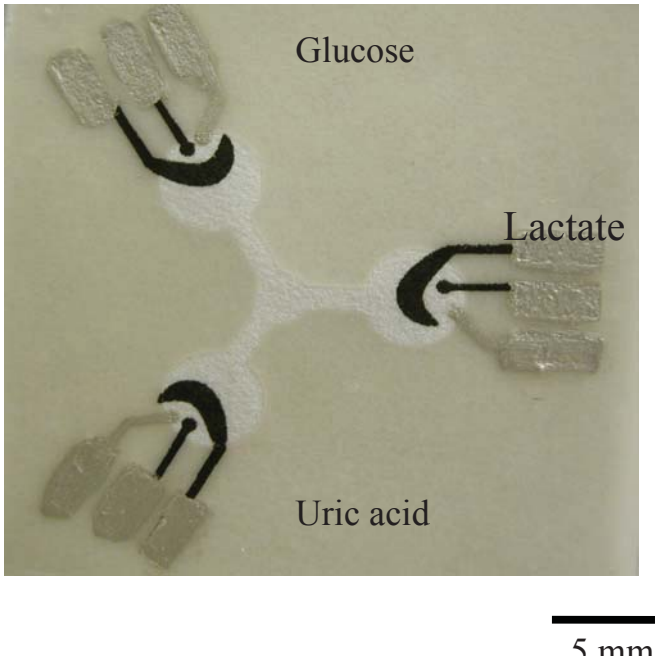

Figure 6.2 Picture of a three electrode paper-based microfluidic devices. The hydrophilic area at center of the device wicks sample into the three separate test zones where independent enzyme reaction occur. The silver electrodes and contact pads are made from Ag/AgCl paste with the black electrode portions are the PB-modified carbon electrodes. The device size is 4 cm x 4 cm.

6.2.5 Human serum sample

Human control serum samples (levels I and II) were obtained from Pointe Scientific (Canton, MI). Levels of analytes were provided by the supplier. All samples were analyzed using electrochemical detection for paper-based microfluidic without any pretreatment.

6.3 Results and discussion

The recent development of paper microfluidics has generated considerable excitement because of their ease of use, very low cost, and portability for point-of-care monitoring. To date, all reported systems have used colorimetric detection. While colorimetric detection is the

simplest detection mode, it has several significant problems as discussed previously. Here we report the development of an electrochemical detection scheme for quantitative analysis in paper microfluidics. Electrochemical detection, while more expensive than visual-based colorimetric detection, is still very low cost and requires minimal instrumentation. Here we demonstrate characterization of screen printed electrodes fabricated on paper microfluidic devices followed by their use for the measurement of clinically relevant analytes in a biological matrix using enzyme modified electrodes.

6.3.1 Characterization of electrochemical detection for paper-based microfluidic devices

Before using the devices for measuring analytes in biological samples, the functionality of the electrodes was established. The electrodes were screen-printed on the hydrophilic and hydrophobic area of paper with the working area of the electrodes on the hydrophilic portion of the device. To demonstrate proper electrode functionality and isolation of the leads by the hydrophobic photoresist underlayer characterization of the PB electrodes using cyclic voltammetry of buffer samples was performed. After dropping solution at the entrance of the microfluidic channel and allowing the test solution to wet the electrode area, cyclic voltammetry was performed. The redox reaction for PB is as follows:

$$Fe^{III}_4[Fe^{II}(CN)_6]_3 + 4K^+ + 4e^- \rightleftharpoons K_4Fe^{II}_4[Fe^{II}(CN)_6]_3 \qquad (10)$$

The characteristic voltammograms as a function of scan rate for PB (Iron (III) hexacyanoferrate (II)) [23] are shown in Figure 6.3. These results agree well with published results for PB electrodes [23]. Next, the dependence of the PB peak current on the scan rate was studied for the electrochemical system on paper. Figure 4.4 shows anodic and cathodic peak currents were directly proportional to the square root of scan rate between 2.5 and 100 mV/s. It should be

noted that the slopes of the forward and reverse sweeps are not identical as would be found at most traditional electrode materials. The differences in slope could be the result of the use of a surface confined redox species (Prussian Blue) coupled with the expected non-ideal behavior of these carbon electrodes [23]. The linearity however indicates the mass transfer in this system is a diffusion controlled process similar to the behavior of traditional electrochemical cells [23-27]. A diffusion controlled process in this system represents the diffusion of potassium ions within the PB lattice in the plating phase of electrode [26-27].

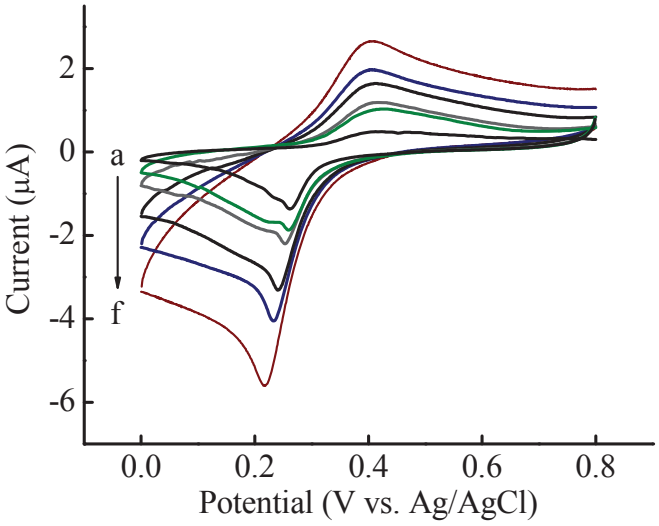

Figure 6.3 Representative cyclic voltammograms of the PB-modified carbon electrodes at various scan rates (a: 2.5, b: 5, c: 10, d: 25, e: 50, f: 100 mV/s) in 0.1 M potassium phosphate buffer (pH 6).

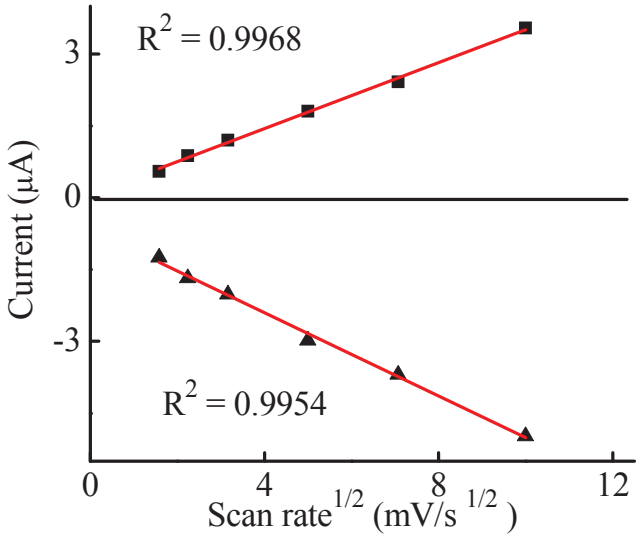

Figure 6.4 The relationship between anodic and cathodic currents and the square root of scan rate.

6.3.2 Choice of detection potential for hydrogen peroxide

The utility of our system was next demonstrated for different oxidase enzymes. Oxidase enzymes catalyze the oxidation of a substrate such as glucose, uric acid, or lactate while reducing oxygen to hydrogen peroxide (H_2O_2). Many electrochemical biosensors using enzymes rely on detection of peroxide for quantification of the analyte. Therefore, it is necessary to have methods for the detection of hydrogen peroxide at a low oxidation potential where few biologically relevant analytes will interfere. The most common electrochemical method is the anodic oxidation of H_2O_2 at a platinum electrode [28-30]. However, platinum is expensive and requires advanced patterning methods that dramatically increase the cost of fabrication [30]. Alternatively, screen-printed carbon electrodes that are significantly cheaper to produce can be used, however the high overpotential and subsequent interference from matrix species such as

ascorbic acid and uric acid represents a significant problem for plain carbon electrodes [31]. One way to minimize the problem is by using the cathodic reduction of H_2O_2 aided by a catalytic redox mediator (e.g., Prussian Blue (PB) [23], cobalt hexacyanoferrate [32], or horseradish peroxidase) [20,33-35]. For the current study, PB was used as the mediator on the electrode because it has been shown to be a selective catalyst for H_2O_2 reduction [36,37]. The catalytic reaction occurs in a relatively low potential region (-0.2 to 0.2 V versus Ag/AgCl) where interferences from endogenous compounds such as uric and ascorbic acid are minimal. Moreover, PB is an inexpensive material that is easy to incorporate with the paper-based screen-printed electrode.

The modified electrode was first characterized in the absence of H_2O_2 (Figure 4.5A, dashed line), and provided the characteristic anodic and cathodic peak of Prussian blue. Next, the catalytic nature of this electrode to the reduction of H_2O_2 was studied. Figure 6.5A (solid line) clearly shows a larger cathodic peak in the presence of 1 mM H_2O_2 relative to the background electrolyte. After characterizing the modified electrodes with cyclic voltammetry, a detailed investigation was conducted using chronoamperometry to optimize the detection potential, generate calibration data, and apply the proposed method to real samples. Chronoamperometry was used instead of cyclic voltammetry because it is a more sensitive, can achieve lower detection limits, and, for long-term applicability, is an easier detection method to implement. Hydrodynamic voltammetry (HDV) was first employed to optimize the detection potential for H_2O_2 in the range of 0.1 to -0.2 V. Analyte solution containing H_2O_2 was deposited in the microfluidic channel and the current measured at a fixed time with different potentials. The cathodic current of the H_2O_2 significantly increased as the detection potentials increased; however, the background current also increased as shown in Figure 6.5B. Therefore, ratios

between H_2O_2 and background current (S/B) were considered. Figure 6.5C shows S/B ratio at each potential. The ratio signal had a maximum of 0 V versus the on-chip Ag/AgCl reference electrode so a detection potential of 0 V was selected for further studies. Higher potentials were not investigated because of the concern over interfering reactions with endogenous compounds.

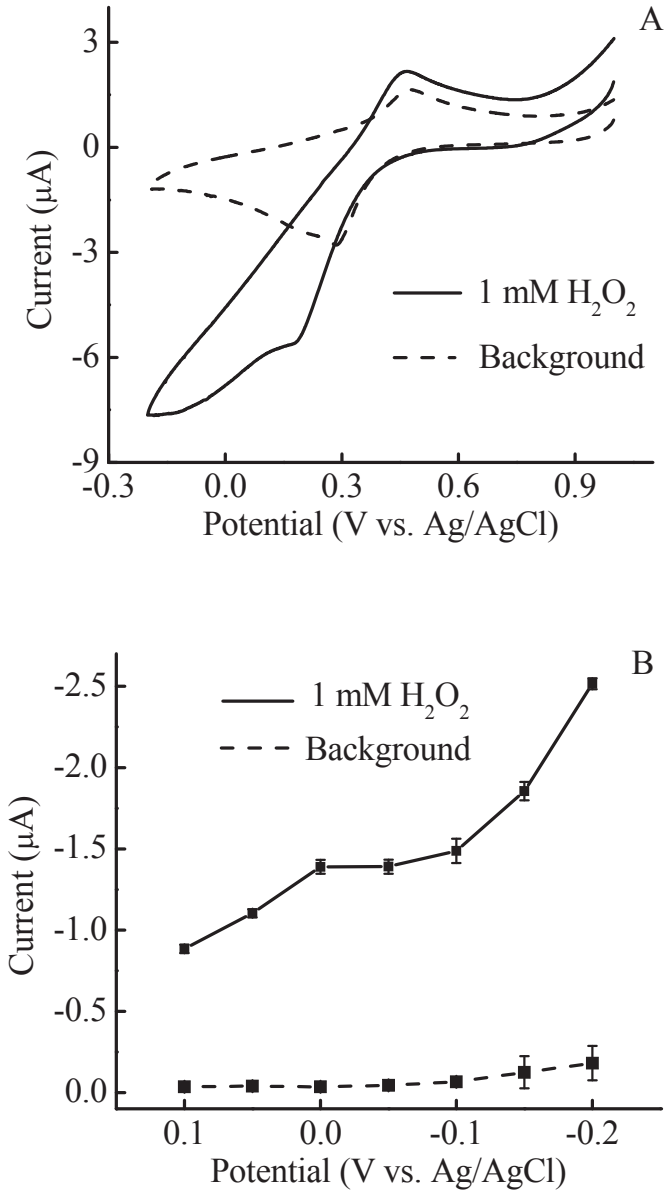

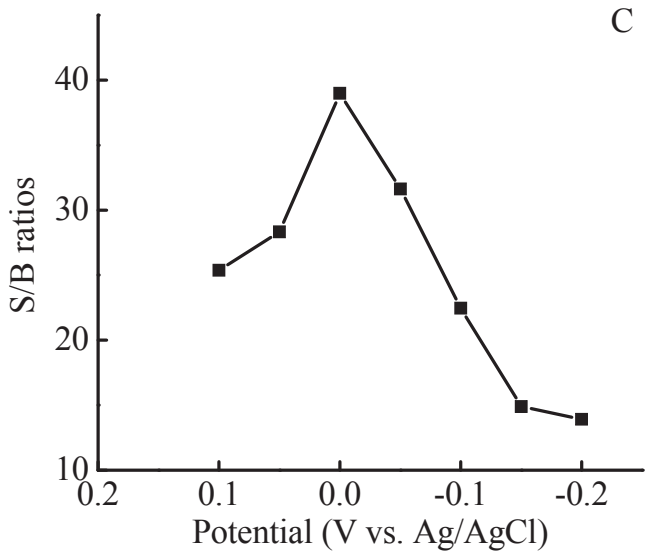

Figure 6.5 (A) Cyclic voltammograms of the carbon mediator Prussian blue electrode in the absence (dashed line) and presence of 1 mM H_2O_2 (solid line) at a 100 mV/s scan rate. (B) Hydrodynamic voltammograms of 1 mM H_2O_2 (solid line), and background (dashed line) for 100 s sampling time, from 3 separate devices. (C) Hydrodynamic voltammogram of signal-to-background ratios extracted from the data shown in B.

Moreover, analytical performance of H_2O_2 using our devices was demonstrated under the optimal detection potential. It obtained that a linear calibration curve between H_2O_2 concentration and the anodic current was between 0 to 0.1 mM (cathodic current, μA = -1.265 (H_2O_2 conc., mM) -0.082, R^2 = 0.9945). The limit of detection (LOD) and limit of quantitation (LOQ) were found at 3.6 ±0.3 and 11.9 ±1.1 μM (conc. ±SD, *n* = 3), respectively as shown in Figure 6.6.

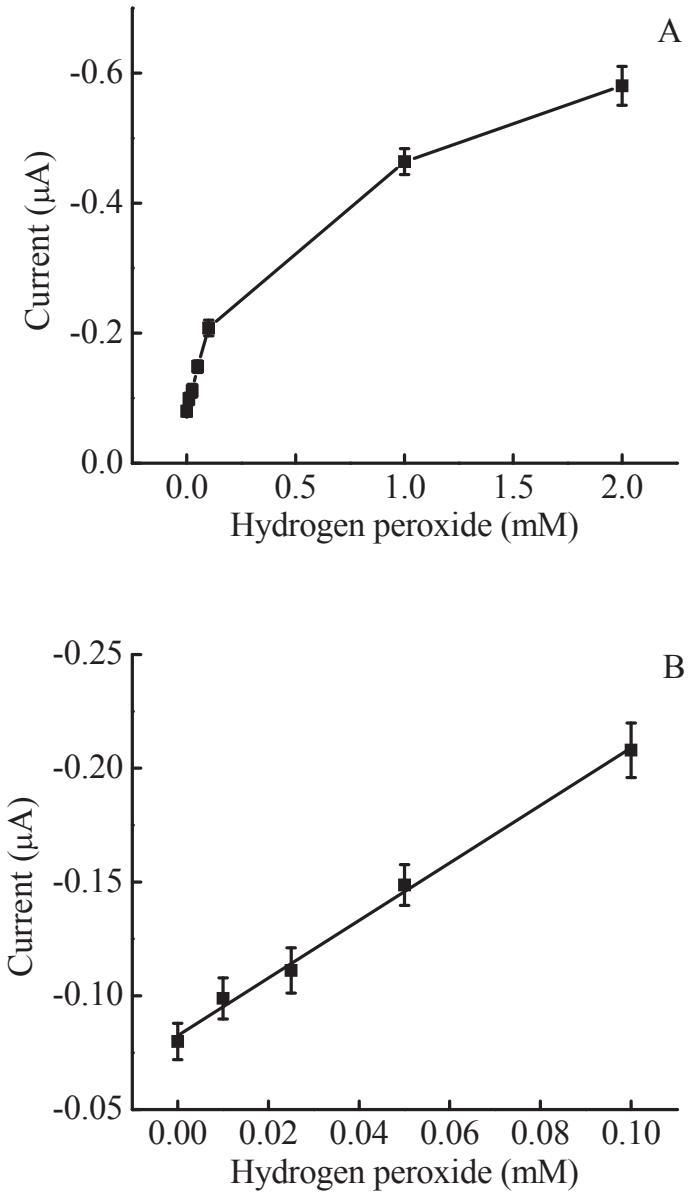

Figure 6.6 The relationship between cathodic current and hydrogen peroxide concentration in the range 0-2 mM (A) and 0-0.10 mM (B).

6.3.3 Analytical performance

After determining the optimal detection potential, the anodic current was recorded at 100 s, the apparent steady state current, to generate a linear calibration curve for a three electrode system consisting of glucose, lactate, and uric acid oxidase on each of three electrodes (Figure 6.7). The average and standard deviation in Figure 6.7 are the mean and relative standard deviation, respectively, from 3 separate devices. The relative standard deviations of all concentrations of glucose, lactate, and uric acid was less than 14% (n=3), demonstrating acceptable reproducibility for this type of device. Calibrations of the anodic current against concentrations generated linear functions for all of the analytes within a range between 0 and 100 mM, and the coefficients of determination (R^2) were higher than 0.993. The limits of detection (LOD) and limit of quantitation (LOQ) were calculated as the concentration which produced the signal at three and ten times, respectively the standard deviation of a blank (n = 10) are summarized in Table 6.1.

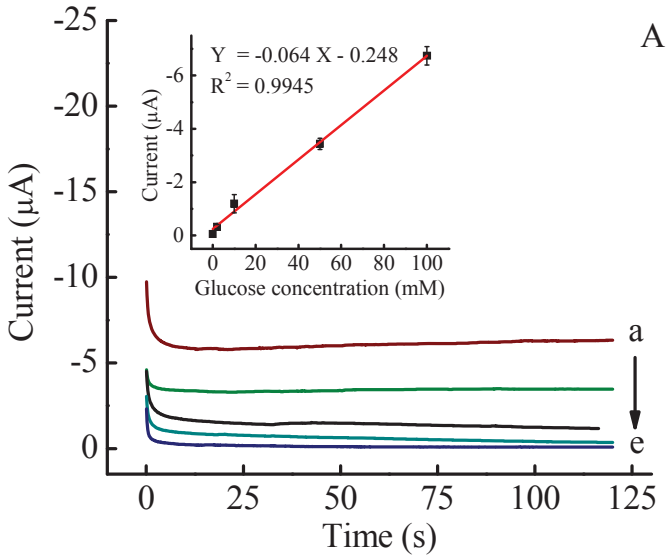

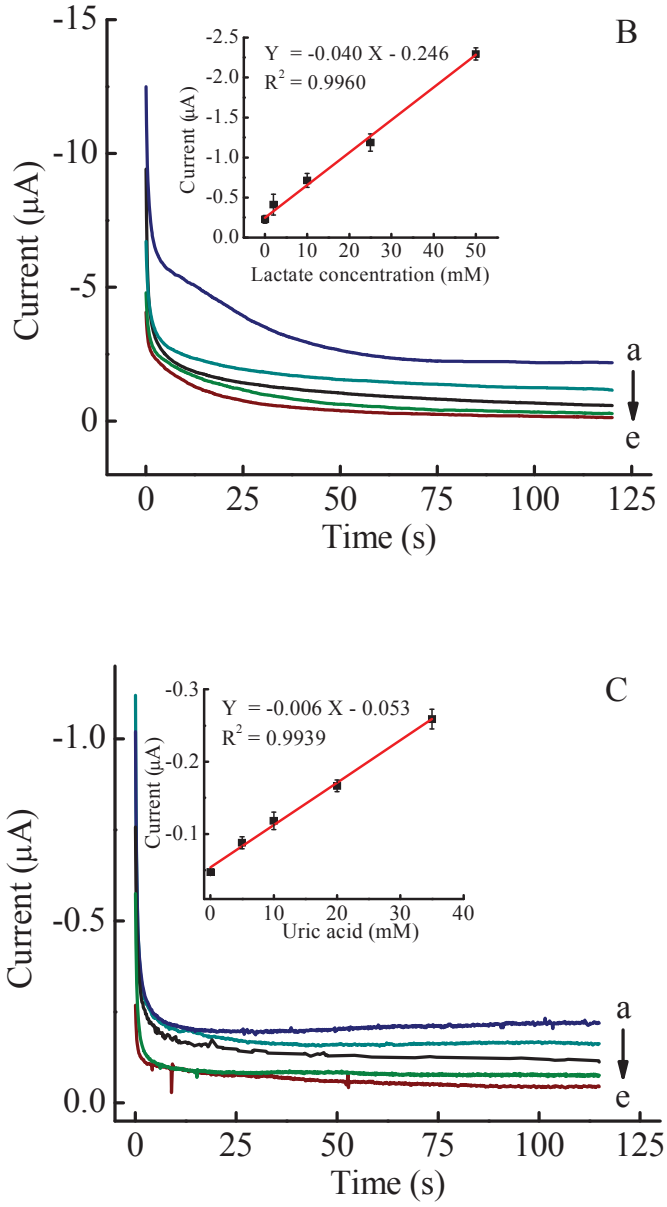

Figure 6.7 Chronoamperograms of (A) glucose (a: 100, b: 50, c: 10, d: 2 mM, e: Background), (B) lactate (a: 50, b: 25, c: 10, d: 2 mM, e: Bg), and (C) uric acid (a: 35, b: 20, c: 10, d: 5 mM, e: Bg) determination at 0 V versus an on-chip Ag/AgCl. The calibration plot of

anodic currents at 100 s of sampling time for determination of three analytes are shown in the insert, $n = 3$.

Table 6.1 Linear dynamic range, limit of detection and limit of quantification of the proposed method

Analyte	Linear dynamic range (mM)	LOQ (mM)	LOD (mM)
Glucose	0-100	0.7	0.2
Lactate	0-50	1.2	0.4
Uric acid	0-35	4.6	1.4

The LOD for glucose was found to be substantially lower (0.2 mM) than the camera detection method (0.5 mM) [13]. The normal level of glucose is 3.5-5.3 mM in whole blood, 2.5-5.3 mM in serum, and 0.1-0.8 mM in urine [38]. Conventional blood glucometers can detect levels as low as 1.7 mM [39], while more modern glucometers can detect glucose as low as 0.6 mM in urine [30]. Our device should therefore be comprehensive for the determination of glucose in all biological samples including serum, blood and urine. The LOD of lactate was found to be 0.4 mM. Even though our LOD is higher than the LOD of conventional lactate kit (0.02 mM) [40], it is sufficient for clinical diagnostics where the normal concentration of lactate is 0.7-1.7 mM in blood, 0.5-1.7 mM in serum, and 5.5-22 mM in urine [38]. Uric acid had a measured LOD of 1.4 mM. Commercially available uric acid assay kits can detect as low as 13

μM [41]. The normal level of uric acid is 0.1-0.4 mM in serum and 1.5-4.4 mM in urine [38]. Further improvements in the LOD for uric acid and the other markers can be obtained by improving the enzyme loading on the paper.

6.3.4 Analytical applications

In order to evaluate the electrochemical paper microfluidic system with real samples, three replicate determinations of glucose, lactate, and uric acid in clinical control samples were carried out using the optimized conditions. The control samples are common systems for determining the accuracy of diagnostic tests in a biologically relevant matrix without worry of blood borne pathogens. The results are shown in Table 6.2. The paired *t*-test was used to validate our method versus the control levels for glucose and lactate. No significant difference was found at the 95% confidence level. Thus, the analyzed values of glucose and lactate in human serum can be accepted. We also tried to measure uric acid in the control samples, but the 0.4 mM concentration was below our LOD (1.4 mM). Therefore, we measured uric acid in spiked samples. The control samples (level I) were spiked with uric acid at 5 and 10 mM and analyzed without any additional treatment. The 5 and 10 mM uric acid spiked samples were measured to contain 5.9 ±0.7 and 10.6 ±1.3 mM, respectively. After subtracting the level of uric acid in control samples (level I: 0.4 mM), recoveries of uric acid were obtained in the range of 102-110%. Although our method cannot detect uric acid in the control serum samples, it can be successfully applied to the determination of uric acid in spiked control samples.

Table 6.2 Determination of glucose, lactate, and uric acid in control samples

Analyte	Concentration (mM ±SD[a])			
	Human serum level I		Human serum level II	
	Certified Value	Proposed method	Certified Value	Proposed method
Glucose	5.3 ±0.3	4.9 ±0.6	16.5 ±0.7	16.3 ±0.7
Lactate	1.4 ±0.1	1.2 ±0.2	3.5 ±0.1	3.2 ±0.3
Uric acid	0.4 ±0.1	ND[b]	0.6 ±0.1	ND[b]

[a] SD: standard deviation (n=3), [b] ND: not detectable

6.4 Summary

We demonstrate here for the first time the coupling of electrochemical detection and paper microfluidics to provide rapid quantitative measurement of critical health markers in blood. In this work, the biological sample matrix and sample color have negligible effect on the glucose, lactate, and uric acid determination in real sample due to both selectivity of enzyme reaction and the working electrode material and detection potential (0 V versus Ag/AgCl). Paper-based microfluidic devices have not been previously applied to real biological samples therefore we have employed electrochemical detection for paper-based microfluidic devices for the determination of glucose and lactate in real world samples for the very first time, which demonstrates the feasibility of using paper microfluidic devices in medical diagnosis.

6.5 References

[1] Altinier, S.; Zaninotto, M.; Mion, M.; Carraro, P.; Rocco, S.; Tosato, F.; Plebani, M. Point-of-care testing of cardiac markers: results from an experience in an Emergency Department. Clin. Chim. Acta. 311 (2001): 67-72.

[2] Sia, S. K.; Kricka, L. J. Microfluidics and point-of-care testing. Lab Chip 8 (2008): 1982-1983.

[3] Burns, M. A.; Johnson, B. N.; Brahmasandra, S. N.; Handique, K.; Webster, J. R.; Krishnan, M.; Sammarco, T. S.; Man, P. M.; Jones, D.; Heldsinger, D.; Mastrangelo, C. H.; Burke, D. T. An Integrated Nanoliter DNA Analysis Device. Science. 282 (1998): 484-487.

[4] Lin, R.; Burke, D. T.; Burns, M. A., Selective extraction of size-fractioned DNA samples in microfabricated electrophoresis devices. J. Chromatogr., A 1010 (2003): 255-268.

[5] Shrinivasan, S.; Norris, P. M.; Landers, J. P.; Ferrance, J. P. A Low-Cost, Low-Power, Consumption Miniature Laser-Induced Fluorescence System for DNA Detection on a Microfluidic Device. J. Assoc. Lab Automation 11 (2006): 254-259.

[6] Wen, J.; Guillo, C.; Ferrance, J. P.; Landers, J. P. Microfluidic-Based DNA Purification in a Two-Stage, Dual-Phase Microchip Containing a Reversed-Phase and a Photopolymerized Monolith. Anal. Chem. 79 (2007): 6135-6142.

[7] Zheng, J.; Webster, J. R.; Mastrangelo, C. H.; Ugaz, V. M.; Burns, M. A.; Burke, D. T. Integrated plastic microfluidic device for ssDNA separation. Sens. Actuators, B 125 (2007): 343-351.

[8] Martinez, Andres W.; Phillips, Scott T.; Butte, Manish J.; Whitesides, George M., Patterned Paper as a Platform for Inexpensive, Low-Volume, Portable Bioassays 13. Angew. Chem. Int. Ed. 46 (2007): 1318-1320.

[9] Zhao, W.; Berg, A. v. d. Lab on paper. Lab Chip 8 (2008): 1988-1991.

[10] Abe, K.; Suzuki, K.; Citterio, D. Inkjet-Printed Microfluidic Multianalyte Chemical Sensing Paper. Anal. Chem. 80 (2008): 6928-6934.

[11] Li, X.; Tian, J.; Nguyen, T.; Shen, W. Paper-Based Microfluidic Devices by Plasma Treatment. Anal. Chem. 80 (2008): 9131-9134.

[12] Martinez, A. W.; Phillips, S. T.; Wiley, B. J.; Gupta, M.; Whitesides, G. M. FLASH: A rapid method for prototyping paper-based microfluidic devices. Lab Chip 8 (2008): 2146-2150.

[13] Martinez, A. W.; Phillips, S. T.; Carrilho, E.; Thomas, S. W.; Sindi, H.; Whitesides, G. M. Simple Telemedicine for Developing Regions: Camera Phones and Paper-Based Microfluidic Devices for Real-Time, Off-Site Diagnosis. Anal. Chem. 80 (2008): 3699-3707.

[14] Wang, J. Electrochemical biosensors: Towards point-of-care cancer diagnostics. Biosens. Bioelectron. 21 (2006): 1887-1892.

[15] Holcomb, R. E.; Kraly, J. R.; Henry, C. S. Electrode array detector for microchip capillary electrophoresis. Analyst. 134 (2009): 486-492.

[16] Matson, W. R.; Langlais, P.; Volicer, L.; Gamache, P. H.; Bird, E.; Mark, K. A. n-Electrode three-dimensional liquid chromatography with electrochemical detection for determination of neurotransmitters. Clin. Chem. 30 (1984): 1477-1488.

[17] Alvarez-Icaza, M.; Bilitewski, U. Mass production of biosensors. Anal.Chem. 65 (1993): 525A-533A.

[18] Martin, R. S.; Gawron, A. J.; Lunte, S. M.; Henry, C. S. Dual-Electrode Electrochemical Detection for Poly(dimethylsiloxane)-Fabricated Capillary Electrophoresis Microchips. Anal. Chem. 72 (2000): 3196-3202.

[19] Jiang, L.; Lu, Y.; Dai, Z.; Xie, M.; Lin, B. Mini-electrochemical detector for microchip electrophoresis. Lab Chip 5 (2005): 930-934.

[20] Tangkuaram, T.; Ponchio, C.; Kangkasomboon, T.; Katikawong, P.; Veerasai, W. Design and development of a highly stable hydrogen peroxide biosensor on screen printed carbon electrode based on horseradish peroxidase bound with gold nanoparticles in the matrix of chitosan. Biosens. Bioelectron. 22 (2007): 2071-2078.

[21] Chiu, M. H.; Wu, H.; Chen, J. C.; Muthuraman, G.; Zen, J. M. Disposable Screen-Printed Carbon Electrodes for Dual Electrochemiluminescence/Amperometric Detection: Sequential Injection Analysis of Oxalate. Electroanalysis. 19 (2007): 2301-2306.

[22] Song, Y. S.; Muthuraman, G.; Chen, Y.-Z.; Lin, C. C.; Zen, J. M. Screen Printed Carbon Electrode Modified with Poly(L-Lactide) Stabilized Gold Nanoparticles for Sensitive As(III) Detection. Electroanalysis. 18 (2006): 1763-1770.

[23] O'Halloran, M. P.; Pravda, M.; Guilbault, G. G. Prussian Blue bulk modified screen-printed electrodes for H_2O_2 detection and for biosensors. Talanta. 55 (2001): 605-611.

[24] Hong, C.; Yuan, R.; Chai, Y.; Zhuo, Y. Amperometric Immunosensor for the Determination of alpha-1-Fetoprotein Based on Core-Shell-Shell Prussian Blue-BSA-Nanogold Functionalized Interface. Electroanalysis. 20 (2008): 2185-2191.

[25] He, X.; Yuan, R.; Chai, Y.; Zhang, Y.; Shi, Y. A new antibody immobilization strategy based on electro-deposition of gold nanoparticles and Prussian Blue for label-free amperometric immunosensor. Biotechnol. Lett. 29 (2007): 149-155.

[26] Moscone, D.; D'Ottavi, D.; Compagnone, D.; Palleschi, G.; Amine, A. Construction and Analytical Characterization of Prussian Blue-Based Carbon Paste Electrodes and Their Assembly as Oxidase Enzyme Sensors. Anal. Chem. 73 (2001): 2529-2535.

[27] Zakharchuk, N. F.; Meyer, B.; Henning, H.; Scholz, F.; Jaworksi, A.; Stojek, Z. A comparative study of Prussian-Blue-modified graphite paste electrodes and solid graphite electrodes with mechanically immobilized Prussian Blue. J. Electroanal. Chem. 398 (1995): 23-35.

[28] Kawakami, M.; Koya, H.; Gondo, S. Immobilization of enzyme to platinum electrode and its use as enzyme electrode. Appl. Biochem. Biotechnol. 28-29 (1991): 211-219.

[29] Santoni, T.; Santianni, D.; Manzoni, A.; Zanardi, S.; Mascini, M. Enzyme electrode for glucose determination in whole blood. Talanta. 44 (1997): 1573-1580.

[30] Miyashita, M.; Ito, N.; Ikeda, S.; Murayama, T.; Oguma, K.; Kimura, J. Development of urine glucose meter based on micro-planer amperometric biosensor and its clinical application for self-monitoring of urine glucose. Biosens. Bioelectron. 24 (2009): 1336-1340.

[31] Tao, H.; Xian-En, Z.; Zhi-Ping, Z.; Li-Qun, C. A Screen-Printed Disposable Enzyme Electrode System for Simultaneous Determination of Sucrose and Glucose. Electroanalysis. 12 (2000): 868-870.

[32] Pauliukaite, R.; Florescu, M.; Brett, C. M. A. Characterization of cobalt- and copper hexacyanoferrate-modified carbon film electrodes for redox-mediated biosensors. J. Solid State Electrochem. 9 (2005): 354-362.

[33] Chen, X.; Li, C.; Liu, Y.; Du, Z.; Xu, S.; Li, L.; Zhang, M.; Wang, T. Electrocatalytic activity of horseradish peroxidase/chitosan/carbon microsphere microbiocomposites to hydrogen peroxide. Talanta. 77 (2008): 37-41.

[34] Zhang, J.; Oyama, M. A hydrogen peroxide sensor based on the peroxidase activity of hemoglobin immobilized on gold nanoparticles-modified ITO electrode. Electrochim. Acta. 50 (2004): 85-90.

[35] Lindgren, A.; Ruzgas, T.; Gorton, L.; Csoregi, E.; Bautista Ardila, G.; Sakharov, I. Y.; Gazaryan, I. G. Biosensors based on novel peroxidases with improved properties in direct and mediated electron transfer. Biosens. Bioelectron. 15 (2000): 491-497.

[36] Arkady, A. K. Prussian Blue and Its Analogues: Electrochemistry and Analytical Applications. Electroanalysis. 13 (2001): 813-819.

[37] Ricci, F.; Amine, A.; Tuta, C. S.; Ciucu, A. A.; Lucarelli, F.; Palleschi, G.; Moscone, D. Prussian Blue and enzyme bulk-modified screen-printed electrodes for hydrogen peroxide and glucose determination with improved storage and operational stability. Anal. Chim. Acta. 485 (2003): 111-120.

[38] Tietz, N. W. Clinical guide to laboratory tests. PA USA: W.B. Saunders Company, 1995.

[39] Magner, E. Treands in electrochemical biosensors. Analyst. 123 (1998): 1967-1970.

[40] Biovision. (Research products). www.biovision.com, 2008.

Chapter VII

Sodium dodecyl sulfate modified electrochemical paper-based analytical device for determination of dopamine levels in biological samples

7.1 Introduction

Dopamine (DA) is an important catecholamine that is involved in neurotransmission within the central and peripheral nervous systems [1] and plays a prominent role in the function of human metabolism, cardiovascular, renal, and hormonal systems [2]. In a healthy human, DA is found in the brain at ~50 nmol g^{-1} and in extracellular fluids at 0.01-1 μM. Abnormally low levels are associated with Parkinson's disease [3] and Alzheimer's disease [4] while abnormally high levels of DA are found in Attention-Deficit Hyperactivity Disorder [5], Huntington's disease [6] and Schizophrenia [7]. Because of the clinical significance of DA in these diseases a number of analytical methods have been developed with the goal of providing fast but sensitive, selective and reliable detection in complex biological samples. A variety of methods for DA detection have been reported previously, and include liquid chromatography [8-10], capillary electrophoresis [11-13], spectrofluorometry [14,15], electrogenerated chemiluminescence [16-18], mass spectrometry [19,20], microchip electrophoresis [21-23] and surface plasmon resonance [24-26]. These methods, however, are generally time-consuming, require complicated expensive instrumentation, and can only be carried out in the laboratory.

Of the common analytical methods for DA detection, electrochemical measurements have attracted increasing interest due to their speed, low cost, portability, high sensitivity and ability to make direct measurements in biological systems [27]. However, a significant problem for electrochemical-based DA detection is the presence of ascorbic acid (AA) and uric acid (UA)

since both AA and UA oxidize at similar potentials as DA and both are typically found at higher levels than DA, making it difficult to obtain selective quantification [28]. Various methods for electrode modification have been explored to improve DA selectivity. For instance, catalytic molecularly imprinted polymers [29], silanized graphene [30], carbon nanotube/magnetic particles [31], single-stranded DNA/poly(anilineboronic acid)/carbon nanotubes [32], and 2,4,6-triphenylpyrylium/zeolite Y [33] have been used to chemically modify electrodes. These methods, however, require expensive materials, as well as complicated and tedious fabrication steps. An alternative method to gain selectivity is through the use of surfactants. The use of surfactants for electrode modification [34] has previously been investigated for DA determination, where the cationic cetylpyridinium chloride [35], cetyltrimethylammonium bromide [36], and tetraoctylammonium bromide [37] were reported to enable the separation and simultaneous determination of AA and DA at micromolar levels in pharmaceutical samples. Sodium dodecyl sulphate (SDS) has been reported to improve DA detection selectivity when directly assembled into the electrode material [38,39] as well as when used as a masking agent [40] or molecular spacer [41]. The negatively charged SDS film formed on the electrode surface has been shown to improve the sensitivity and lower the detection limit as well as shift the oxidation potential for DA detection [28,29].

Here, a paper-based analytical device (PAD) is used to determine DA in the presence of SDS. PADs represent a new trend in analytical chemistry that builds on the combination of age old lateral flow immunoassays and paper-spot tests with modern abilities to perform photolithography to define small structures on a monolithic substrate [42]. PADs have several advantages, including low cost of materials, lightweight, flexibility, disposability, biodegradability, and power-free flow generation using capillary action. While the majority of

work with PADs has used colorimetric detection, other detection modes, such as chemiluminescence [43], electrochemiluminescence [44], mass spectrometry [45] and surface enhanced Raman spectroscopy [46], have been demonstrated. Electrochemical detection has also been used in this format. Dungchai et al. [47] demonstrated PADs with electrochemical detection (or ePADs) for the determination of glucose, lactate and UA in serum using oxidase enzymes to produce hydrogen peroxide for electrochemical detection. Nie et al. [48] reported a new design of ePADs for biosensors and metal detection applications, whilst Dossi et al. [49] proposed an amperometric gas sensor as a detector in flow injection analysis using paper-based screen-printed carbon electrodes (SPCE) with room temperature ionic liquids for the determination of 1-butanethiol vapors. Tan et al. [50] reported the use of a paper disk that was impregnated with zinc as an internal standard and bismuth for *in situ* electrode modification, respectively, for a more sensitive determination of Pb (II) levels in drinking water than the commercial SPCE without modified paper disk.

Here, we report the development of an ePAD-based assay for DA detection that possesses an enhanced selectivity and sensitivity through the use of the anionic surfactant SDS, impregnated in one layer of the device. The potential benefits of this device, including ease of operation, small sample volume, low cost, high selectivity for DA via electrostatic interactions with the negatively charged SDS, low detection limits from sample preconcentration, and a high reproducibility using a commercial SPCE, were evaluated. The time required to measure DA, the limit of detection (LOD) and the effect of biologically relevant interfering compounds were evaluated. Finally, this device was used for the determination of DA in human control serum samples.

7.2 Experimental

7.2.1 Materials and equipment

SU-8 negative photoresist and developer were purchased from MicroChem Corp. (Newton, MA). For square-wave voltammetry (SWV), a commercially available potentiostat (ED201 e-corder, eDAQ) was used. Disposable SPCEs on a ceramic substrate with a 4-mm disk carbon working electrode were obtained from Dropsens and connected to the potentiostat through a standard edge connector (Llanera, Spain). Electrochemical measurements were made in a Faraday cage to reduce electronic noise. All experiments were done at room temperature (22 ± 2 °C). Filter paper (No. 1, 11 cm diameter) was obtained from Whatman. 18 MΩ cm^{-1} resistance water was obtained from a Millipore Milli-Q water system. The supporting phosphate buffered saline (PBS) electrolyte was prepared as 0.8% (w/v) NaCl, 0.02% (w/v) KCl, 0.144% (w/v) Na_2HPO_3, 0.024% (w/v) KH_2PO_4 in Milli-Q water. All reagents, including DA, norepinephrine-bitartrate salt (NE), SDS, tetradecyltrimethylammonium bromide (TTAB) Sigma) and polyoxyethylene (20) sorbitan monolaurate (Tween-20) from Sigma, trichloroacetic acid (TCA), KH_2PO_4 and KCl from Fisher, Na_2HPO_4 (Mallinckrodt) and NaCl (Macron), were used as received without further purification. For the determination of DA levels in real serum samples, lyophilized human control serum sample (level I) was obtained from Pointe Scientific (Canton, MI). Prior to use, deionized water (5.0 mL) was added to rehydrate the human serum. All samples with TCA precipitation and sample pH adjustment as indicated were analyzed using electrochemical detection.

7.2.2 Fabrication of the Paper-Based Analytical Device (ePAD)

Patterned papers were fabricated using previously described methods [42,47]. Briefly, the transparency film photomask was designed with Adobe Illustrator CS5 software (Adobe Systems, Inc.) and printed by Chaiyaboon Co. (Bangkok, Thailand). The filter paper was coated with 4 g of SU-8 negative photoresist using a spin coater (G3P-8). After baking at 95 °C for 10 min, the photomask was placed above the coated paper and exposed to ultraviolet (UV) light with 100% intensity for 10 s (Intelli-ray 400). Areas exposed with UV light remained hydrophobic while unexposed areas were hydrophilic. The exposed paper was baked at 95 °C for 10 min followed by soaking in the SU-8 developer and then isopropanol for 3 min each, respectively. Finally, the patterned paper was dried in a hood at room temperature (22 ± 2 °C). Prior to use, paper microfluidic devices were exposed to air plasma (Harrick PDC-32G) for 2 min.

7.2.3 Electroanalytical Procedure for the Selective Determination of DA levels

The device consisted of three layers; (i) a layer of patterned paper containing a 7 mm diameter hydrophilic area for sample preconcentration, (ii) a 50 mm x 25 mm transparency film connector layer with two 5-mm diameter holes 5 mm apart, the second of which contains the selective, SDS-modified, transfer paper to wick the sample to (iii) a commercial SPCE for electrochemical detection of DA (Fig. 7.11A). The two holes in the transparency were designed to allow for sample preconcentration, by repeated 20 μl sample applications and drying, in the first hole followed by selective sample transfer through the second hole containing treated filter paper to the SPCE (third layer) (Fig. 7.1B).

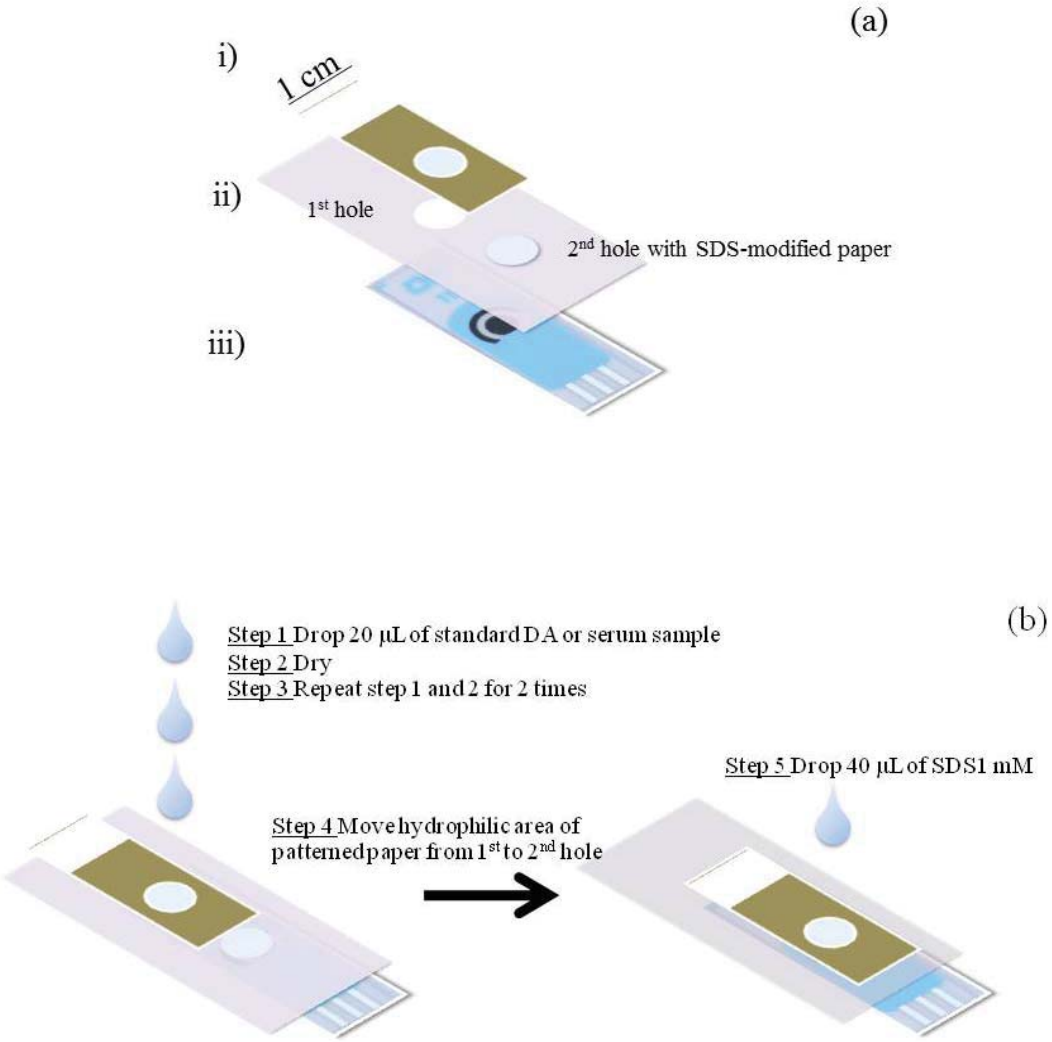

Figure 7. 1. (a) Schematic representation of the paper-based analytical device for determination of DA consisting of: (i) the patterned paper for sample preconcentration, (ii) the transparency film connector with two holes for sample preconcentration and for selective transport of DA

using a SDS-modified paper disk and wicking solution, respectively, and (iii) a commercial SPCE. **(b)** Sequence of operation steps for the selective determination of DA in human serum.

7.2.4 ePAD Operation

For operation, the selective transfer paper was prepared by adding 20 μL of 1 mM SDS in PBS adjusted to pH 2 with 3 M HCl and the paper was then placed into the second hole of the connector layer (Fig. 7.1B). Preconcentration of the analyte on the spot assay was first performed by adding 20-μL aliquots of the test sample to the hydrophilic circle (7 mm diameter) on the first layer, aligned above the first hole of the middle layer, and allowed to dry between applications. The hydrophobic barrier prevents the sample from spreading out and dispersing the analyte across the paper, whilst the first hole (without paper disk) of the middle layer prevents the leakage of the solution from the bottom of the patterned paper through to the third layer (SPCE) by making a space between the patterned paper and the commercial SCPE. This procedure was repeated two more times (unless otherwise noted) so as to non-specifically concentrate the sample. Next, the patterned paper was moved manually from first hole to the second hole of the connector (middle) layer, and 60 μL of the selective wicking solution (1 mM SDS in PBS at pH 2 except where specified otherwise) was added to the patterned paper. The solution was then transferred by wicking from the patterned paper to the SPCE (third layer) and SWV was performed without oxygen removal. The use of a commercial SPCE was chosen as the third layer because of the cost, stability, and availability of these electrodes.

The optimum parameters for SWV measurement were found in preliminary trials (data not shown) to be a pulse amplitude of 0.15 V, square wave frequency of 30 Hz, and a step height of 0.005 V for scanning the potential between -0.2 V to 0.8 V *vs*. Ag/AgCl, and so these

parameters were used throughout this study. Protein precipitation using TCA was used for serum sample preparation [51]. The sample was vortexed for 5 min following TCA addition to 0.6 M followed by centrifugation at 1073 rcf for 10 min and harvesting of the supernatant.

7.3 Results and discussion

7.3.1 Electrochemical Characterization of DA

Prior reports have shown that SDS can improve the specificity and sensitivity of DA detection in the presence of interfering analytes, such as AA and UA, through electrostatic interactions between the surfactant film on the electrode surface and the cationic DA [41]. In the presence of SDS, the electrode surface becomes negatively charged and preconcentrates the cationic catecholamines [52]. At the same time, the negatively charged surface of the electrode rejects common anionic interferences. To show this concept worked with the designed combination of a paper-spot device and a commercial SPCE, the detection of DA with and without SDS was investigated. The peak current for DA increased by approximately two-fold relative to a single sample application when three 20-μL (80 μM DA) sample applications (4.8 nmol total) were applied when no SDS was present in the wicking PBS buffer. However, 1 mM SDS was present in the same wicking solution the DA current increased approximately five-fold compared to the system without preconcentration and SDS (Fig. 7.2). SDS also shifted the oxidation potential down from 558 ± 21 mV to 419 ± 9 mV. This increase in peak current is believed to be the result of an increase in the mass of DA transported from the top layer to the middle layer contacted to electrode surface as well as the ability of the anionic surfactant to preconcentrate the DA at the electrode surface. The peak potential shift is most likely the result

of favorable interactions between the anionic head groups of the surfactant and the cationic DA [36].

Next, the quantity of 20-μL sample applications and the SDS concentration in the selective wicking solution were optimized. The highest numerical DA current response was observed after five 20-μL sample applications (8 pmol total) were applied to the preconcentration spot, but there was no statistically significant difference in the obtained current responses obtained from three to five sample applications. That additional applications did not significantly increase the peak current any further is most likely due to surface saturation. The SDS concentration in the wicking solution also had a significant effect on the DA peak current. When the SDS concentration was higher than 1 mM, electrode fouling occurred and the peak current decreased. In contrast, if the SDS concentration was less than 1 mM, the AA and DA oxidation peaks overlapped. Thus, SDS at 1 mM gave the optimal DA detection and so three 20-μL sample applications and a 40 μL PBS/ 1 mM SDS wicking solution were used for all remaining studies.

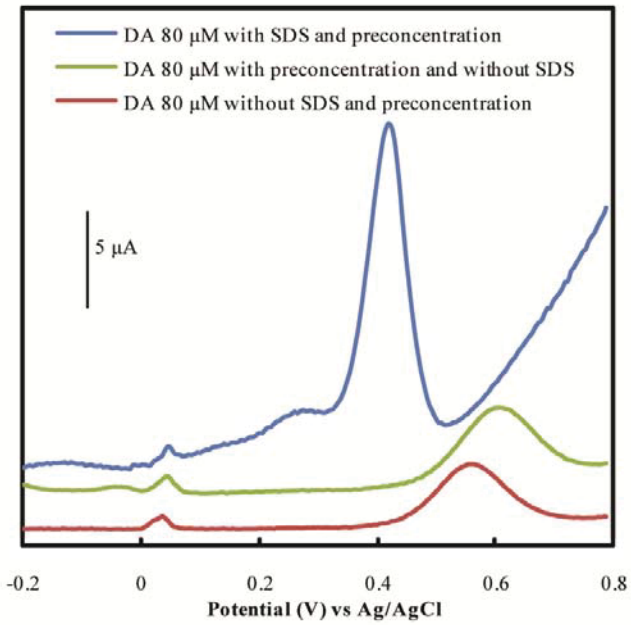

Figure 7.2. Representative DA voltammograms with or without preconcentration (three or one 20-µL applications of an 80 µM sample, respectively, yielding 4.8 or 1.6 nmol DA total) and with or without 1 mM SDS wicking solution. SWV detection conditions: pulse amplitude = 0.15 V, square wave frequency = 30 Hz, and step height = 0.005 V.

7.3.2 Analytical Performance and Interferences

AA and UA are generally present in biological samples at concentrations of 100- to 1000-fold higher than DA [52], whilst the highest AA and UA levels in normal human serum are 80 µM and 400 µM, respectively [47,53]. Therefore, the ability to selectively determine DA in the presence of AA and UA was studied using the highest anticipated serum concentrations for AA (80 µM) and UA (400 µM). In the absence of SDS in the wicking solution, the response of these compounds completely overlapped at ~ 600 mV. In contrast, their responses in the presence of 1 mM SDS in the wicking solution showed separate peaks at ~400 and 600 mV and a potential

difference ($E_{UA} - E_{DA}$) of around 200 mV (Fig. 7.3a). The individual voltammograms for DA, AA and UA, as well as the mixture of all three compounds, revealed that the anodic peak of AA was not observed under these conditions (Fig. 7.3). At pH 2, the separation of well-defined peaks with oxidation potentials for DA (red line) and UA (purple line) were 400 mV and 600 mV, respectively. These results clearly show the ability of the SDS-containing wicking solution and paper to provide selective determination of DA in the presence of AA and UA.

The linear range was found to be 1-100 μM, with a correlation coefficient (r^2) of 0.9949 and RSD of 4.32% (n = 3) (Fig. 7.4a-b). The LOD, evaluated using a signal-to-noise (S/N) ratio of three, was found to be 0.37 μM, which is similar to previously published studies using surfactant-modified electrodes. However, the limit of quantitation (LOQ), evaluated using a S/R ratio of 10, was 1.22 μM, which is lower than some previously published results using modified carbon electrodes [35,37,40]. Although the LOD and LOQ values reported here are higher than those obtained with a modified Pt electrode, the CPSE based e-PAD reported here does not require the complicated electrode modification strategies to achieve detection at physiologically relevant levels [52].

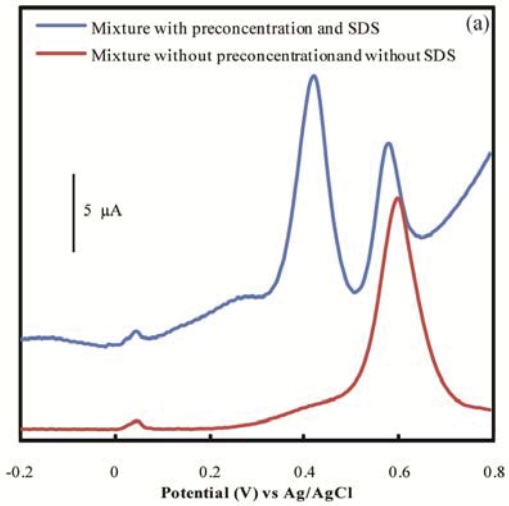

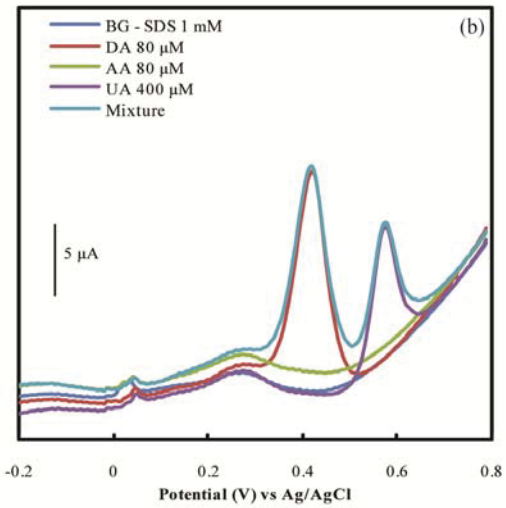

Figure 7.3. (a) Discrimination of the SDS enhancement effect between square-wave voltammograms for the mixture of samples of AA (80 µM), DA (80 µM) and UA (400 µM) with or without preconcentration (three or one 20-µL application, respectively) in presence or absence of 1 mM SDS in the wicking solution. **(b)** Representative voltammograms of no sample application (background; BG) or samples of AA (80 µM), DA (80 µM) and UA (400 µM) (4.8, 4.8 and 24 nmol total for AA, DA and UA, respectively) alone or a mixture of all three, using this system with optimum conditions (see Fig. 7.2 legend).

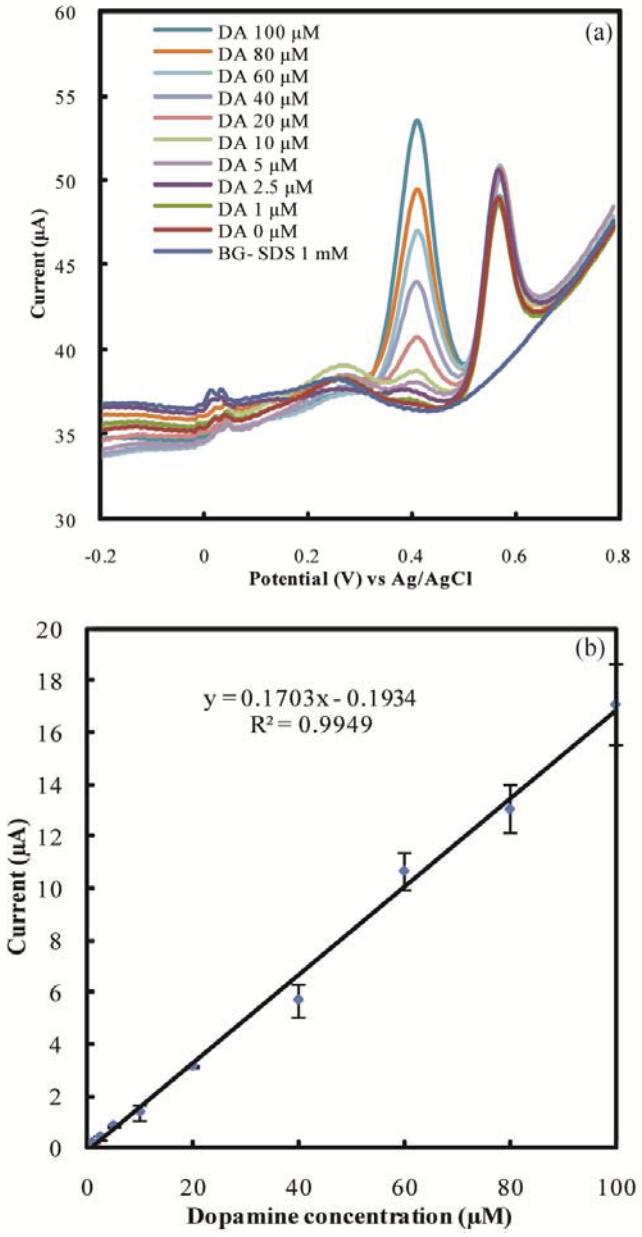

Figure 7.4. (a) Representative square-wave voltammograms and **(b)** the derived calibration curve for DA detection over a concentration range of 1 to 100 µM in the copresence of AA and UA at 80 µM and 400 µM (4.8 and 24 nmol total), respectively, and with 1 mM SDS in the PBS pH 2 wicking solution.

7.3.3 Analytical Application

To evaluate the performance of this system on complex biological samples, DA was analyzed in control serum samples. Control serum samples are used to standardize clinical assays and so to validate new diagnostic assays. Known concentrations of DA were added to the serum and then the protein precipitated by TCA and centrifugation. The protein-free serum supernatant was then added to the ePAD as three 20-μL applications as described previously. The resulting voltammograms revealed a dose-dependent DA response (Fig. 7.5a), from which the standard curve (Fig. 7.5b) showed acceptable linearity with a correlation coefficient (r^2) of 0.9979 (n = 3). These results clearly indicate the ability to measure DA levels in a biologically relevant sample.

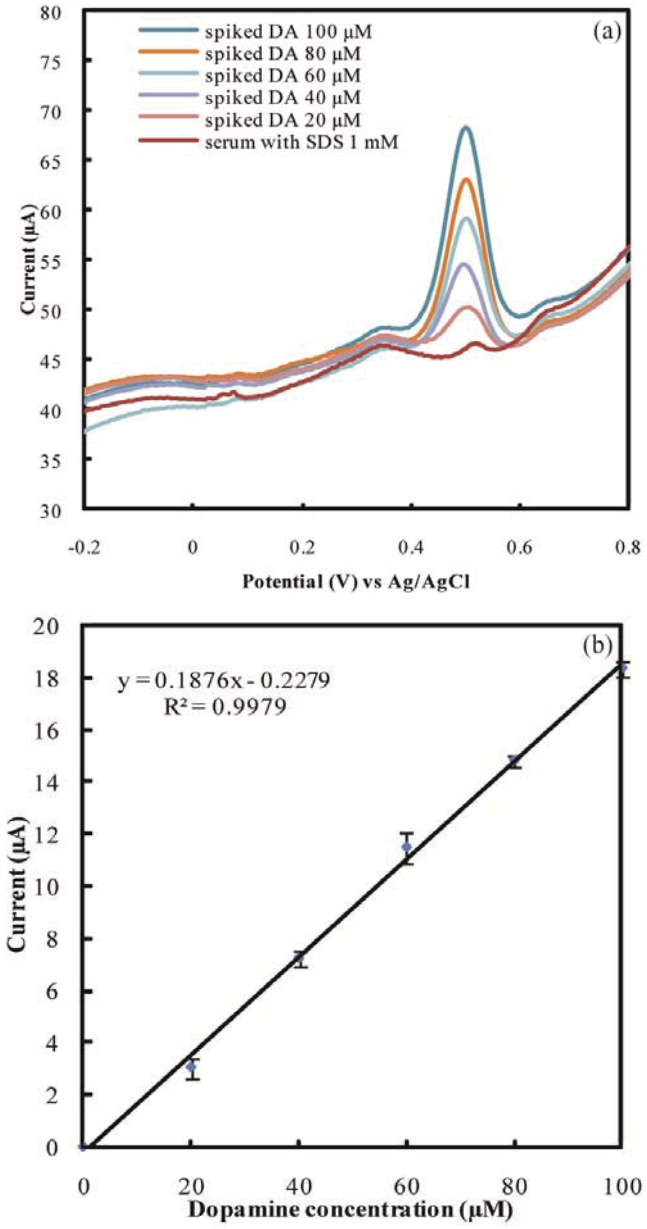

Figure 7.5. (a) Representative square-wave voltammograms and **(b)** the derived calibration curve of different spiked DA concentrations (20-100 µM; 1.2-6 nmol total) in human serum after the TCA protein precipitation step

7.3.4 Mechanism for Enhancement and Selective Detection of DA

The effect of surfactant chemistry on the performance of the ePAD was studied using the anionic SDS in comparison to the cationic TTAB and nonionic Tween-20 as representative members of the three charge classes of surfactants in the wicking solution. At pH 2, the anodic UA peak was barely visible at 600 mV in the TTAB-containing wicking solution and AA and DA signals were not detected (Fig. 7.6). This is due to repulsion between the positively charged compounds and the positively charged surfactant. In the case of Tween-20, the AA, DA and UA signals were not seen at any surfactant concentration, most likely due to electrode fouling [54,55]. Next, NE (pK_a = 8.6 [56]), a structurally similar catecholamine to DA, was studied with these surfactants to determine if structural variations in the analyte had any effect on the results. The anodic peak of NE was seen in the SDS system but not with TTAB or Tween-20 (Fig. S.D. 3), suggesting that the selectivity mechanism is primarily governed by the electrostatic interactions and not the structure of the compound.

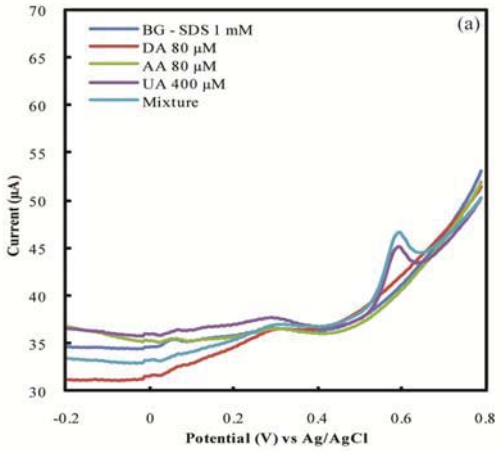

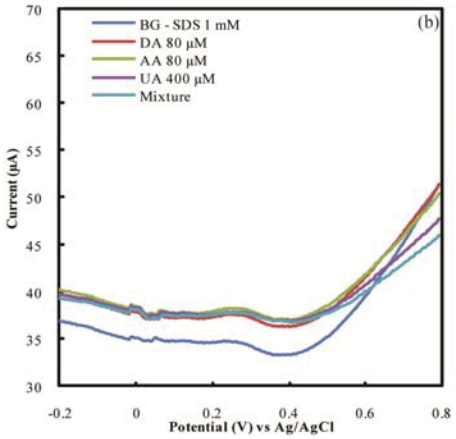

Figure 7. 6. Representative voltammograms of preconcentrated (three 20-µL applications) DA (80 µM), AA (80 µM) and UA (400 µM) (4.8, 4.8 and 24 nmol total for AA, DA and UA, respectively), applied individually or as a mixture of all three, and with no sample application (background; BG), using PBS pH 2 with **(a)** the cationic TTAB or **(b)** the nonionic Tween-20 surfactant as the wicking solution.

Finally, the impact of the pH of the wicking solution on the subsequent detection of DA was evaluated between pH 2 and 10 in the presence of 1 mM SDS. The peak potentials of DA and UA were dependent on the pH, whilst at 80 µM AA (4.8 nmol total applied DA) was not detectable at any tested pH (Fig. 7.7). This is because at a low pH, the generation of two protons during the electrooxidation is unfavorable [57,58], while at a higher pH, the negatively charged AA is difficult to oxidize because of the repulsion at the negative SDS film. In the presence of SDS, the DA response was highest and lowest at pH 2.0 and 5.0, respectively, with a current difference of 10.82 µA, while the peak current for UA was highest and lowest at pH 2.0 and 10.0, respectively, with a current difference of 7.63 µA. The trend in response was attributed to the ionization of DA and UA in the cationic form at a lower pH value (Fig. 7.7).

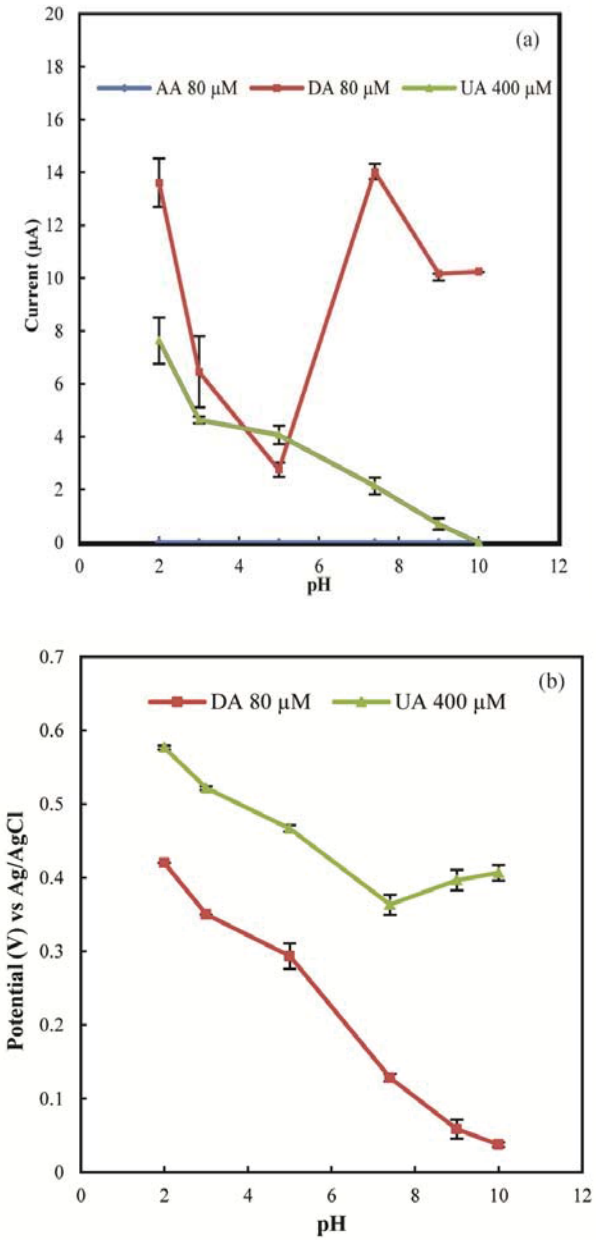

Figure 7.7. The effect of the pH value on **(a)** the peak current of AA (blue line), DA (red line) and UA (green line); and on **(b)** the oxidation peak potential of DA (red line) and UA (green line). Samples were preconcentrated as three 20-µL applications (DA and AA at 80 µM (4.8 nmol total), UA at 400 µM (24 nmol total)) and wicked with 1 mM SDS in PBS at the indicated pH values.

7.4 Summary

Here, a novel ePAD was demonstrated for determination of DA levels in serum that made use of a multilayer paper device coupled with selective transport of the cationic DA to the working electrode. Using a series of paper membranes and the addition of multiple aliquots of the test DA-containing sample, a significant preconcentration was achieved, along with an increase in the selectivity due to a shift in the oxidation potential. The system was tested with human serum, and the serum was shown to have a negligible effect on DA determination. The mechanism behind the selective enhancement of the signal is primarily the result of electrostatic interactions of the analytes with the anionic SDS.

7.5 References

[1] R.A. Wise, Nat. Rev. Neurosci. 5 (2004), 483-494.

[2] M. Heien, A.S. Khan, J.L. Ariansen, J.F. Cheer, P.E.M. Phillips, K.M. Wassum, R.M. Wightman, Proc. Natl. Acad. Sci. U. S. A. 102 (2005), 10023-10028.

[3] L. Studer, M. Psylla, B. Buhler, L. Evtouchenko, C.M. Vouga, K.L. Leenders, R.W. Seiler, C. Spenger, Brain Res. Bull. 41 (1996), 143-150.

[4] L.L. Liu, Q. Li, N.J. Li, J.H. Ling, R. Liu, Y.X. Wang, L.X. Sun, X.H. Chen, K.S. Bi, J. Sep. Sci. 34 (2011), 1198-1204.

[5] T. Puumala, J. Sirvio, Neuroscience 83 (1998), 489-499.

[6] R.J. Jakel, W.F. Maragos, Trends Neurosci. 23 (2000), 239-245.

[7] K.L. Davis, R.S. Kahn, G. Ko, M. Davidson, Am. J. Psychiat. 148 (1991), 1474-1486.

[8] P. Song, O.S. Mabrouk, N.D. Hershey, R.T. Kennedy, Anal. Chem. 84 (2012), 412-419.

[9] P. Uutela, L. Karhu, P. Piepponen, M. Kaenmaki, R.A. Ketola, R. Kostiainen, Anal. Chem. 81 (2009), 427-434.

[10] G. C. Davis, P. T. Kissinger, Anal. Chem. 51 (1979), 1960-1965.

[11] S.R. Wallenborg, L.Nyholm, C.E. Lunte, Anal. Chem. 71 (1999), 544-549.

[12] M.S. Shou, C.R. Ferrario, K.N. Schultz, T.E. Robinson, R.T. Kennedy, Anal. Chem. 78 (2006), 6717-6725.

[13] Y.M. Liu, C.Q. Wang, H.B. Mu, J.T. Cao, Y.L. Zheng, Electrophoresis 28 (2007), 1937-1941.

[14] Z.E. Seckin, M. Volkan, Anal. Chim. Acta 547 (2005), 104-108.

[15] H. Huang, Y. Gao, F.P. Shi, G.N. Wang, S.M. Shah, X.G. Su, Analyst 137 (2012), 1481-1486.

[16] L.L. Li, H.Y. Liu, Y.Y. Shen, J.R. Zhang, J.J. Zhu, Anal. Chem. 83 (2011), 661-665.

[17] Y.F. Hu, W. Xu, J.P. Li, L.J. Li, Luminescence 27 (2012), 63-68.

[18] F. Li, Y.Q. Pang, X.Q. Lin, H. Cui, Talanta 59 (2003), 627-636.

[19] H.B. Wei, H.F. Li, S.F. Mao, J.M. Lin, Anal. Chem. 83 (2011), 9306-9313.

[20] M. Grundmann, M. Rothenhofer, G. Bernhardt, A. Buschauer, F.M. Matysik, Anal. Bioanal. Chem. 402 (2012), 2617-2623.

[21] Q. Guan, C.S. Henry, Electrophoresis 30 (2009), 3339-3346.

[22] S.L. Zhao, Y. Huang, M. Shi, R.J. Liu, Y.M. Liu, Anal. Chem. 82 (2010), 2036-2041.

[23] C.M. Kang, S. Joo, J.H. Bae, Y.R. Kirn, Y. Kim, T.D. Chung, Anal. Chem. 84 (2012), 901-907.

[24] S. Kumbhat, D.R. Shankaran, S.J. Kim, K.V. Gobi, V. Joshi, N. Miura, Biosens. Bioelectron. 23 (2007), 421-427.

[25] L. Shang, S.J. Dong, Nanotechnology 19 (2008).

[26] M.A. Malvindi, R. Di Corato, A. Curcio, D. Melisi, M.G. Rimoli, C. Tortiglione, A. Tino, C. George, V. Brunetti, R. Cingolani, T. Pellegrino, A. Ragusa, Nanoscale 3 (2011), 5110-5119.

[27] R.M. Wightman, Science 311 (2006), 1570-1574.

[28] W. Siangproh, W. Dungchai, P. Rattanarat, O. Chailapakul, Anal. Chim. Acta 690 (2011), 10-25.

[29] D. Lakshmi, A. Bossi, M.J. Whitcombe, I. Chianella, S.A. Fowler, S. Subrahmanyam, E.V. Piletska, S.A. Piletsky, Anal. Chem. 81 (2009), 3576-3584.

[30] S.F. Hou, M.L. Kasner, S.J. Su, K. Patel, R. Cuellari, J. Phys. Chem. C 114 (2010), 14915-14921.

[31] E. Baldrich, F.X. Munoz, Anal. Chem. 83 (2011), 9244-9250.

[32] S.R. Ali, Y.F. Ma, R.R. Parajuli, Y. Balogun, W.Y.C. Lai, H.X. He, Anal. Chem. 79 (2007), 2583-2587.

[33] A. Domenech, H. Garcia, M.T. Domenech-Carbo, M.S. Galletero, Anal. Chem. 74 (2002), 562-569.

[34] R. Vittal, H. Gomathi, K.J. Kim, Adv. Colloid Interface Sci. 119 (2006), 55-68.

[35] A.P. dos Reis, C.R.T. Tarley, N. Maniasso, L.T. Kubota, Talanta 67 (2005), 829-835.

[36] X.L. Wen, Y.H. Jia, Z.L. Liu, Talanta 50 (1999), 1027-1033.

[37] S. Shahrokhian, H.R. Zare-Mehrjardi, Sens. Actuator B-Chem. 121 (2007), 530-537.

[38] J.W. Mo, B. Ogorevc, Anal. Chem. 73 (2001), 1196-1202.

[39] J.B. Zheng, X.L. Zhou, Bioelectrochemistry 70 (2007), 408-415.

[40] G. Alarcon-Angeles, S. Corona-Avendano, M. Palomar-Pardave, A. Rojas-Hernandez, M. Romero-Romo, M. Ramirez-Silva, Electrochim. Acta 53 (2008), 3013-3020.

[41] A. Marino, A. Brajtertoth, Anal. Chem. 65 (1993), 370-374.

[42] A.W. Martinez, S.T. Phillips, M.J. Butte, G.M. Whitesides, Angew. Chem.-Int. Edit. 46 (2007), 1318-1320.

[43] J.H. Yu, L. Ge, J.D. Huang, S.M. Wang, S.G. Ge, Lab Chip 11 (2011), 1286-1291.

[44] L. Ge, J.X. Yan, X.R. Song, M. Yan, S.G. Ge, J.H. Yu, Biomaterials 33 (2012), 1024-1031.

[45] J. Ho, M.K. Tan, D.B. Go, L.Y. Yeo, J.R. Friend, H.C. Chang, Anal. Chem. 83 (2011), 3260-3266.

[46] W.W. Yu, I.M. White, Anal. Chem. 82 (2010), 9626-9630.

[47] W. Dungchai, O. Chailapakul, C.S. Henry, Anal. Chem. 81 (2009), 5821-5826.

[48] Z.H. Nie, C.A. Nijhuis, J.L. Gong, X. Chen, A. Kumachev, A.W. Martinez, M. Narovlyansky, G.M. Whitesides, Lab Chip 10 (2010), 477-483.

[49] N. Dossi, R. Toniolo, A. Pizzariello, E. Carrilho, E. Piccin, S. Battiston, G. Bontempelli, Lab Chip 12 (2012), 153-158.

[50] S.N. Tan, L.Y. Ge, W. Wang, Anal. Chem. 82 (2010), 8844-8847.

[51] F. Bugamelli, C. Marcheselli, E. Barba, M.A. Raggi, J. Pharm. Biomed. Anal. 54 (2011), 562-567.

[52] N.F. Atta, A. Galal, R.A. Ahmed, Bioelectrochemistry 80 (2011), 132-141.

[53] N. Chauhan, J. Narang, C.S. Pundir, Analyst 136 (2011), 1938-1945.

[54] J.F. Rusling, Colloid Surf. A-Physicochem. Eng. Asp. 123 (1997), 81-88.

[55] R.A. Mackay, Colloid Surf. A-Physicochem. Eng. Asp. 82 (1994), 1-28.

[56] S.H. Huang, H.H. Liao, D.H. Chen, Biosens. Bioelectron. 25 (2010), 2351-2355.

[57] T. Hinoue, N. Kuwamoto, I. Watanabe, J. Electroanal. Chem. 466 (1999), 31-37.

[58] P. Karabinas, D. Jannakoudakis, J. Electroanal. Chem. 160 (1984), 159-167.

Chapter VIII

Fabrication of paper-based devices by lacquer spraying method for the determination of nickel (II) ion in waste water

8.1 Introduction

Paper-based device have the potential to be good alternative analytical devices for healthcare related applications because they are portable, easy to use, have a low sample volume requirement and provide rapid analysis [1, 2, 3]. Paper-based device is a device made of paper in which the main component is cellulose fiber. Paper is a low-cost material that is readily available and easy to manipulate. Therefore, paper-based devices have been widely popular and have many potential benefits in fields as diverse as environmental monitoring and clinical research. Currently, paper-based devices have become an interesting technology for research units, resulting in the development of method for the fabrication of paper-based devices. A lot of methods for fabricating the pattern on paper have been proposed, including photolithography [4-11], polydimethylsiloxane (PDMS) plotting [12], inkjet printing [13], cutting [14], plasma etching [15], wax printing [16,17,18], wax screen-printing [19], and wax dipping [20]. Each fabrication method has its own advantages and limitations that are similar and/or difference. The first reported method was based on photolithography. This method can provide approximately 200 μm of teeny barrier line width between hydrophilic and hydrophobic areas [6]. However, photolithography method concerned the use of organic solvents, expensive photoresists and photolithography apparatus. Moreover, the fabrication process involves many complicated processes. The PDMS plotting method also override the problems of physical inflexibility of devices using photolithography [11]. This method does not use expensive photoresists, organic solvent and photolithography instrument. Unfortunately, this method needs a customized plotter [10]. The inkjet printing method involves the use of organic solvent to print onto the polymer-soaked paper by inkjet printer

for creating hydrophilic area on the paper. Plasma etching is a method to detract sizing agent [19] coating on the paper using plasma treatment. However, paper-based devices created by photolithography, inkjet printing and plasma etching methods all still require organic solvents and polymers to create hydrophilic areas. In cutting method, a knife plotter is used to cut paper to create pattern of microfluidic channels. However, this method has to use tape to cleave the paper pattern, which is difficult in implementation. Wax printing method utilizes a commercially available wax printer for the fabrication of paper-based devices. This method is easy and fast to generate a patterned paper by wax printer. However, this method has a shallower barrier than photolithography (~850 μm of minimal barrier) because the spread of the wax is difficult to handle when a wax was melted on hotplate. So, careful infiltration of wax must be regarded before creation of the pattern in this method. Wax screen-printing method is similar to wax printing method by using a commercial wax for the fabrication of paper-based devices, but wax screen-printing does not require wax printer for fabrication. This method can create a pattern by using screen-printed block instead of the commercial printer. The advantages of wax screen-printing method are low-cost, simplicity, and rapidness. Nevertheless, wax screen-printing is difficult to produce the exact designed pattern with high barrier due to the spread of the wax. Recently, a new fabrication method for creating paper-based devices has been reported as wax dipping. Wax dipping does not demand expensive equipments and organic solvents. However, the hydrophobic areas generated by the wax printing, wax screen-printing and wax dipping methods still used the hot plate for melting wax. Moreover, limitations of these previous methods by wax are wax spreading before creating the pattern and the trained personnel for using and maintaining the instruments. To overcome these limitations, a simple, rapid and low-cost fabrication method, that also provides several advantages, needs to be developed. A spraying method with lacquer was therefore developed for the fabrication of paper-based devices.

Acrylic lacquer is made of acrylic resin. One of main characteristic features of acrylic resin is high transparency. Acrylic lacquer is one of polymer (resin) generated through chemical reaction by applying polymerization. The advantages of acrylic resin are water resistance, good adhesion and fast drying [22].

The objective of this work is to present a new concept of spraying method with lacquer for the fabrication of paper-based devices. To evaluate efficiency of this developed method, paper-based devices with electrochemical detection were used to determine nickel in waste water of a jewelry factory using the differential pulse anodic stripping voltammetry (DPASV) and copper-enhancing solution was used for increasing the sensitivity of nickel determination**.**

8.2 Materials and methods

8.2.1 Materials and chemicals

Whatman No. 1 (11μm porosity) and No. 4 (20-25 μm porosity) filter paper were purchased from Cole-Parmer (Vernon Hills, IL). Iron mask (1 mm thick) was made-to-order by a laser cutting shop in Bangkok. Magnetic plate and acrylic lacquer Leyland® manufactured by Nakoya Paint (Thailand) Co, Ltd. were purchased from a local area shop in Bangkok. Carbon ink was purchased from Gwent group (Torfaen, UK). Silver chloride ink (Electrodag 7019) was obtained from Acheson Colloids Company (Port Huron, MI). Electrochemical measurements were performed using a potentiostat (Autolab PGSTAT 30). All solutions were prepared in 18 $M\Omega cm^{-1}$ resistance deionized water (obtained from a Millipore Milli-Q purification system. A standard solution CertiPUR®, 1000 mgL^{-1} $Ni(NO_3)_2$ in HNO_3 2-3% was purchased from Merck and was used as the stock solution. Sodium chloride (NaCl) (99.5%) (Merck) and copper sulfate ($CuSO_4$) (99%) (BDH) were used as received

8.2.2 Spraying method with lacquer for fabrication of patterned on paper

The spraying method with lacquer was used to fabricate the pattern on a filter paper. The iron mask (Fig. 8.1a), which was designed by an Adobe Illustrator and was manufactured using laser cutting technique, was used to create cover pattern on the paper. Hydrophobic area was created by spraying method. To fabricate paper-based devices (Fig. 8.1b), the paper was first put on a magnetic plate. Next, the iron mask was placed on the other side of the paper and it was temporarily attached by means of magnetic force with a magnetic plate placed on the backside of the paper. Then, the paper was sprayed with lacquer creating the hydrophobic barrier around the iron mask. After that, the paper was air-dried and the iron mask was removed from the paper. Finally, the images of hydrophobic and hydrophilic areas of the pattern on the paper were characterized using an optical microscope and scanning electron microscopy (SEM).

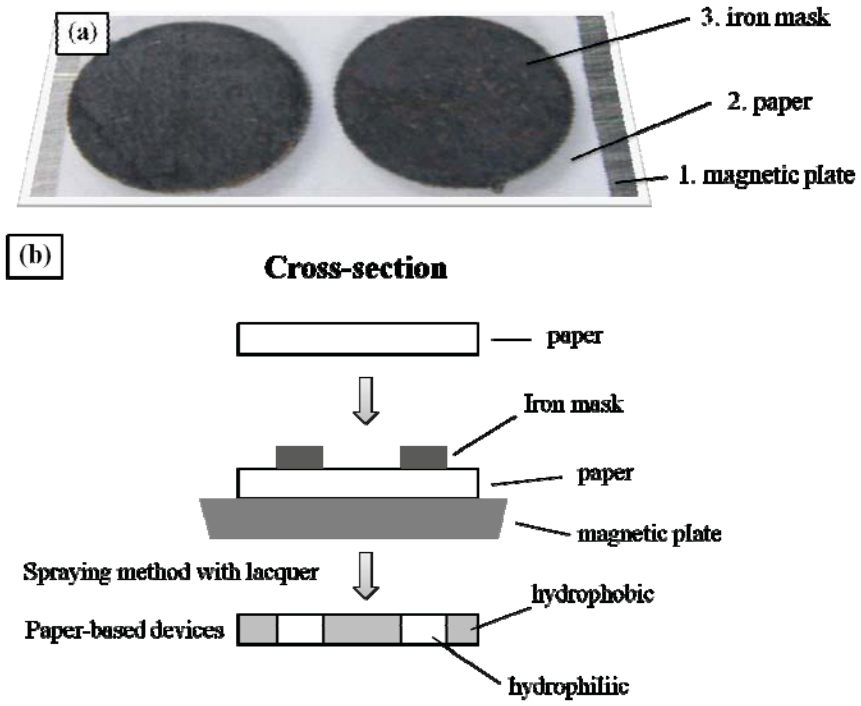

Figure 8.1. Schematic representation of the procedure for the fabrication of the paper-based devices by the lacquer spraying method (a) in top view (b) in cross section view

8.2.3 Preparation of electrochemical detector for paper-based devices.

The screen-printed electrodes were prepared in-house. The three electrodes were fabricated using screen-printing method. The carbon ink was used as the working electrode (WE) and the counter electrode (CE) and the silver/silver chloride ink was used as the reference electrode (RE) and conductive pads. All electrodes were screened on the patterned paper and were cured in the oven at 65 ^{o}C for 30 min. The paper-based devices coupled with electrochemical detection are shown in Fig. 8.2.

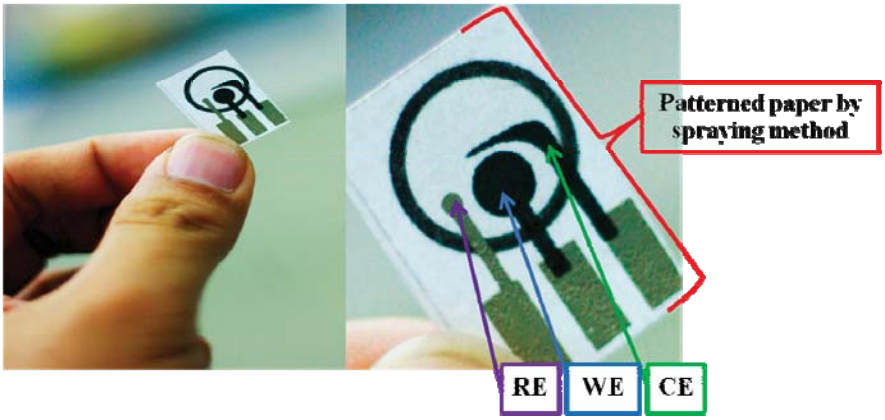

Figure 8.2. Paper-based devices coupled with electrochemical detection showing the carbon ink based working (WE) and counter (CE) electrodes, plus the silver/silver chloride based reference electrode (RE).

8.2.4 Applicability of paper-based devices for the determination of nickel in waste water sample of a jewelry factory

The waste water sample of a jewelry factory was received from The Gem and Jewelry Institute of Thailand (Public Organization). The jewelry waste sample was prepared by filtration of 20 mL of the waste water with Whatman No. 1 filter paper. Then the sample was mixed with 20 mL of HNO_3 and the solution was heated at 200 ^{o}C to evaporate the solvent. After that, the sample was made up with 20 mL of MilliQ water and was heated at 100 ^{o}C

until dryness (repeated 3 times). Next, the sample was rinsed with mixed solution between 20 mL of 0.1 M NaCl and Cu solution 4.5 ppm (pH 6.7). Finally, the sample was sonicated for 30 min and clear solution was ready for analysis.

8.3 Results and discussions

8.3.1 The effect of lacquer type for the fabrication of paper-based devices

In this work, the effect of lacquer type was studied. Three types of acrylic lacquer were investigated, including paint lacquer, matte spray lacquer and gloss spray lacquer. For paint lacquer, the paper was painted with paint lacquer instead of spraying. The results indicated that it was inappropriate for fabrication of pattern on paper because the penetration of lacquer into the filter paper and the diffusion under the iron mask could not be controlled (Fig. 8.3a). To study the matte spray lacquer and gloss spray lacquer, the spraying method was used as the lacquer application method. With the matte spray lacquer (Fig. 8.3b), the hydrophobic and hydrophilic areas can be generated on the paper-based devices, however, the uniformity of pattern on paper was difficult to observe. For gloss spray lacquer, the results indicated that the hydrophobic and hydrophilic areas were clearly distinguished (Fig. 3c). Therefore, the gloss spray lacquer was chosen for fabricating the paper-based devices throughout the following work.

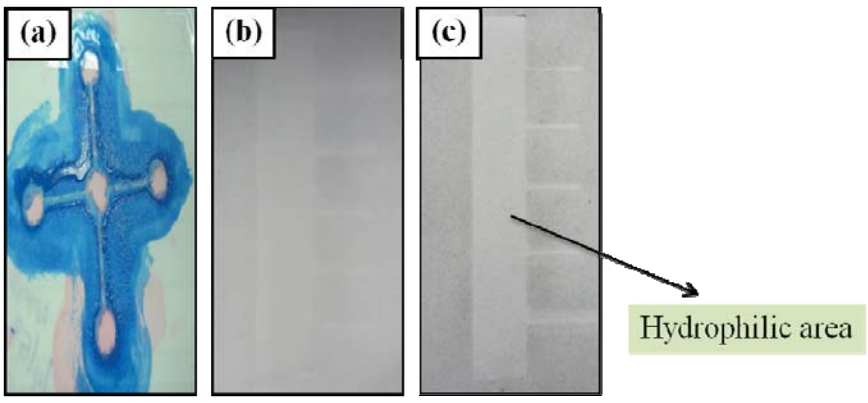

Figure 8.3 The effect of the lacquer type for fabrication of the paper-based devices: (a) paint lacquer (blue color), (b) matte spray lacquer (colorless) and (c) gloss spray lacquer (colorless).

8.3.2 The effect of particle retention efficiency of filter paper for fabrication of paper-based devices

Since the distribution of the lacquer could not be controlled, the effect of particle retention efficiency of filter paper was studied. The particle retention efficiency of a depth-type filter is expressed in terms of the particle size (in μm). A retention level of 98% of the total number of particles was obtained [23]. The Whatman filter paper No. 1 and No. 4 were used to study in this work. The particle retention efficiency of Whatman filter paper No. 1 and No. 4 were 11μm and 20-25 μm respectively. The results indicated that Whatman filter paper No. 4 gave better results than Whatman filter paper No. 1 because the former has larger porosity (Fig. 8.4). Therefore, the lacquer was easily and rapidly penetrated into the fiber of filter paper No. 4. In this work, the Whatman filter paper No. 4 was thus chosen to fabricate paper-based devices.

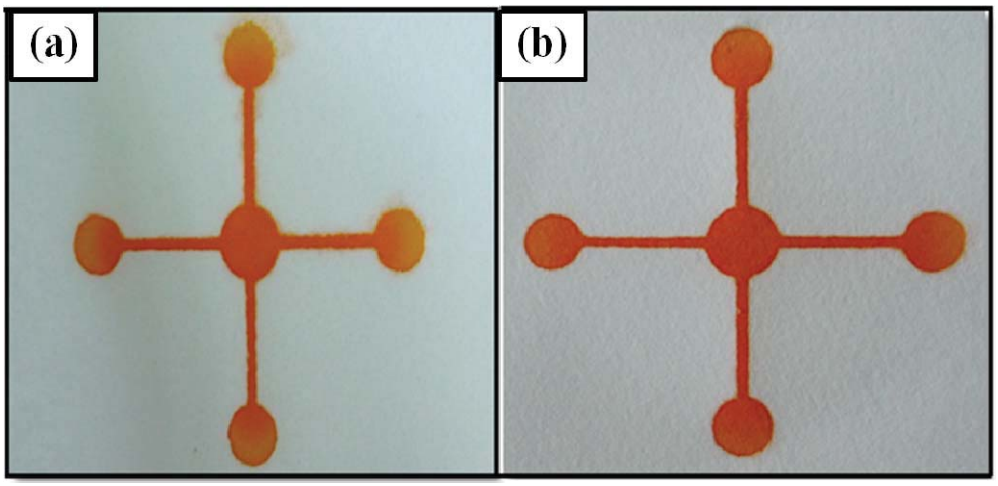

Figure 8.4. The effect of the filter paper particle retention efficiency in the fabrication of a paper-based device (a) Whatman filter paper No. 1 with a porosity of 11 µm and (b) Whatman filter paper No. 4 with a porosity of 20-25 µm.

8.3.3 The characterization of hydrophilic and hydrophobic areas on paper-based devices

The hydrophobic area was created by the sprayed lacquer on filter paper while the hydrophilic area was protected by the iron mask. The lacquer was not absorbed into the hydrophilic area. Therefore, the pattern of hydrophobic and hydrophilic areas was generated on the paper. The fabricated pattern on the paper was observed by an optical microscope (Olympus CX31), as shown in Fig. 8.5a and 8.5b. It was clearly seen that the surface of the paper was significantly changed as a result of lacquer coating. From Fig. 8.5a, the right side of the paper is the native surface, whereas the left side was coated with lacquer and completely turned into a hydrophobic area. In Fig. 8.5b, it was indicated that a colored food dye was not able to percolate into the hydrophobic area because of lacquer coating. Fig. 5c shows the hydrophobicity of our paper-based devices following a drop of a colored food dye comparing to that of the hydrophilic zone.

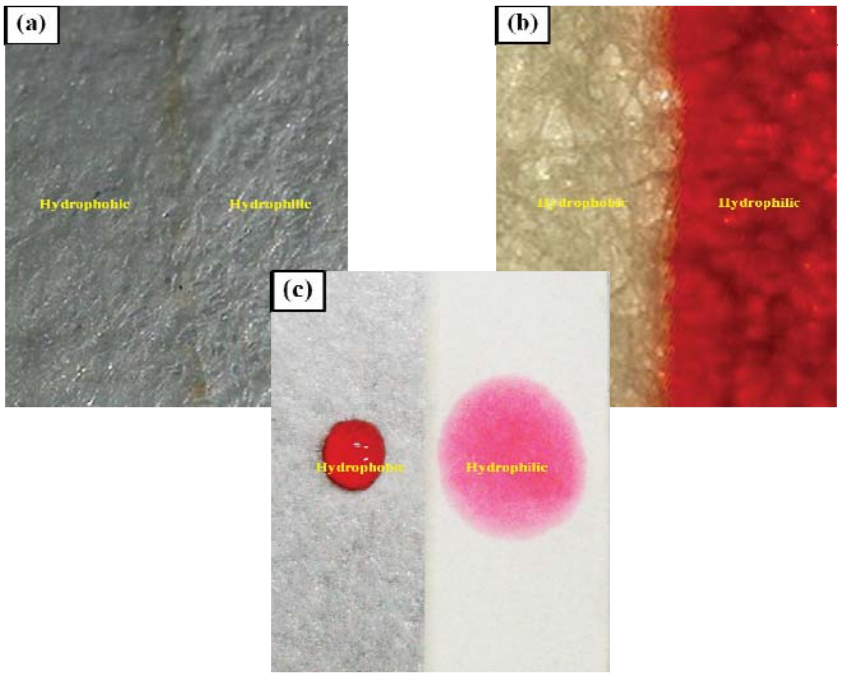

Figure 8.5. The paper-based device fabricated by the gloss lacquer spraying method, showing: (a) the hydrophobic (left side) and hydrophilic (right side) area captured under an optical microscope at 4x magnification, (b) the hydrophilic zone soaked with food dye color and (c) a comparison of the hydrophilic and hydrophobic area of the paper after applying a drop of colored food dye.

Then, the surface image of the pattern paper was taken by scanning electron microscope (JSM-6400) as shown in Fig. 8.6a and 8.6b. Fig. 6a shows the cross section of the surface paper uncoated with lacquer, and Fig 6b shows the cross section of the surface paper coated with lacquer, which clearly demonstrated the infiltration of the lacquer through the porosity of the filter paper.

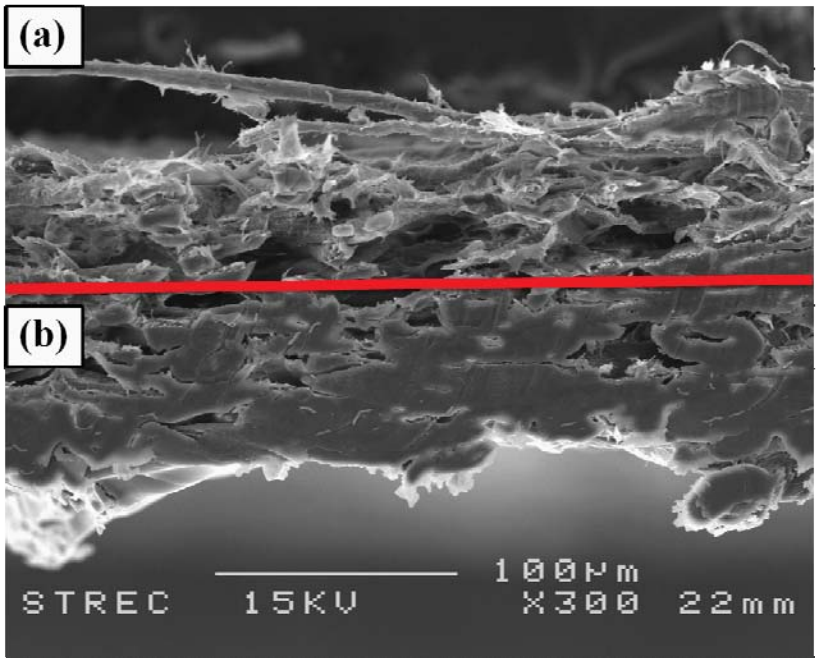

Figure 8.6. SEM image (300x magnification) of the cross section surface of the Whatman filter paper No. 4, either (a) uncoated or (b) coated with gloss spray lacquer.

8.3.4 The effect of Cu-enhancer solution for the determination of nickel

Based on earlier finding, copper solution is known to enhance the sensitivity for the determination of mercury [24]. Hence in this study, we are interested in using copper to enhance the determination of nickel with the fabrication paper-based devices. The effect of the concentration of copper was studied in range from 0.5 to 7.5 ppm. The relationship between current and concentration of copper was shown in Fig. 8.7. The peak current increased until the concentration of copper of 4.5 ppm. Then peak current decreased, it could be explained that unsuitable concentration of copper may be disturbed the signal of nickel. Therefore, the optimum concentration of copper at 4.5 ppm was chosen.

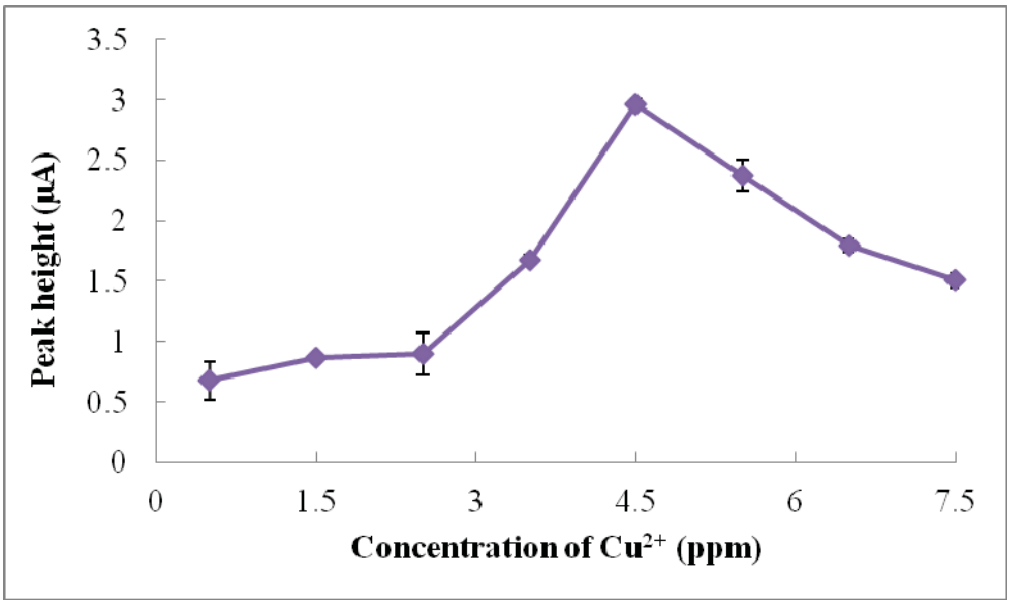

Figure 8.7. The effect of the Cu^{2+} concentration on enhancing the 0.5 ppm Ni^{2+} signal in 0.1 M NaCl

8.3.5 Analytical performance

Under the optimum experimental conditions, the electrochemical performance of the DPASV for the determination of nickel using paper-based devices coupled with

electrochemical detection on screen-printed carbon electrode were studied. A 50 µL of solution was dropped on the hydrophilic area of paper-based device. Peak potential of nickel was obtained in potential region between -0.20 to -0.10 V (*versus* Ag/AgCl). The obtained voltammograms provided well-defined oxidation peaks. Therefore, the developed paper-based devices are clearly an effective tool to determine nickel. The relative standard deviation of all concentrations of nickel were within 1.25% (n=3), demonstrating acceptable reproducibility for this device. Calibration curve of the anodic current against concentrations generated linear range between 1 to 50 ppm with a high coefficient of 0.9971 (Fig. 8.8). The limit of detection (LOD) and the limit of quantitation (LOQ) were found to be 0.5 and 1.97 ppm, respectively.

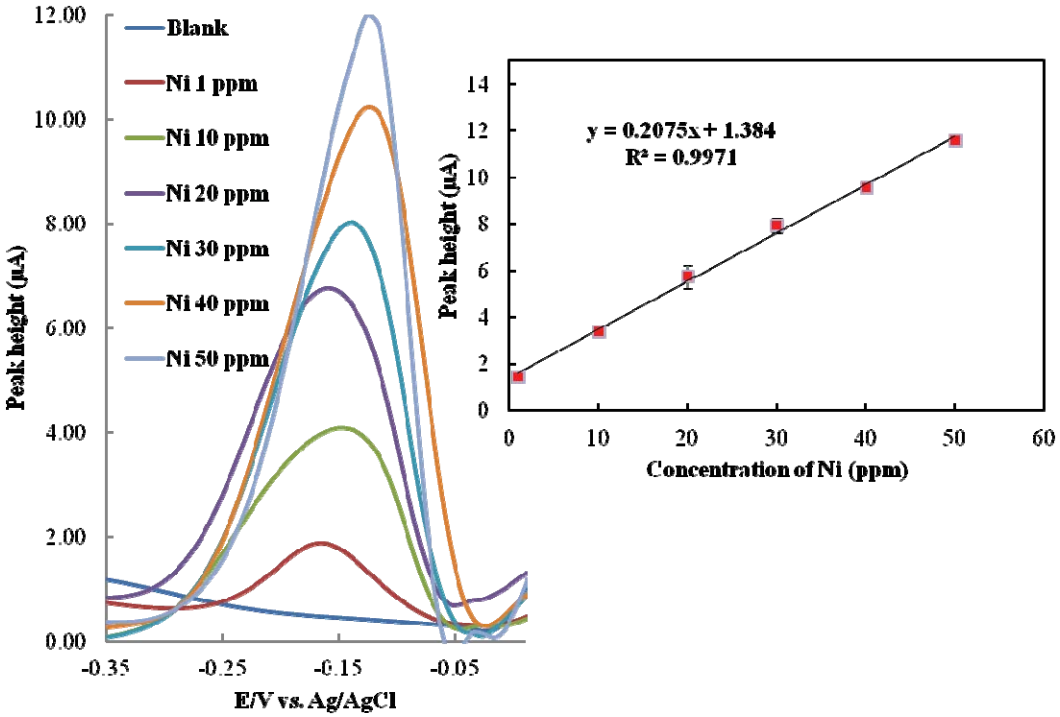

Figure 8.8 (a) Anodic stripping voltammogram of Ni^{2+} (1-50 ppm) determination with the screen-printed carbon electrode on a Whatman No. 4 paper-based device at a deposition

potential of -0.9 V *versus* Ag/AgCl. (b) The calibration plot of anodic currents at 180 s of deposition time for determination of the Ni^{2+} level. Data are (a) representative of, or (b) derived from, three independent repeats.

8.3.6 Analytical Application

To evaluate the efficiency of this developed method, the paper-based devices with electrochemical detection were used to detect nickel in waste water of a jewelry factory. The determination of nickel in real sample was carried out using the optimal conditions. In addition, this proposed method was compared with ICP-OES method. The results indicated that the concentration of nickel in waste water were found to be 4.15±0.043 ppm for electrochemical detection and 4.06±0.013 ppm for ICP-OES method (n=3). The paired t-test was used to validate our method versus the ICP-OES method. No significant difference of the analyzed values of nickel in the jewelry waste water was found at the 95% confidence level.

8.4 Summary

The lacquer spraying method was successfully employed for the fabricating paper-based devices. This spraying method is an alternative method due to its ease of use, affordability and simplicity. In addition, there is no requirement for complicated and expensive instruments or organic solvents. The iron mask was used to create the pattern of hydrophilic area and hydrophobic area was obtained by spraying with lacquer. The spraying method does not suffer from problems of interference from residues remaining in the hydrophilic area after fabrication. Moreover, the paper-based devices were shown to be useful for electrochemical detection methods, and were applied for the determination of nickel in real samples. Therefore, to fabricate paper-based devices, the spraying method with lacquer is one of the effective promising methods.

8.5 References

[1] F. S. R. R. Teles, L. A. P. D. T. Tavira, L. J. P. Fonseca, Crit. Rev. Clin. Lab. Sci. 3 (2010) 139-169.

[2] S. Haeberle, R. Zengerle, Lab Chip 7 (2007) 1094-1110.

[3] S. Sun, M. H. Yang, Y. Kostov, A. Rasooly, Nature 442 (2006) 412-418.

[4] A. W. Martinez, S. T. Phillips, G. M. Whitesides, E. Carrilho, Anal. Chem. 82 (2009) 3–10.

[5] A. W. Martinez, S. T. Phillips, M. J. Butte, G. M. Whitesides, Angew. Chem., Int. Ed. 46 (2007) 1318–1320.

[6] A. W. Martinez, S. T. Phillips, E. Carrilho, S. W. Thomas, H. Sindi, G. M. Whitesides, Anal. Chem. 80 (2008) 3699–3707.

[7] A. W. Martinez, S. T. Phillips, B. J. Wiley, M. Gupta, M. Whitesides, Lab Chip 8 (2008) 2146–2150.

[8] W. Dungchai, O. Chailapakul, C. S. Henry, Anal. Chem. 81 (2009) 5821–5826.

[9] Z. Nie, C. A. Nijhuis, J. Gong, X. Chen, A. Kumachev, A. W. Martinez, M. Narovlyansky, G. M. Whitesides, Lab Chip 10 (2010) 477–483.

[10] R. F. Carvalhal, M. Sima˜o Kfouri, M. H. de Oliveira Piazetta,A. L. Gobbi, L. T. Kubota, Anal. Chem., 2010, 82, 1162–1165.

[11] A. Apilux, W. Dungchai, W. Siangproh, N. Praphairaksit,C. S. Henry, O. Chailapakul, Anal. Chem., 2010, 82, 1727–1732.

[12] D. A. Bruzewicz, M. Reches, G. M. Whitesides, Anal. Chem. 2008, 80, 3387–3392.

[13] K. Abe, K. Suzuki and D. Citterio, Anal. Chem. 80 (2008) 6928–6934.

[14] E. M. Fenton, M. R. Mascarenas, G. P. L_opez, S. S. Sibbett, ACS Appl. Mater. Interfaces 1 (2008) 124–129.

[15] X. Li, J. Tian, T. Nguyen, W. Shen, Anal.Chem.80 (2008) 9131–9134.

[16] E. Carrilho, A. W. Martinez, G. M. Whitesides, Anal. Chem. 81 (2009) 7091–7095.

[17] L. Y. Shiroma, M. Santhiago, A. L. Gobbi, L. T. Kubota, Anal. Chim. Acta. 725 (2012) 44-50.

[18] M. Santhiago, L. T. Kubota, Sens. Act. B. 177 (2013) 224-230.

[19] W. Dungchai, O. Chailapakul, C. S. Henry, Analyst 136 (2011) 77-82.

[20] T. Songjaroen,W. Dungchai, W.; Chailapakul, W. Latwattanapaisal, Talanta 85 (2011) 2587-2593.

[21] X. Li, J. Tian, G. Garnier, W. Shen, Colloids Surf. B: Biointerf 76 (2010) 564-570.

[22] R. Lu, T. Honda, T. Ishimura, T. Miyakoshi, PolymJ 37 (2005) 309-315

[23] <http://www.Whatman.com/References/FiltrationSimplified.pdf>.

[24] A. Apilux, W. Siangproh, N. Praphairaksit, C. S. Henry, O. Chailapakul, Talanta 97 (2012) 288-394.

Chapter IX

The development of lab-on-paper for simultaneous determination of gold and iron by dual electrochemical / colorimetric detection

9.1 Introduction

Lab-on-paper has recently been developed for use in biological assays. Lab-on-paper is very attractive because it is portable, easy to use, has a low sample volume requirement and is inexpensive [1-3]. Paper is a cellulose fiber web with a high surface area and is abundant and inexpensive. It can be patterned into channels of hydrophilic surfaces separated by hydrophobic walls of photorest-based polymer. To date, lab-on-paper devices have primarily used colorimetric detection methods for the qualitative analysis of multiplex analytes [4]. However, quantitative analysis is still needed when a "yes" or "no" answer is insufficient. Much effort has, therefore, been directed towards the development of quantitative detection for the lab-on-paper using cameras and optical scanners. Recently, Dungchai et al. [5] successfully fabricated paper-based microfluidic devices with electrochemical detection. Electrochemical detection is attractive because of its simplicity, speed and high sensitivity. However, electrochemical detection cannot detect all the species present in complex samples. To combine the advantages of colorimetric detection for screening with the usefulness of electrochemical detection for quantitative analysis, in this study a lab-on-paper device with dual electrochemical / colorimetric detection was developed. The utility of this device was demonstrated with the simultaneous determination of Au(III) and Fe(III).

Gold is one of the important noble metals present at a low abundance on earth and thus possesses a high economic value. It has been extensively used in many fields, including electronics, batteries, dentistry and jewelry, amongst others. Nowadays, the recovery of gold from industrial waste solutions has become important for both economic and environmental

reasons. As industrial demand continues to develop, the demand for the ability to perform a rapid Au(III) analysis for quantifying Au(III) in waste solutions and so providing information about the effectiveness of the recovery processes is essential.

Several methods have been used to determine gold levels, including atomic absorption spectroscopy (AAS), [6-9] atomic emission spectroscopy (AES) [10] and inductively coupled plasma mass spectrometry (ICP-MS) [11-13]. However, these methods require expensive and complicated instrumentation and can generally only be done in the laboratory. In order to overcome these problems, electrochemical methods using modified carbon electrodes, [14-19] solid electrodes [20] and carbon fiber ultramicroelectrodes [21] have been reported for gold analysis. None of the above methods have, however, pursued the portable sensing of Au(III) in waste streams. As a result, there is increasing recognition of the need to develop a simple and portable device with improved ability to analyze small sample volumes. Lab-on-paper approach has considerable promise in this area. The aim of this work is to develop a dual electrochemical / colorimetric detection using lab-on-paper for a fast, simple, portable and simultaneous detection of Au(III) and Fe(III) in waste streams. The optimized system was capable of achieving detection limits of 1 ppm for Au(III) while only requiring 1 min to complete the assay. In the potential region where Au(III) is reduced, Fe(III) is noted as a significant source of interference when present at a substantially high value. By applying the dual detection technique Fe(III) could be accounted for, confirming the result of Au(III) determination. Finally, the sensor was applied to the determination of Au(III) in gold refining waste solutions.

9.2 Experimental Method

9.2.1 Chemicals and Materials

A negative photoresist SU-8 3025 and developer were purchased from Microchem Corp (company city, USA). Carbon ink (ELECTRODEDAGPF-407C) and silver/silver

chloride ink (ELECTRODAG7019 (18DB19C)) were purchased from Acheson. Filter paper (No.1, 100 cm diameter) was obtained from Whatman. Analytical grade reagents and 18 $M\Omega cm^{-1}$ resistance water (Millipore Milli-Q purification system) were used throughout this experiment. A standard solution of 1000 ppm Au(III) was purchased from Merck and used as the stock solution. The supporting electrolyte aqua regia solution (0.1 M HCl + 0.05 M HNO_3) used in the experiments diluted was prepared by dilution of hydrochloric and nitric acid (Merck). The following chemicals were used as received: isopropanol, 1,10-phenanthroline hydrate, iron chloride hexahydrate ($FeCl_3.6H_2O$), platinum (Pt) and rhodium (Rh) standard solution (Merck), potassium ferricyanide $K_3[Fe(CN)_6]$ (Riedeel-dellaen), potassium chloride (KCl) (Univar), copper sulphate ($CuSO_4$), zinc nitrate $Zn(NO_3)_2$ and L-ascorbic acid (all from BDH), nickel nitrate ($Ni(NO_3)_2$) (Aldrich) and silver nitrate ($AgNO_3$) (Carloerba).

9.2.2 Fabrication of Patterned paper

Devices were fabricated using previously described methods [22]. The mask was designed with Adobe Illustrator software (Adobe Systems incorporated) and fabricated by Chaiyaboon Co. (Bangkok, Thailand). The filter paper was coated with 4 g of SU-8 negative photoresist using a spin coater (G3P-8) at 1900 rpm for 5 seconds and then baked at 95 ^oC for 10 min. The mask was then placed on the coated paper and exposed to UV light for 10 seconds (Intelli-ray 400). After that, the exposed paper was baked at 95 ^oC for 10 min, followed by soaking in SU-8 developer for 3 min then rinsed with isopropanol. Finally, the patterned paper was dried in a hood at room temperature. For electrochemical detection, the electrodes were screen printed in house. Three electrodes were screened on patterned paper using carbon ink as the working electrode (WE) and counter electrode (CE) and silver/silver chloride ink as the reference electrode (RE) and conductive pads. After each printing step, the

paper was placed into an oven at 65 °C for 30 min to cure the inks. The finished product is illustrated in Figure 9.1.

Cyclic voltammetry (CV) and square wave voltammetry (SWV) experiments were performed by a CHI 1232A electrochemical analyzer (CH Instruments. Inc. USA). All voltammetric experiments were performed using only the electrodes on the paper without removal of oxygen from the solution. For voltammetric experiments, the potential was scanned from 1200 mV to 0 mV vs. Ag/AgCl. Cyclic voltammetry was performed at a scan rate 100 mVs^{-1}. Square wave voltammetry was performed at , the pulse amplitude at 50 mV, a square wave frequency of 15 Hz and a step height of 5 mV in the potential range from 1200 mV to 0 mV vs. Ag/AgCl.

The colorimetric method on the lab-on-paper was prepared by dropping 0.7 μL of 1000 ppm 1-10 phenanthroline on the colorimetric test zone and allowing the reagents to dry in the air. Then, 0.7 μL of 1000 ppm ascorbic acid was added and left until dry.

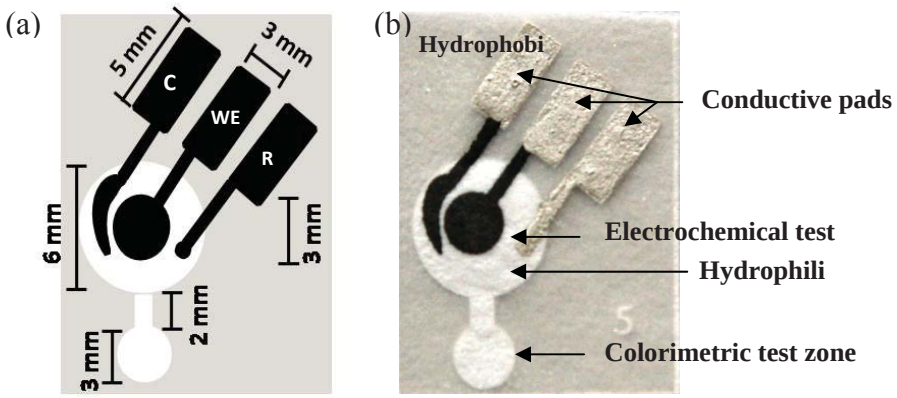

Figure 9.1 The dual electrochemical/ colorimetric lab-on-paper device. (a) The basic design of the electrochemical detection cell (WE, working electrode; RE, reference electrode; CE, counter electrode). (b) The lab-on-paper device consisting of the electrochemical and colorimetric test zones.

9.3 Results and Discussion

9.3.1 Electrochemical behavior of Au(III)

First, the electrochemistry of Au(III) on the paper system was investigated. A cyclic voltammogram of 50 ppm Au(III) in dilute aqua regia electrolyte is shown in Figure 9.2. A well defined reduction peak of Au(III) at around 260 mV vs. Ag/AgCl can be observed corresponding to the reaction $AuCl_4^- + 2e^- \rightarrow AuCl_2^- + 2\ Cl^-$. Although it has been reported that the reduction potential of Au(III) to Au(I) is about 0.6 V vs. Ag/AgCl/KCl(sat) in 0.1 M HCl,[21], the significantly lower potential observed in this study could have arisen from many reasons, such as the type of reference electrode, working electrode materials, supporting electrolytes and experimental conditions [52]. From the cyclic voltammogram, the oxidation peak of Au was not observed due to its difficulty to occur without pretreatment. In addition, the electrodes were characterized using $Fe(CN)_6^{3-}$ as the model electroactive analyte.

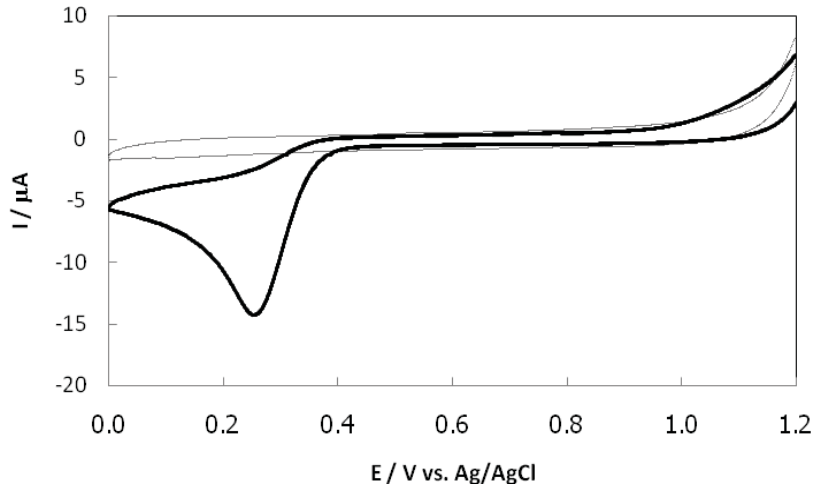

Figure 9.2 Cyclic voltammogram of 50 ppm Au(III) in dilute aqua regia as the electrolyte (black line), and the dilute aqua regia background (grey line), at a 100 mVs^{-1} scan rate.

In order to achieve a low detection limit for metals, differential pulse or square wave voltammetry (SWV) is typically used. The square wave voltammogram of Au(III) is shown

in Figure 9.3, where a reduction peak for 50 ppm Au(III) in dilute aqua regia at 287 ± 12 (n = 10) mV vs. Ag/AgCl is clearly observed. In addition, a reduction peak was also observed at 85 ± 15 (n = 10) mV, which may be attributed to contaminants in the carbon ink because it was also found in the blank (inset of Figure 9.3).

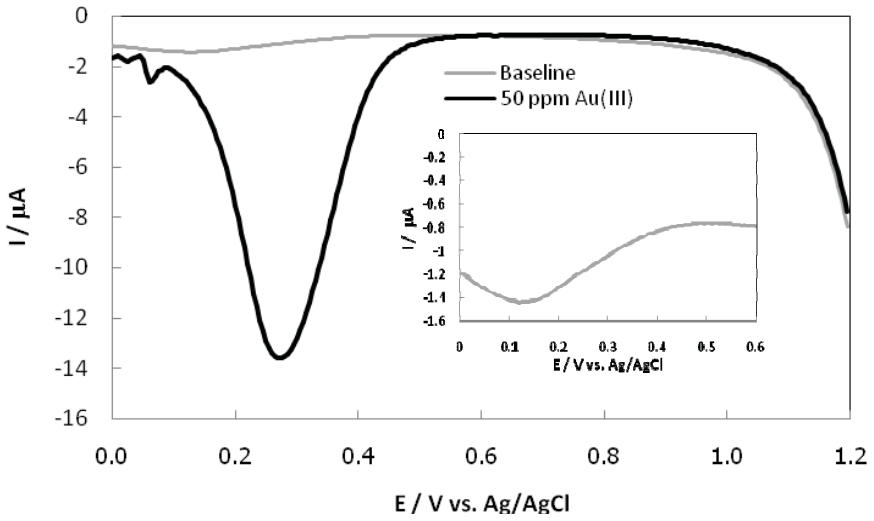

Figure 9.3 Square wave voltammogram of 50 ppm Au(III) in dilute aqua regia. Pulse amplitude = 50 mV, square wave frequency = 15 Hz, step height = 5 mV. Inset: Square wave voltammogram of baseline.

The peak current obtained from SWV is dependent on various instrumental parameters, including the pulse amplitude, square wave frequency and step height and so the optimal conditions for the analysis of Au(III) were determined. The pulse amplitude was varied from 10 mV to 100 mV, where the peak intensity increased with growing pulse amplitude but slightly deceased above 50 mV vs. Ag/AgCl and the peak width increased. Therefore, the amplitude of 50 mV vs. Ag/AgCl was selected for subsequent experiments. The effect of square wave step height (1 - 10 mV) on the peak current of 50 ppm Au(III) in the dilute aqua regia electrolyte was studied next. The peak intensity increased with

increasing square wave step height and then slightly decreased above 7 mV. However, as the step height approached 7 mV, the peak became broad and, therefore, 5 mV was selected as the optimal condition. Square wave frequencies from 10 – 25 Hz were also examined and the peak intensity increased with increasing square wave frequency up to 15 Hz. Since above this frequency, the peak height slightly decreased and the peak width also increased, then a frequency of 15 Hz was chosen for further studies. The resulting optimal SWV parameters for the detection of Au(III) were set as; pulse amplitude = 50 mV, square wave frequency = 15 Hz and step height pulse height = 5 mV.

9.3.2 Standard curves

The relationship between the reduction peak current and the concentration of Au(III) in the dilute aqua regia electrolyte under optimal conditions was examined using SWV. The square wave voltammograms of Au(III) and the corresponding calibration curve are shown in Figure 9.4. The peak position shifts slightly from run to run however it does not affect the results. This curve showed a linear range between 1 and 200 ppm (correlation coefficient (R^2) of 0.997), with a sensitivity of approximately 0.2 μA/ppm. The limits of detection (LOD) and quantization (LOQ) were 1 and 4 ppm, respectively, based on 3x and 10x SD, respectively. Reproducibility of the Au(III) SWV response was assessed as the relative standard deviation of 10 consecutive measurements of 10 and 100 ppm Au(III) and was found to be 2.6 and 5.1%, respectively.

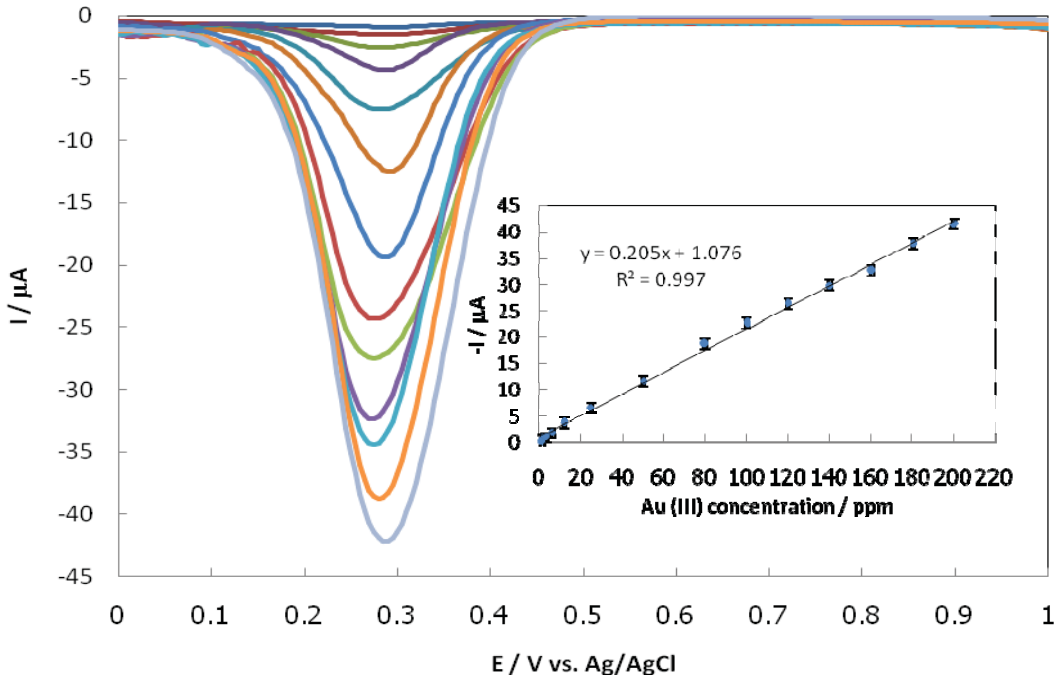

Figure 9.4 Square wave voltammograms for Au(III) (1, 3, 6, 12, 25, 50, 80, 100, 120, 140, 160, 180 and 200 ppm) in dilute aqua regia electrolyte, measured under the optimal experimental conditions. The inset shows the calibration curve.

9.3.3 Interferences

Cu(II), Ni(II), Zn(II), Fe(III), Pt(II), Rh(II) and Ag(I) are some of the most common elements used in the jewelry and electronics industries, and so were examined as potential interferences in the determination of Au(III). Among of 5 - 500 ppm Cu(II), Ni(II) and Zn(II), 5 - 250 ppm of Fe(III), 5 - 100 ppm of Pt(II) and Rh(II) and 1 - 10 ppm of Ag(I) were added into a fixed 10 ppm Au(III) solution to represent that of a real waste sample. It was found that a 50-fold excess of Cu(II), Ni(II), Zn(II), Pt(II), Rh(II) and Ag(I) did not interfere with the determination of Au(III) by this technique, as shown in Figure 9.5. However, the peak current for Au(III) decreased in the presence of a 2.5-fold excess concentration of Fe(III) (Figure 9.5G, c line, blue triangle symbol) and no current response of Au(III) was detected in the presence of a 25-fold excess of Fe(III), as shown in Figure 9.5G (f line, pink

circle symbol). From the Figure 9.5G (c, d and e), it is apparent that the reduction current response of Fe(III) overlapped with that of Au(III) due the closed reduction potential or the formation of intermetallic compound.

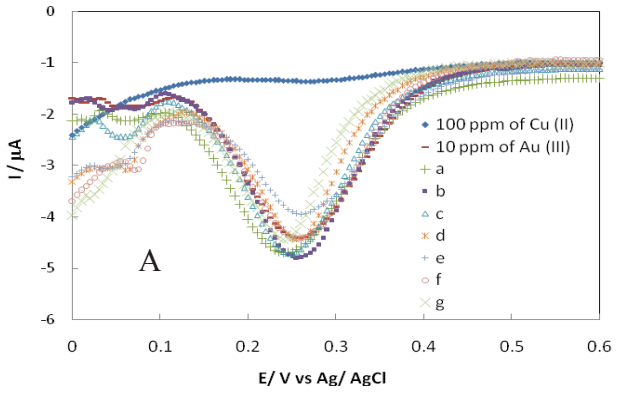
A
100 ppm of Cu (II)
10 ppm of Au (III)
a
b
c
d
e
f
g
I / µA
E/ V vs Ag/ AgCl

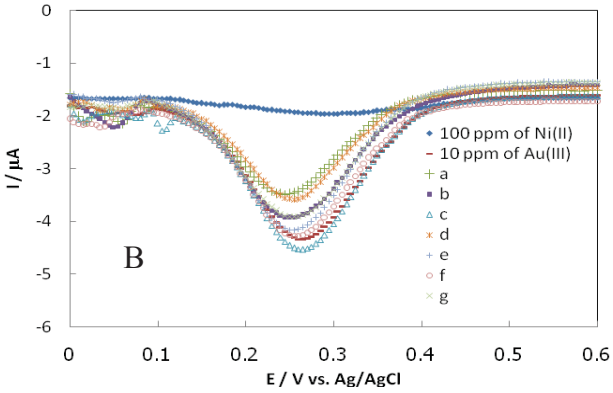
B
100 ppm of Ni(II)
10 ppm of Au(III)
a
b
c
d
e
f
g
I / µA
E / V vs. Ag/AgCl

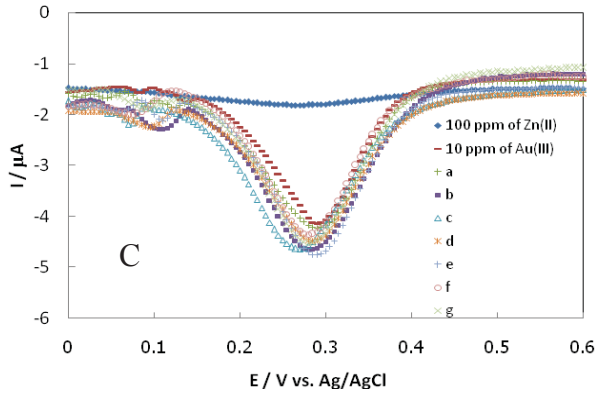
C
100 ppm of Zn(II)
10 ppm of Au(III)
a
b
c
d
e
f
g
I / µA
E / V vs. Ag/AgCl

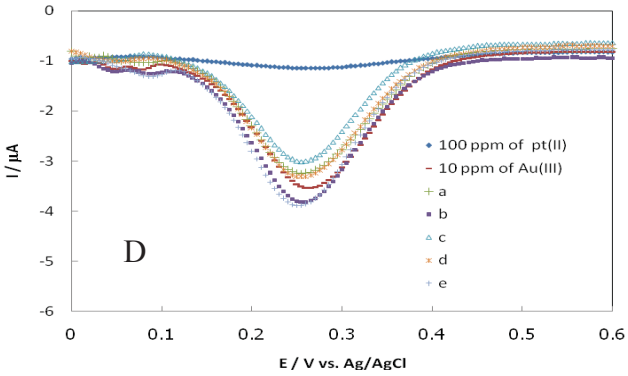
D
100 ppm of pt(II)
10 ppm of Au(III)
a
b
c
d
e
I / µA
E / V vs. Ag/AgCl

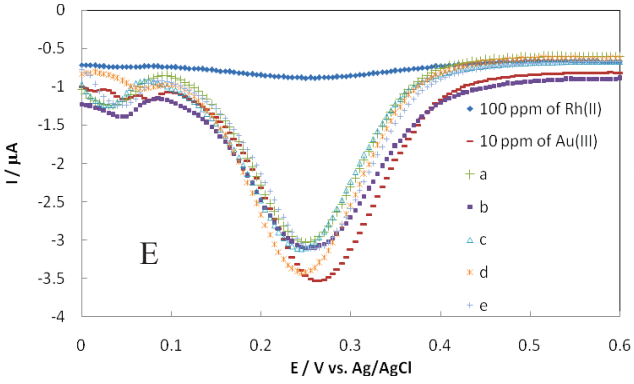
E
100 ppm of Rh(II)
10 ppm of Au(III)
a
b
c
d
e
I / µA
E / V vs. Ag/AgCl

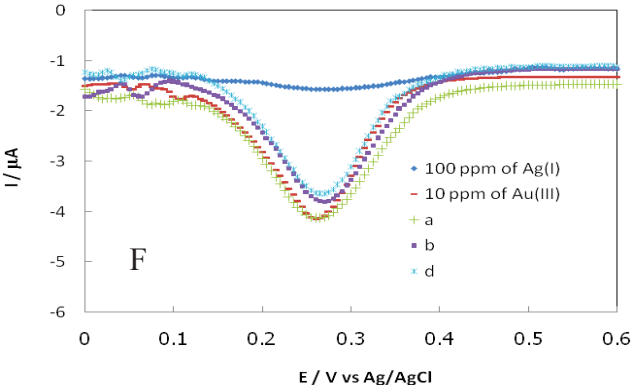
F
100 ppm of Ag(I)
10 ppm of Au(III)
a
b
d
I / µA
E / V vs Ag/AgCl

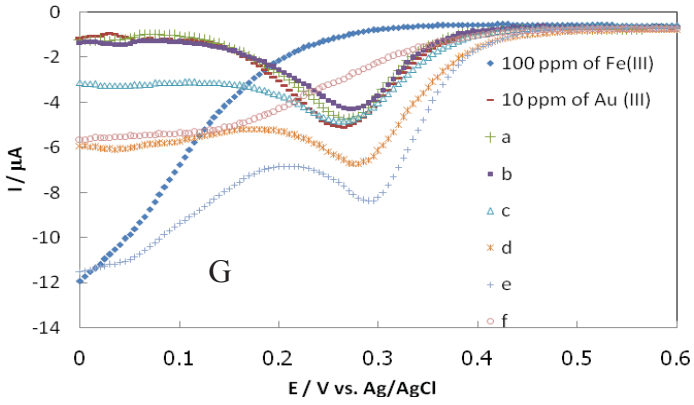
G
100 ppm of Fe(III)
10 ppm of Au (III)
a
b
c
d
e
f
I / µA
E / V vs. Ag/AgCl

Figure 9.5 Square wave voltammograms of 10 ppm Au (III) with added 5 (a), 10 (b), 25 (c), 50 (d), 100 (e), 250 (f) and 500 (g) ppm of the cations: (A) Cu(II), (B) Ni(II), (C) Zn(II), (D) Pt(II), (E) Rh(II), (F) Ag(I) and (G) Fe(III) in the dilute aqua regia electrolyte. Pulse amplitude = 50 mV, step height = 5 mV and square wave frequency = 15 Hz.

9.3.4 Colorimetric Determination of Fe(III)

Because of the potential interference of Fe(III), a simple colorimetric assay was developed to determine if Fe(III) was interfering with the Au(III) assay. To determine the Fe ion levels, a colorimetric method based on the reaction of Fe(II) with 1,10-phenanthroline was used. Since Fe ion in acidic solution is Fe(III) form, ascorbic acid was added to reduce Fe(III) to Fe(II) form. The colorimetric test zone consists of ascorbic acid and 1,10-phenanthroline at a 1:1 (v/v) ratio. The resulting color intensity is proportional to the concentration of the Fe(II) complex with 1,10-phenanthroline, and was assessed visually. Moreover, we found that no significant difference in color was observed in the co-presence of Au(III), Cu(II), Ni(II), Zn(II), Pt(II), Rh(II) and Ag(I) in the dilute aqua regia, indicating the selectivity of the assay for Fe(III).

9.3.5 Analytical application

The performance of the device for the determination of Au(III) was tested on gold refining waste solutions, collected from the precious metals assay laboratory of the Gem and Jewelry Institute of Thailand, and the results were validated with ICP-AES. The results obtained for Au(III) analysis in gold refining waste samples 1 and 2 using the lab-on-paper device were evaluated as 17.48 ± 0.55 and 45.70 ± 1.23 ppm, respectively, which were in good agreement (95.6% and 96.0%, respectively) with the values of 18.28 ± 0.29 and 47.59 ± 0.44 ppm, respectively, measured by ICP-AES. These results clearly show the ability of

paper microfluidic devices to provide accurate results for the determination of Au(III) in these waste streams.

The reliability of the system was then investigated by recovery studies. The average percentage recovery obtained for a gold waste sample spiked with Au(III) standard solutions, containing 5 and 10 ppm Au(III) for sample 1 and 10 and 20 ppm Au(III) for sample 2, were measured. The results, shown in table 9.1, revealed a recovery in the range of 91 – 93% with a precision (% RSD) in the range of 2.7 – 4.4%, respectively.

Finally, the dual electrochemical and colorimetric based lab-on-paper device developed here was next evaluated for the simultaneous determination of Au(III) in the presence of Fe(III). The sample solution was dropped on the electrode side of the device. Au(III) was electrochemically analysed while the solution flowed to the colorimetric detection zone, where the ascorbic acid reduced the Fe(III) to Fe(II). The color developed by the reaction of Fe(II) and the complexing reagent 1,10-phenanthroline was then compared to the calibration chart by naked eye. As described in the interference part, only Fe(III) concentrations which were higher than a 2.5-fold excess of the Au(III) concentration were observed to interfere with the reduction peak of Au(III). For the two real samples studied, it was found that the color of Fe(III) concentrations matched with the color of the standard Fe(III) concentrations of 5 and 10 ppm (0.3-fold and 0.2-fold that of the Au(III) concentration) for samples 1 and 2, respectively (Figure 9.6). No effect of Fe(III) on the determination of Au(III) in the real samples was observed, presumably due to the fact that the concentration of Fe(III) was less than 2.5 fold concentration that of Au(III) in these samples. Detection of Fe(III) by the visual comparison with standards was screening method which was sufficient for this study. The precision of this colorimetric measurement was low; therefore, to obtain high precision results, using the other devices such as camera phone or scanner was needed.

Table 9.1 Determination of Au(III) in real sample

Sample	Au(III) (ppm)		%Recovery	% RSD (n = 10)
	Added	Found		
Gold refining waste solution (sample 1)	0	17.48 ± 0.55	0	2.9
	5	22.05 ± 1.03	91	4.4
	10	26.65 ± 1.11	92	4.0
Gold refining waste solution (sample 2)	0	45.70 ± 1.23	0	2.7
	10	54.96 ± 1.68	93	3.1
	20	64.11 ± 1.98	92	3.1

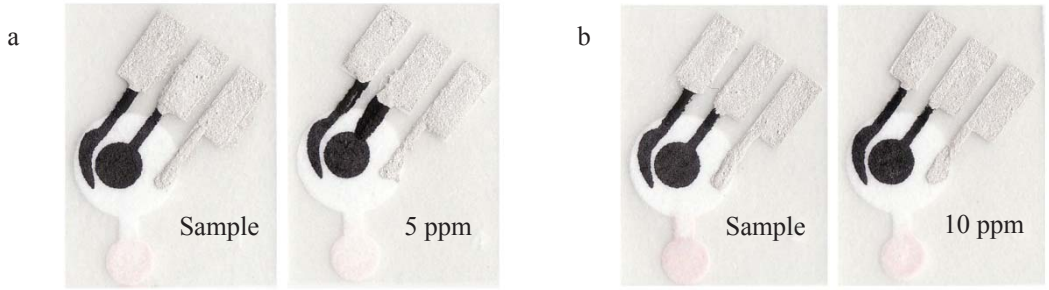

Figure 9.6 The intensity of the observed color is proportional to the complex concentration of sample 1(a) and sample 2(b) compared with the Fe(III) reference.

9.4 Summary

The dual electrochemical and colorimetric based lab-on-paper device developed here displayed a simple and rapid quantitation of Au(III) using electrochemistry while screening for Fe(III) using colorimetry. Well defined square wave voltammograms of Au(III) were obtained and the optimal experimental conditions for square wave voltammetry were established. Under these optimized conditions, the device was able to detect Au(III) as low

as 1 ppm, with a linear dynamic range from 1 to 200 ppm. Fe(III), as the interference of Au(III) determination was screened for using a simple colorimetric method. The procedure has been successfully applied to the determination of Au(III) in real gold refining waste solutions. The easy and rapid analysis using dual detection with lab-on-paper makes the approach especially attractive for a wide range of environment samples for heavy metals.

9.5 References

[1] Martinez, A. W.; Phillips, S. T.; Carrilho, E.; Thomas, S. W.; Sindi, H.; Whitesides, G. M., Anal. Chem., 80 (2008): 3699-3707.

[2] Martinez, A. W.; Phillips, S. T.; Butte, M. J.; Whitesides, G. M., Angew. Chem. Int. Ed., 46 (2007): 1318-1320.

[3] Zhao, W. A.; Ali, M. M.; Aguirre, S. D.; Brook, M. A.; Li, Y. F., Anal. Chem., 80 (2008): 8431-8437.

[4] Zhao, W. A.; van den Berg, A., Lab Chip, 8 (2008): 1988-1991.

[5] Dungchai, W.; Chailapakul, O.; Henry, C. S., Anal. Chem., 81 (2009): 5821-5826.

[6] Shamsipur, M.; Ramezani, M., Talanta, 75 (2008): 294-300.

[7] Du, X. G.; Xu, S. K., Fresenius J. Anal. Chem., 370 (2001) : 1065-1070.

[8] Yu, M. Q.; Sun, D. W.; Huang, R.; Tian, W.; Shen, W. B.; Zhang, H. C.; Xu, N., Anal. Chim. Acta, 479 (2003): 225-231.

[9] Fazli, Y.; Hassan, J.; Karbasi, M.-H.; Sarkouhi, M., Miner. Eng., 22 (2009): 210-212.

[10] Senofonte, O.; Caroli, S., J. Anal. At. Spectrom., 15 (2000): 869-872.

[11] Duan, X. C.; McLaughlin, R. L.; Brindle, I. D.; Conn, A., J. Anal. At. Spectrom., 17 (2002): 227-231.

[12] Jin, X. D.; Zhu, H. P., J. Anal. At. Spectrom., 15 (2000): 747-751.

[13] Juvonen, R.; Lakomaa, T.; Soikkeli, L., Talanta, 58 (2002): 595-603.

[14] Lack, B.; Duncan, J.; Nyokong, T., Anal. Chim. Acta, 385 (1999): 393-399.

[15] Navratilova, Z.; Kula, P., Fresenius' J. Anal. Chem., 367 (2000): 369-372.

[16] Hu, R. Z.; Zhang, W. D.; Liu, Y. Y.; Fu, J. K., Anal.Commun., 36 (1999): 147-148.

[17] Turyan, I.; Mandler, D., Fresenius' J. Anal. Chem., 349 (1994): 491-496.

[18] Bergamini, M. F.; Santos, D. P.; Zanoni, M. V. B., J. Braz. Chem. Soc., 20 (2009): 100-106.

[19] Gevorgyan, A. M.; Vanyukov, V. V.; Vakhnenko, S. V., J. Anal. Chem., 57 (2002): 253-254.

[20] Bond, A. M.; Kratsis, S.; Mitchell, S.; Mocak, J., Analyst, 122 (1997): 1147-1152.

[21] Alarnes-Varela, G.; Costa-Garcia, A., Electroanalysis, 9 (1997): 1262-1266.

[22] Wang, J.; Tian, B.; Nascimento, V.B.; Angnes, L., Electrochim. Acta., 43 (1998): 3459-3465.

Chapter X

Simple and rapid determination of ferulic acid in food and cosmetic samples using paper-based platforms

10.1 Introduction

Antioxidants are compounds that the human body needs to prevent the oxidative damage caused by free radicals, which may contribute to various diseases such as cancer, cardiovascular diseases and cataracts. Interest in natural antioxidants has increased significantly in the past few years. The antioxidant activities of plants have been attributed mostly to their phenolic content which is one class of natural antioxidant. Therefore, plants containing high-level of phenolic have great importance as natural antioxidants. Ferulic acid (4-hydroxy-3-methoxycinnamic acid) is one of many ubiquitous phenolic acids in the plant kingdom. Ferulic acid is more easily absorbed into the body and stays in the blood longer than any other antioxidant, even longer than vitamin C. Because of these features, ferulic acid is considered to be a superior antioxidant and, thus, is widely used in healthy foods and nutrition restoratives. Ferulic acid has been touted as an anti-microbial, anti-inflammatory, anti-arrhythmic and anti-thrombosis pharmacological agent [1]. Ferulic acid is also used in a wide range of cosmetics such as skin lighteners, moisturizers and sunscreens, because it has the ability to protect skin from ultraviolet radiation. Ferulic acid is also reduce nerve cell damage and may help to repair damaged cells. Furthermore, ferulic acid is a popular sports supplement; because it is an antioxidant, it can neutralize free radicals in muscle tissue and, thus, can alleviate muscle soreness, loss of endurance and muscle fatigue. In addition, a study about diabetes in rats showed that ferulic acid was able to alleviate oxidative stress in diabetics and lower blood glucose levels [2]. Thus, the antioxidant properties of ferulic acid might be beneficial for diabetics. More recently, a study showed that ferulic acid supplements can reverse the damage of the organs in diabetic rats. In addition, ferulic acid has been shown

to be effective in treating menopausal hot flashes which may be caused by inflammation and oxidation of tissues and also has properties of an immune stimulant [3]. Ferulic acid has also been shown to suppress many types of cancer such as lung, liver and digestive tract cancers. In rats, it was found that ferulic acid can increase the good cholesterol, HDL, and decrease total cholesterol and triglycerides [4]. Thus, the development of a new method for the quantification of ferulic acid is very important.

Currently, the main quantitative techniques for ferulic acid detection are high–performance liquid chromatography (HPLC) [5-7], thin-layer chromatography [8-10], the capillary tube electrophoresis method [11-13], and spectrophotometry [14-16]. Among these methods, the detection limits of selected detectors are typically low enough to detect ferulic acid in samples; however, these assays require laborious sample preparation steps, high equipment costs and a significant amount of labor and analytical resources, which can potentially cause substantial delays in obtaining results.

Paper-based analytical devices have the potential to be good alternative analytical devices for healthcare related applications because they are portable, easy to use, require only a small volume of sample and provide rapid analysis [17-19]. For patterning channels of hydrophilic surfaces on filter paper, there are several methods such as photolithography, wax printing, wax screen-printing. Whitesides *et al*. first introduced photolithography for a simple method using negative photoresist to create a small hydrophilic channel in millimeter scale on chromatography paper [17]. Moreover, Dungchai *et al*. exhibited wax screen-printing for the fabrication of patterned paper. This fabrication is environmentally user-friendly, inexpensive and simple method than photoresist. Recently, our research group successfully fabricated a paper-based analytical device coupled to colorimetric and electrochemical detection for many application areas [20-22]. The use of a colorimetric and electrochemical detection is an alternative detection method and has the benefits of simplicity, speed, low cost, and

portability. However, because of the lack of the selectivity for both detection modes, the sample preparation step is extremely required. Additionally, there is very little information about the combination of the sample preparation and paper-based analytical device. Vella *et al*. introduced the multilayer paper-based colorimetric device with filter membrane for detecting the biomarkers for liver function [23]. Songjaroen *et al*. successfully created a single device consisting of blood separation membranes and colorimetric paper-based microfluidic device for total protein assay in the blood [24]. Govindarajan *et al*. fabricated a paper-based origami for the bacterial DNA extraction from viscous sample [25]. Hence, efforts to extend the developed methodology and/or to create new sample preparation devices for ferulic acid detection have been challenging. To reach these goals, two platforms of paper-based analytical electrochemical device and TLC coupled with paper-based colorimetric devices were proposed and developed to rapidly detect ferulic acid in variety samples.

To assess the amount of ferulic acid in various samples, we further have innovated two designs of paper-based analytical device. In this work, ferulic acid content in the simple matrix sample was directly electrochemically determined by paper-based screen-printed electrode. For the complicated samples, the use of TLC separation and colorimetric paper device for the minimizing the interference effect and detecting ferulic acid colorimetrically, was introduced. The amount of ferulic acid can be determined by monitoring oxidative current and the color intensity at the zone of detection. Strong analytical figures with limits of detection in the low ppm range, good sensitivity, excellent response precision and stability were observed with electrochemical detection as well as from colorimetric detection. Therefore, this innovative concept could contribute to the development of a practical, rapid, highly sensitive and accurate method for assaying ferulic acid levels in variety of food and cosmetic samples.

10.2 Experimental Section

10.2.1 Apparatus

Cyclic voltammetry (CV) and differential pulse voltammetry (DPV) experiments were performed by a potentiostat (Autolab PGSTAT 30). For voltammetric experiments, CV was performed at a scan rate of 100 mV s^{-1} and the potential was scanned from –0.2 V to 0.8 V vs Ag/AgCl. DPV was performed at pulse amplitude of 50 mV and a step potential of 7 mV in the potential range from 0 V to 1.0 V vs. Ag/AgCl. For the colorimetric method, a digital camera (EOS 1000D, Canon) was used to capture the picture. The picture was then recorded in terms of mean intensity in the histogram using Adobe Photoshop [26].

10.2.2 Reagents and Solutions

A negative photoresist SU-8 3025 and developer were purchased from MicroChem Corp. (Newton, MA). Carbon ink (Electrodag PF-407C) and silver/silver chloride ink (Electrodag 7019) were purchased from Acheson (California, USA). Ferulic acid was purchased from Fluka (Buchs, Switzerland) and was prepared immediately before use in each of the experiments. A 0.1 mol L^{-1} acetate buffer, which served as a supporting electrolyte, was prepared from sodium acetate trihydrate and concentrated acetic acid)100% (which were obtained from Fluka (Buchs, Switzerland) and Merck (Darmstadt, Germany), respectively. TLC plates (silica gel 60 F_{254}) were obtained from Merck (Darmstadt, Germany). The Folin-Ciocalteau reagent was acquired from Carlo Erba (Strada Rivoltana, Italy) Sodium carbonate, chloroform, formic acid and methanol were obtained from Merck (Darmstadt, Germany). All reagents were analytical grade. The 18 MΩ cm^{-1} resistance water, obtained from a Millipore Milli-Q purification system, was used throughout these experiments.

10.2.3 Fabrication of the paper-based electrochemical device using photolithography method

The photolithography method was used to fabricate the device as described previously [17]. For the fabrication of the device (Figure 10.1), a spin coater (G3P-8) was used to coat 4 g of SU-8 negative photoresist onto the filter paper (No. 1, 100 cm diameter, Whatman), which was subsequently baked at 95 °C for 10 min. Afterward, the photomask, which was designed with Adobe Illustrator software (Adobe Systems, Inc.) and fabricated by Chaiyaboon Co. (Bangkok, Thailand), was placed onto the SU-8-covered paper, irradiated with ultraviolet (UV) light (Intelli-ray 400) for 10 s, and then baked at 95 °C for 10 min. Next, the unpolymerized photoresist layer was removed from the paper by soaking it in a SU-8 developer for 3 min and then rinsing with isopropanol. Finally, the patterned paper was dried in a hood at room temperature.

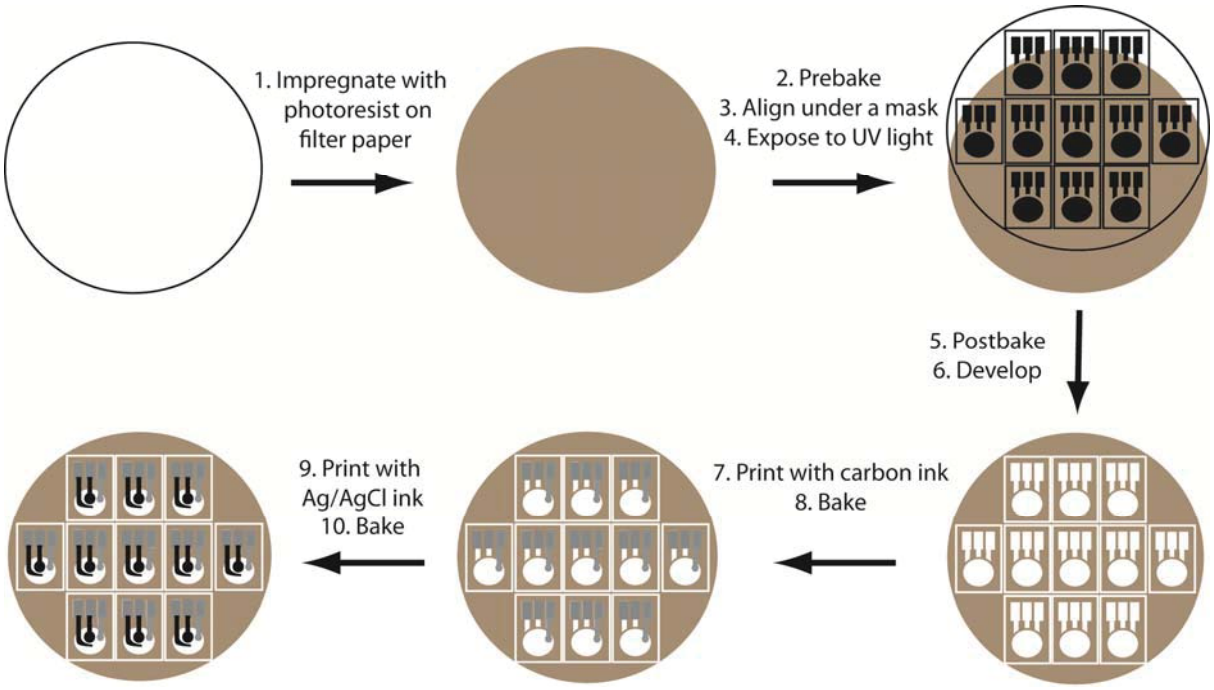

Figure 10.1 Schematic of representation of photolithography and screen printing for paper-based electrochemical device.

For the electrode preparation, the screen-printed electrodes were prepared in-house [20]. Carbon ink was used for the working electrode (WE) and the counter electrode (CE); silver/silver chloride ink was used for the reference electrode (RE) and conductive pads. All electrodes were screened on patterned paper and then were cured in the oven at 65 °C for 30 min. The paper-based device designed in this study for electrochemical detection is illustrated in Figure 10.2a.

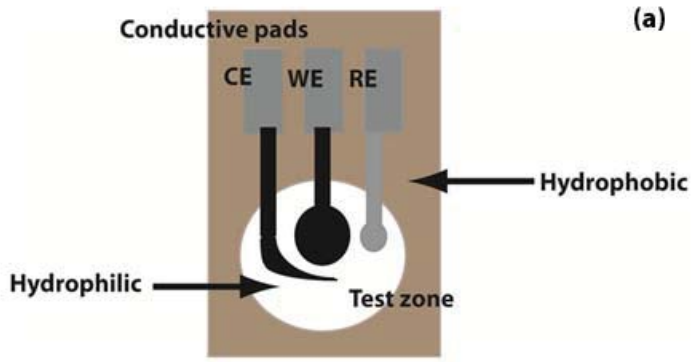

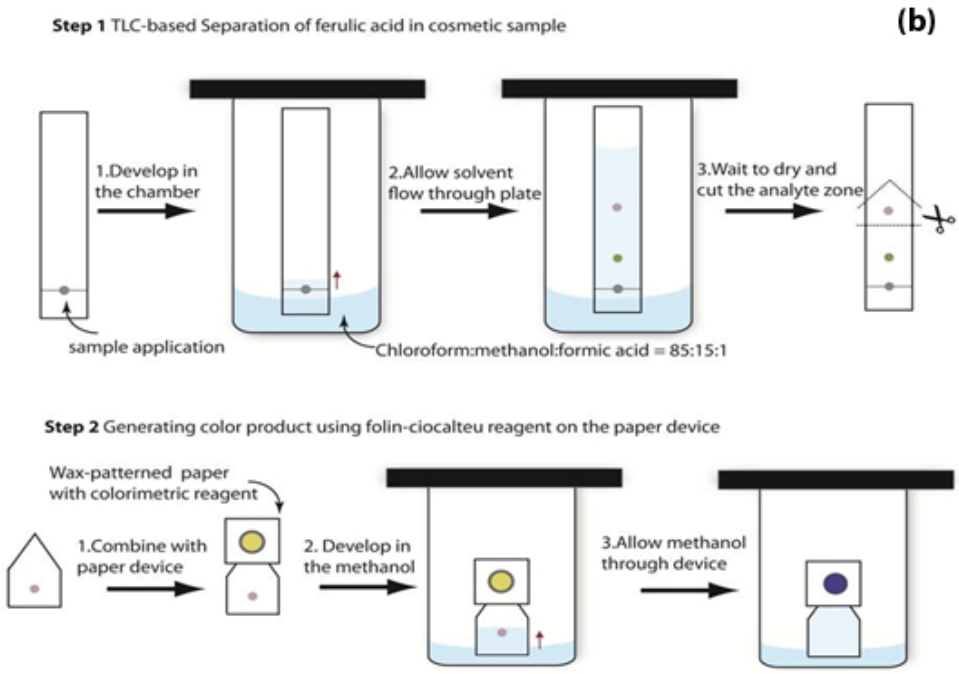

Figure 10.2 (**a**) Schematic of paper-based electrochemical device consisting of the electrochemical WE, working electrode; RE, reference electrode; CE, counter electrode. (**b**) Separation and quantitative analysis of ferulic acid by coupling thin layer chromatography with paper-based device.

10.2.4 Separation and quantitative analysis of ferulic acid by thin layer chromatography coupled with paper-based colorimetric platform

The wax screen-printing method was used to fabricate the patterned paper using previously described method as shown in Figure 10.3 [27]. The filter paper was positioned on the hot plate at 100^{o}C. Then, the solid wax was placed on the block screen. After wax was melted, it was printed through the perforated screen and allowed to be absorbed into the paper. The patterned paper was ready to use after the wax was cooled to room temperature.

Ferulic acid was determined by the colorimetric method on paper-based device using the Folin-Ciocalteau reagent [28, 29]. 2 μL of Folin-Ciocalteau reagent was applied to the colorimetric test zone. Afterward, 2.5 μL of 10% sodium carbonate was dripped onto this area. Then, paper-based device was allowed to dry at room temperature.

Figure 10.2b shows the conceptual separation and detection of ferulic acid using TLC coupled with paper-based colorimetric device. For the separation of ferulic acid by thin layer chromatography, TLC plate was cut into the strip (2 cm x 15 cm). Standard ferulic acid and ascorbic acid were applied on plate and developed with chloroform: methanol: formic acid (85:15:1) in a pre-saturated chromatographic chamber [8]. After separation, TLC area consisted of ferulic acid was cut and attached with paper-based colorimetric device. Then, ethanol was used to drive ferulic acid to react with reagent on paper-based device. The color of test zone was captured by digital camera. The color intensities were then analyzed using Adobe photoshop [26].

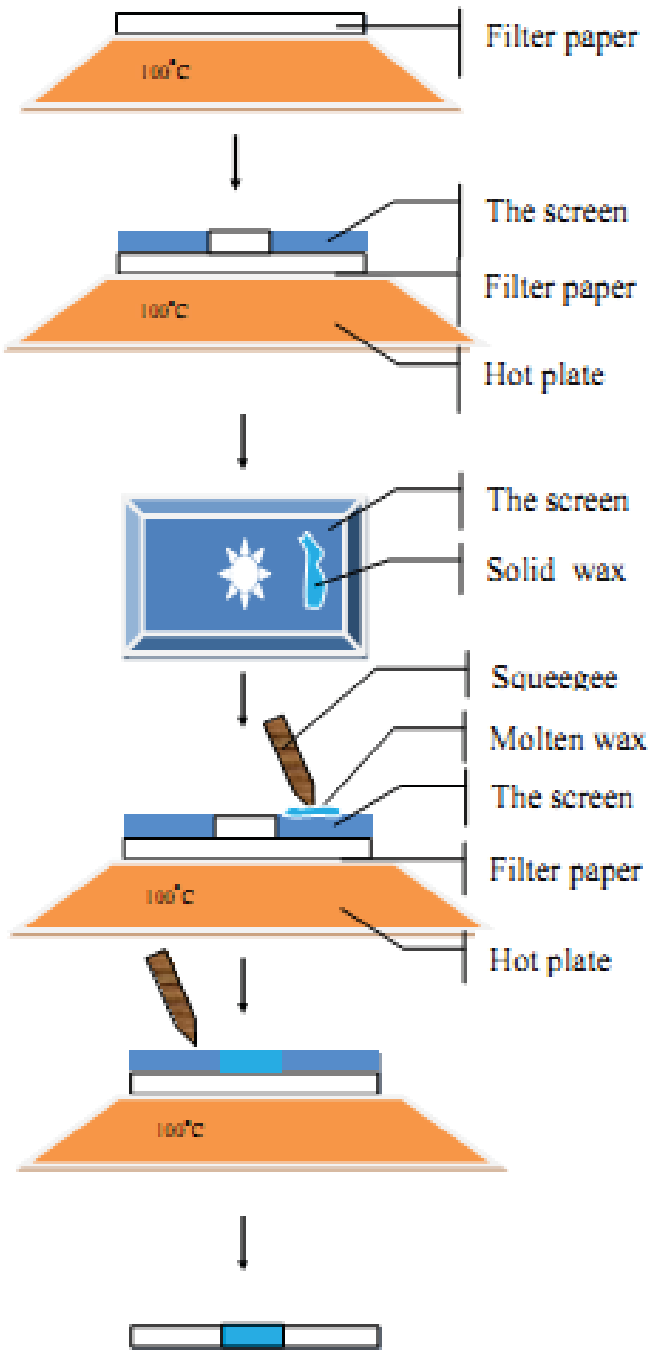

Figure 10.3 Schematic of representation of melting wax screen printing for colorimetric paper-based analytical device

10.2.5 Sample preparation

Corn milk solution was prepared by weighing 5 g of commercially available corn milk and heating it at 90 °C in 50 mL of Milli-Q water. The samples were then filtered and used for analysis. For corn cider, the sample was used without any further preparation. However, all of the samples were diluted once for determination of ferulic acid by electrochemical detection. For colorimetric detection, the three samples of cosmetic serums were used without any preparation.

10.3 Results and Discussion

10.3.1 Paper-based electrochemical device for direct detection of ferulic acid

10.3.1.1 Electrochemical behavior of ferulic acid

First, cyclic voltammetry was used to investigate the electrochemistry of ferulic acid on paper-based electrodes. Acetate buffer solution was used as the supporting electrolyte for ferulic acid detection, because it provides a well-defined peak at the carbon electrode [30]. The cyclic voltammogram of 50 ppm feruic acid in 0.1 mol L^{-1} acetate buffer solution (pH 5) is shown in Figure 10.4. Ferulic acid exhibited a well-defined oxidation peak during the scan of the potential toward the positive direction at the carbon electrode at approximately 0.4 V vs. Ag/AgCl.

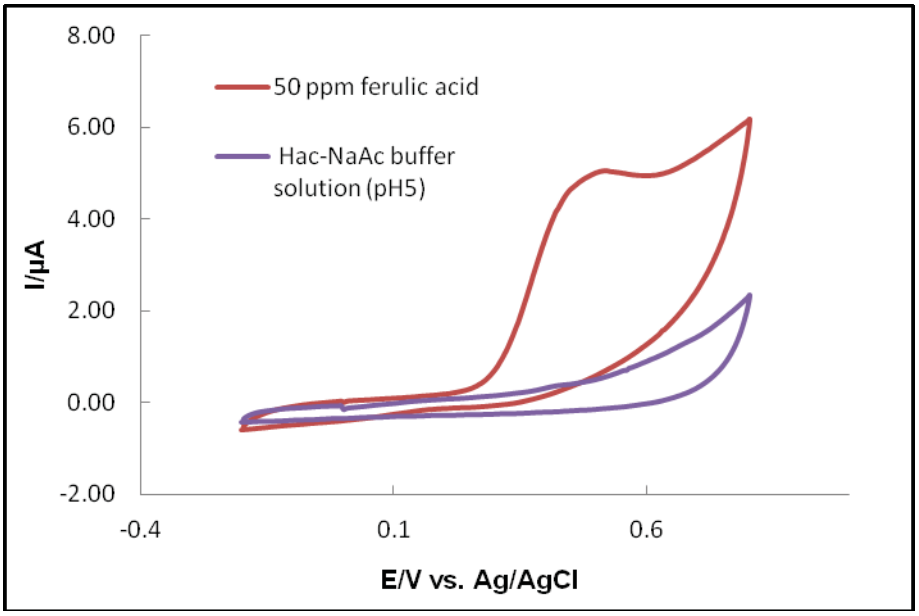

Figure 10.4 Cyclic voltammogram of 50 ppm ferulic acid in 0.1 mol L^{-1} acetate buffer solution (pH 5). Scan rate 100 mV/s, electrode area 0.8 cm^2. Voltammograms shown are representative of at least five independent repetitions.

These results indicated that the paper-based carbon electrode offers great performance and substantial sensitivity for ferulic acid detection. Therefore, the electrochemical behavior of ferulic acid can be investigated by this system.

10.3.1.2 Effect of pH

In any electrochemical detection method, the supporting electrolyte pH has a significant impact on the ionization and redox reaction of each analyte. Therefore, the optimization of the supporting electrolyte pH was carried out for the electrochemical detection of ferulic acid. The effect of pH values on the peak potential and oxidation current were examined in the pH range 3.0 – 7.0. All buffers contained a 0.1 mol L^{-1} acetate buffer. Figure 10.5a displays the relationship obtained from plotting the pH values and the oxidation peak potentials from cyclic voltammogram. It can be observed that ferulic acid is easily oxidized when the pH

increases because the potentials shifted negatively at a higher pH. Moreover, the relationship between the oxidation peak currents and pH was investigated. As shown in Figure 10.5b, it is evident that a buffer with pH 5.0 exhibited the highest current signal using carbon electrodes. Accordingly, this buffer was selected as a suitable pH for all subsequent work.

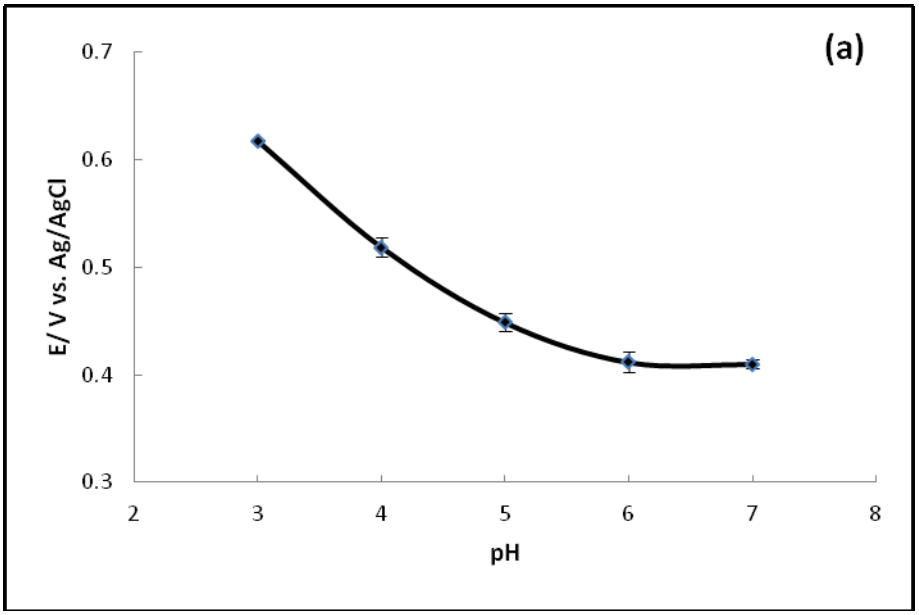

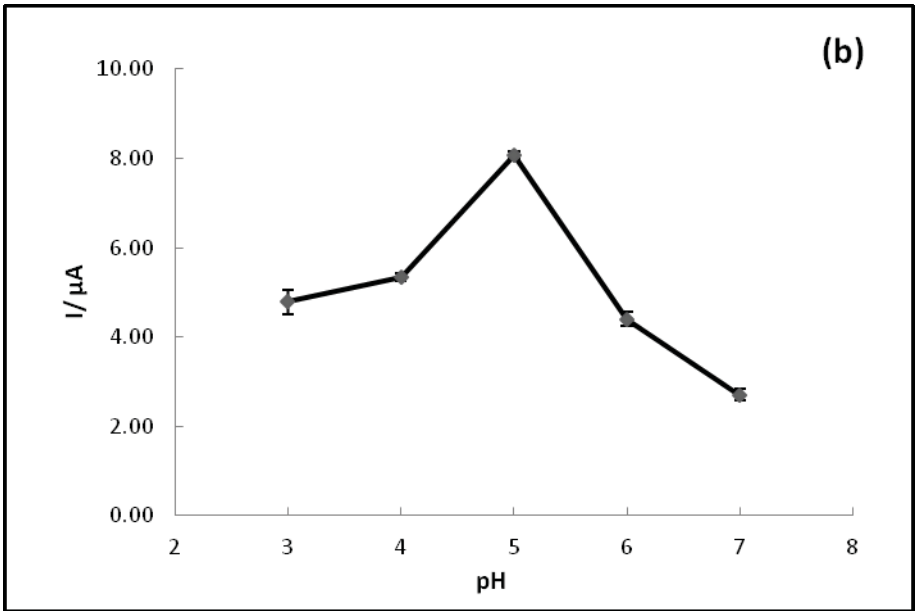

Figure 10.5 (**a**) The influence of pH on the oxidation peak potential. (**b**) The influence of pH on the oxidation peak currents. Other conditions same in Figure 3**.**

10.3.1.3 Effect of the scan rate

The influence of the scan rate was also investigated to authenticate the adsorption of ferulic acid on the carbon electrode surface. The experiment was carried out by cyclic voltammetry in the potential range from 50 mV s^{-1} to 500 mVs^{-1}, data not shown. The oxidation peak currents increased linearly as the square root of the scan rate increased as shown in Figure 10.6. Hence, this result confirmed that the reaction was controlled by the diffusion process and that ferulic acid is slightly adsorbed on the electrode surface.

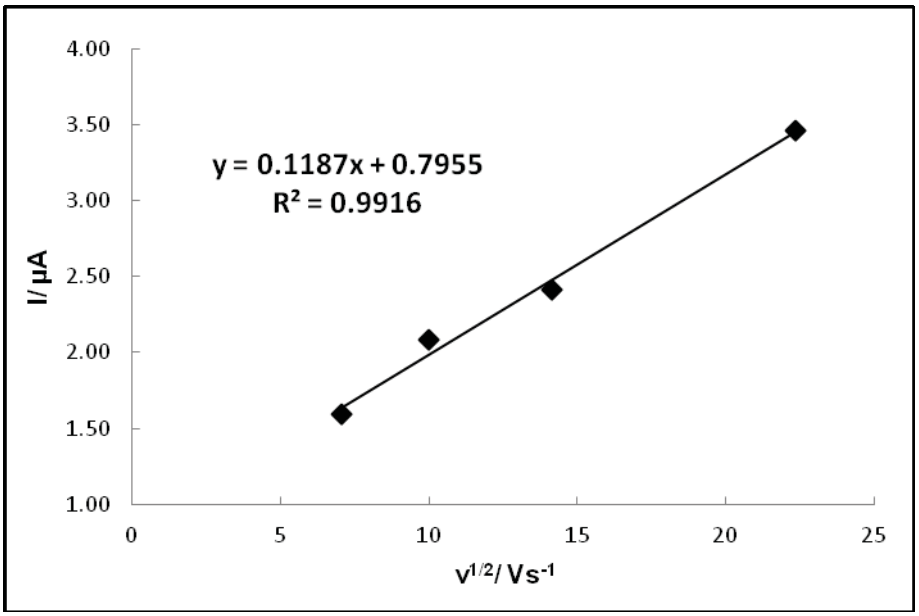

Figure 10.6 The influence of scan rate on the oxidation peak currents of 50 ppm ferulic acid in 0.1 mol L^{-1} HAc- NaAc buffer solution.

10.3.1.4 Effect of differential pulse voltammetric parameters

Differential pulse voltammetry (DPV) is the technique typically used to achieve a lower detection limit than cyclic voltammetry. Therefore, differential pulse voltammetry was selected as a technique to determine ferulic acid. The differential pulse voltammogram of ferulic acid is clearly observed. However, to obtain the optimal conditions for the quantitative analysis of ferulic acid, the effects of the pulse amplitude and step potential on peak current were examined. The pulse amplitude was varied from 50 mV to 250 mV. As expected, the peak currents of ferulic acid increased as the pulse amplitude increased, however, broadening of the peaks was also observed. Therefore, the pulse amplitude of 50 mV was chosen as a trade-off between the peak height and peak broadening. Figure 10.7 displays the effect of the step potential. The step potential was varied within the range of 2 mV–10 mV and the optimal value was found to be 7 mV because the increment in the peak intensity slightly decreased above 7 mV.

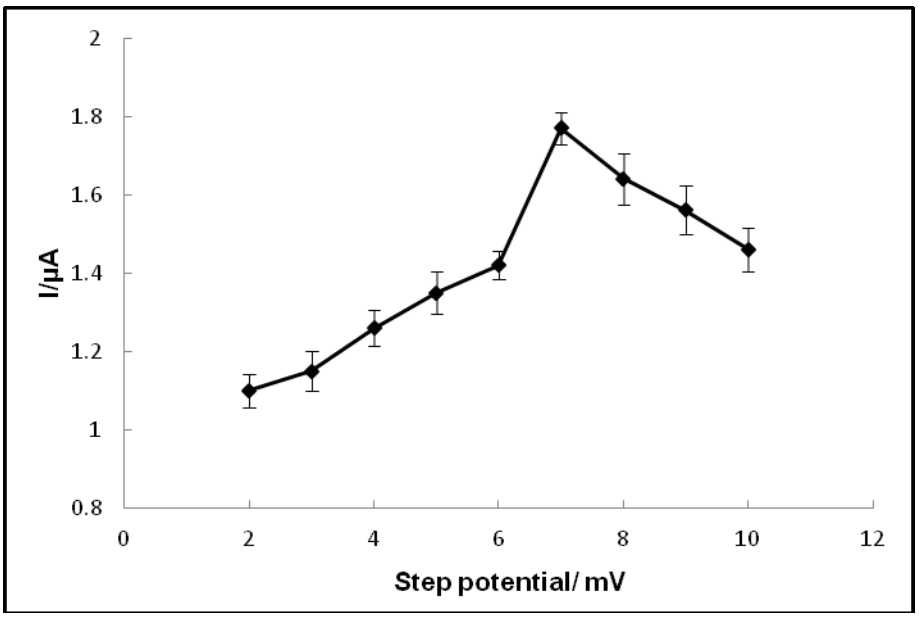

Figure 10.7 The influence of step potential on the oxidation peak currents.

10.3.1.5 Analytical performances for electrochemical detection of ferulic acid

As shown in Figure 10.8, the ferulic acid solutions were investigated by DPV under optimal conditions. Defined peaks with currents proportional to the analyte concentration were observed. The oxidation peak current of ferulic acid showed a linear relationship with its concentration in the range of 3 ppm to 140 ppm (correlation coefficient of $R^2 = 0.9994$). The resulting calibration plots are linear with the sensitivity of 0.0246 μA/ppm. The limit of detection (LOD) was obtained from experiment at concentrations as low as 1 ppm based on a signal-to-noise ratio (S/N) of 3, and the limit of quantization (LOQ) was also found to be 3 ppm based on a signal-to-noise ratio (S/N) of 10.

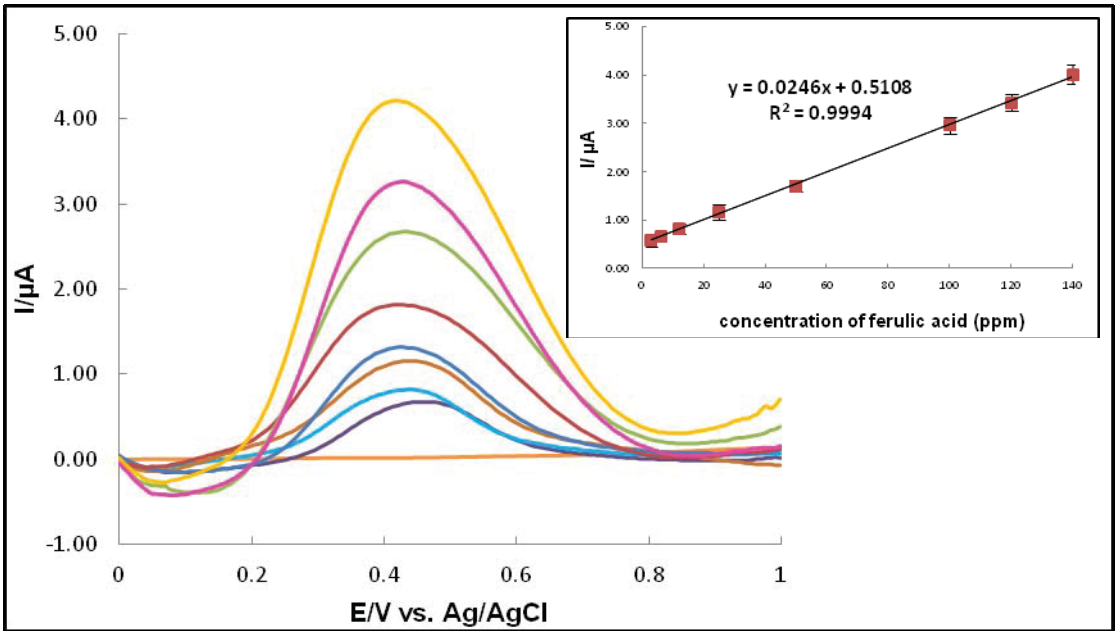

Figure 10.8 Differential pulse voltammograms of ferulic acid (3, 6, 12, 25, 50, 100, 120, 140 ppm) in 0.1 mol L^{-1} acetate buffer solution (pH 5), measured under optimal experimental conditions.

10.3.2 Thin layer chromatography coupled with colorimetric paper-based analytical device for separation and detection of ferulic acid

10.3.2.1 Effect of sodium carbonate concentration

The colorimetric detection based on the Folin-Ciocalteau Total Phenolic Assay has gained popularity and has been commonly used to determine the phenolic content. This assay works by measuring the change in color when metal oxides are reduced. The Folin-Ciocalteau reagent reacted with phenolic compounds under basic conditions obtained by adjusting with sodium carbonate. The effect of concentration of sodium carbonate was optimized. The result shows that 10% sodium carbonate offered the great color response as illustrated in the Figure 10.9.

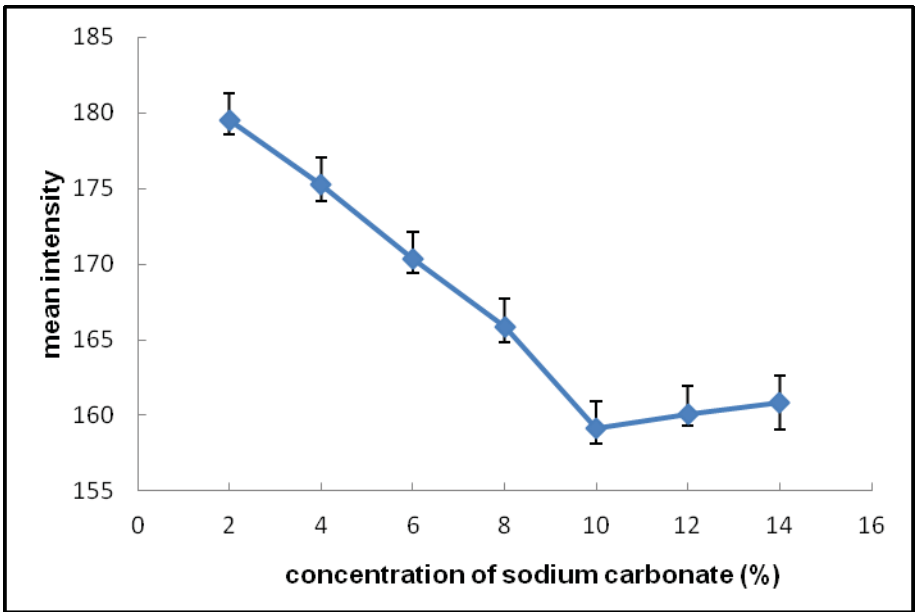

Figure 10.9 The effect of concentration of sodium carbonate on mean intensity.

10.3.2.2 Separation and quantitation of ferulic acid

In this section, the use of paper-based colorimetric devices coupled with thin layer chromatography was designed for separation and detection of ferulic acid in the presence of ascorbic acid. Ascorbic acid is a naturally antioxidant and can be colorimetrically detected by

Folin-Ciocalteau reagent as well [31]. Therefore, the separation of ferulic acid before detecting is in need particularly. First, the separation of ascorbic acid and ferulic acid by thin layer chromatography was examined. Chloroform: methanol: formic acid (85:15:1) was used as the mobile phase in the separation system (Figure 10.10). It was found that two analytes can be separated clearly with R_f of 0.70± 0.01 and 0.10 ± 0.01 for ferulic and ascorbic acid, respectively (Table 10.1).

Figure 10.10 Separation of ferulic acid and ascorbic acid by thin-layer chromatography (**a**) Spot of ferulic acid. (**b**) Spot of ascorbic acid. (**c**) Spot of ferulic acid and ascorbic acid.

Table 10.1. R_f value of ferulic acid and ascorbic acid in solvent system chloroform: methanol: formic acid (85: 15: 1).

		R_f value	**Average R_f**
Ferulic acid	1	0.72	0.70 ± 0.01
	2	0.70	
	3	0.71	
Ascorbic acid	1	0.10	0.10 ± 0.00

After separation, zone of ferulic acid was obtained on paper. Then this zone was leached out by solvent and reacted with Folin-Ciocalteau reagent. Finally, the color at the reaction zone was captured by camera and converted to intensity by Adobe Photoshop program. Figure 10.11 shows the resulting color intensity, which is proportional to the concentration of ferulic acid.

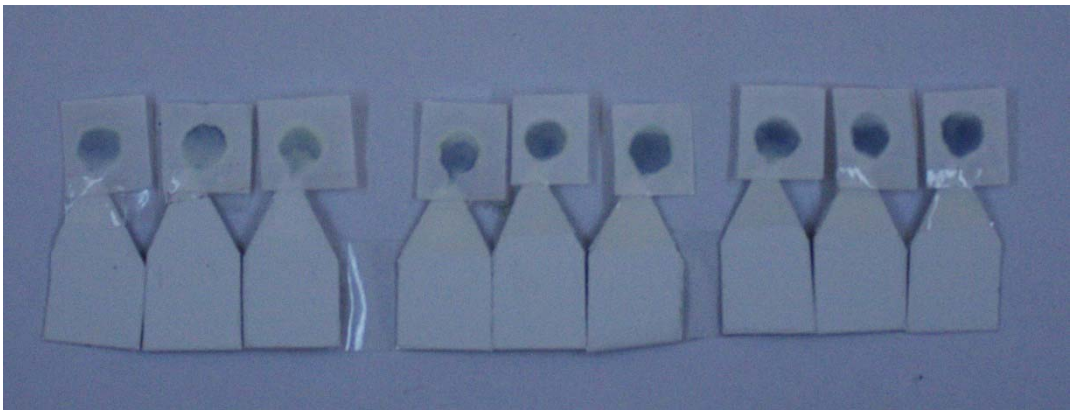

Figure 10.11 Thin- layer chromatography couple with colorimertric paper-based analytical device. Intensity of the observed color is proportional to the concentration of ferulic acid.

10.3.2.3 Analytical performances for colorimetric detection of ferulic acid

The standard curve was generated by using various concentrations (1-200 ppm) of ferulic acid. The color intensity of ferulic acid from three replicate runs was examined using Adobe Photoshop and the mean intensity was recorded in a histogram. By plotting the mean intensity value versus the ferulic acid concentration, Figure 10.12 shows a linear range between 20 and 140 ppm (correlation coefficient of $R^2 = 0.9974$) and the limit of detection was found to be 7 ppm based on a signal-to-noise ratio (S/N) of 3.

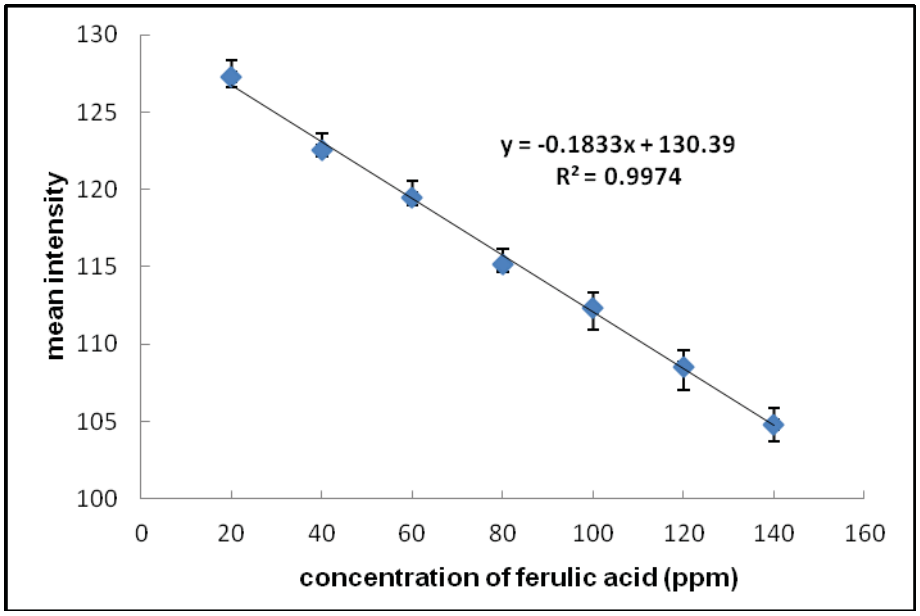

Figure 10.12 Calibration curve of ferulic acid using paper-based colorimetric detection.

10.3.3 Analytical application in a real sample

To verify the applicability of the proposed paper-based analytical devices and methodology developed in this present work, ferulic acid in samples of corn cider and corn milk obtained from local supermarkets, were determined by electrochemical detection using standard addition method. The determination of ferulic acid was performed using the same experimental conditions reported above. Two different samples were divided into two portions and then spiked with 20 and 50 ppm of ferulic acid, respectively. The recovery efficiencies, using electrochemical detection, obtained for the samples spiked with ferulic acid revealed a recovery in the range of 96.85 % – 99.92 % and 96.94 % –103.20 % for corn cider and corn milk, respectively (Table 10.2). For colorimetric detection in the second design, the results obtained for ferulic acid analysis in three cosmetic samples were found as following (1) 39.76 ± 0.21 ppm, (2) 47.40 ± 0.34 ppm and (3) 31.19 ± 0.23 ppm, respectively.

Table 10.2. Determination of ferulic acid in real samples using proposed paper-based device with electrochemical detection and conventional HPLC-UV.

Samples	**Ferulic acid (ppm ± SD, n = 3)**			**% Recovery**	**% RSD**
	Added	Found			
		Proposed method	HPLC-UV		
Corn cider	0	0.24 ± 0.11	0 ± 0.00	0	7.68
	20	19.61 ± 0.16	18.96 ± 0.37	96.85	5.91
	50	50.20 ± 0.40	51.01 ± 0.53	99.92	8.92
Corn milk	0	0.94 ± 0.01	1.09 ± 0.09	0	9.19
	20	21.58 ± 0.04	20.47 ± 0.27	103.20	5.47
	50	49.41 ± 0.13	48.01 ± 0.27	96.94	8.76

In addition, HPLC-UV method was used to validate both proposed devices [32]. The results obtained from those two methods were in good agreement and showed no significant differences between the proposed method and standard method. For using TLC coupled with paper-based colorimetric device, the concentration of ferulic acid in three cosmetic samples which were also obtained from HPLC-UV method were found as following : (1) 40.09 ± 0.14 ppm, (2) 48.76 ± 0.26 ppm and (3) 29.11 ± 0.16 ppm. Consequently, the methods for the determination of ferulic acid using paper-based analytical devices reported here are acceptable and potentially feasible for use with real samples.

10.4 Summary

The practical, rapid, highly sensitive and accurate method for quantitative determination of ferulic acid in complicated and uncomplicated matrix was successfully developed using paper-based analytical device. For direct determination using paper-based electrochemical device, the differential pulse voltammogram provided a well-defined oxidation peak of ferulic acid. The calibration curve of ferulic acid showed a good linearity in the concentration range of 3 – 140 ppm with a correlation coefficient of 0.9994. The limit of detection (LOD) of the proposed method was found to be 1 ppm. In the second design for monitoring ferulic acid in complicated matrix, the device can detect ferulic acid content as low as 7 ppm, with a linear dynamic range from 20 ppm to 140 ppm. In both platforms, this proposed methodology displayed a simple and rapid quantification of ferulic acid and completely covered the ferulic acid detection in any types of sample matrix. Furthermore, this method was successfully used for the quantification of ferulic acid in fruit juice and cosmetic serum. In conclusion, these proposed paper-based analytical platforms provide an attractively alternative method for the determination of ferulic acid in food and cosmetic samples. This method may prove to be useful for nutritional and clinical investigations of ferulic acid levels in a variety of samples.

10.4 References

[1] Zhang, Y.T.; Xu, M.T.; Du, M.; Zhou, F.M. Comparative studies of the interaction between ferulic acid and bovine serum albumin by ACE and surface plasmon resonance. *Electrophoresis* **2007**, *28*, 1839-1845.

[2] Balasubashini, M.S.; Rukkumani, R.; Viswanathan, P.; Menon, V.P. Ferulic acid alleviates lipid peroxidation in diabetic rats. *Phytotherapy Research* **2004**, *18*, 310-314.

[3] Philp, H.A. Hot flashes--a review of the literature on alternative and complementary treatment approaches. *Altern Med Rev* **2003**, *8*, 284-302.

[4] Kim, H.K.; Jeong, T.S.; Lee, M.K.; Park, Y.B.; Choi, M.S. Lipid-lowering efficacy of hesperetin metabolites in high-cholesterol fed rats. *Clinica Chimica Acta* **2003**, *327*, 129-137.

[5] Weon, J.B.; Ma, J.Y.; Yang, H.J.; Ma, C.J. Simultaneous determination of ferulic acid, hesperidin, 6-gingerol and glycyrrhizin in Insampaedok-san by HPLC coupled with diode array detection. *Journal of Analytical Chemistry* **2012**, *67*, 955-959.

[6] Silva, C.L.; Pereira, J.; Wouter, V.G.; Giro, C.; Camara, J.S. A fast method using a new hydrophilic-lipophilic balanced sorbent in combination with ultra-high performance liquid chromatography for quantification of significant bioactive metabolites in wines. *Talanta* **2011**, *86*, 82-90.

[7] Laokuldilok, T.; Shoemaker, C.F.; Jongkaewwattana, S.; Tulyathan, V. Antioxidants and Antioxidant Activity of Several Pigmented Rice Brans. *Journal of Agricultural and Food Chemistry* **2011**, *59*, 193-199.

[8] Sharma, O.P.; Bhat, T.K.; Singh, B. Thin-layer chromatography of gallic acid, methyl gallate, pyrogallol, phloroglucinol, catechol, resorcinol, hydroquinone, catechin, epicatechin, cinnamic acid, p-coumaric acid, ferulic acid and tannic acid. *Journal of Chromatography A* **1998**, *822*, 167-171.

[9] Borges, M.F.M.; Pinto, M.M.M. Separation of the diastereoisomers of ethyl-esters of caffeic, ferulic, and isoferulic acids by thin-layer and high-performance liquid-chromatography. *Journal of Liquid Chromatography* **1994**, *17*, 1125-1139.

[10] Ellnain-Wojtaszek, M.; Zgorka, G. High-performance liquid chromatography and thin-layer chromatography of phenolic acids from Ginkgo biloba L-leaves collected within vegetative period. *Journal of Liquid Chromatography & Related Technologies* **1999**, *22*, 1457-1471.

[11] Choudhary, G.; Chakel, J.; Hancock, W.; Torres-Duarte, A.; McMahon, G.; Wainer, I. Investigation of the potential of capillary electrophoresis with off-line matrix-assisted laser desorption/ionization time-of-flight mass spectrometry for clinical analysis: Examination of a glycoprotein factor associated with cancer cachexia. *Analytical Chemistry* **1999**, *71*, 855-859.

[12] Lima, D.L.D.; Duarte, A.C.; Esteves, V.I. Optimization of phenolic compounds analysis by capillary electrophoresis. *Talanta* **2007**, *72*, 1404-1409.

[13] Aturki, Z.; Fanali, S.; D'Orazio, G.; Rocco, A.; Rosati, C. Analysis of phenolic compounds in extra virgin olive oil by using reversed-phase capillary electrochromatography. *Electrophoresis* **2008**, *29*, 1643-1650.

[14] Ozyurt, D.; Demirata, B.; Apak, R. Determination of total antioxidant capacity by a new spectrophotometric method based on Ce(IV) reducing capacity measurement. *Talanta* **2007**, *71*, 1155-1165.

[15] Shpigun, L.K.; Zamyatina, N.N.; Shushenachev, Y.V.; Kamilova, P.M. Flow-injection methods for the determination of antioxidant activity based on free-radical processes. *Journal of Analytical Chemistry* **2012**, *67*, 801-808.

[16] Garcia, R.; Rakotozafy, L.; Telef, N.; Potus, J.; Nicolas, J. Oxidation of ferulic acid or arabinose-esterified ferulic acid by wheat germ peroxidase. *Journal of Agricultural and Food Chemistry* **2002**, *50*, 3290-3298.

[17] Martinez, A.W.; Phillips, S.T.; Butte, M.J.; Whitesides, G.M. Patterned paper as a platform for inexpensive, low-volume, portable bioassays. *Angewandte Chemie-International Edition* **2007**, *46* (8), 1318-1320.

[18] Martinez, A W.; Phillips, S.T.; Carrilho, E.; Thomas, S.W.; Sindi, H.; Whitesides, G.M. Simple telemedicine for developing regions: Camera phones and paper-based microfluidic devices for real-time, off-site diagnosis. *Analytical Chemistry* **2008**, *80*, 3699-3707.

[19] Martinez, A.W.; Phillips, S.T.; Whitesides, G.M. Three-dimensional microfluidic devices fabricated in layered paper and tape. *Proceedings of the National Academy of Sciences of the United States of America* **2008**, *105*, 19606-19611.

[20] Dungchai, W.; Chailapakul, O.; Henry, C.S. Electrochemical Detection for Paper-Based Microfluidics. *Analytical Chemistry* **2009**, *81*, 5821-5826.

[21] Apilux, A.; Dungchai, W.; Siangproh, W.; Praphairaksit, N.; Henry, C.S.; Chailapakul, O. Lab-on-Paper with Dual Electrochemical/Colorimetric Detection for Simultaneous Determination of Gold and Iron. *Analytical Chemistry* **2010**, *82*, 1727-1732.

[22] Rattanarat, P.; Dungchai, W.; Siangproh, W.; Chailapakul, O.; Henry, C.S. Sodium dodecyl sulfate-modified electrochemical paper-based analytical device for determination of dopamine levels in biological samples. *Analytica Chimica Acta* **2012**, *744*, 1-7.

[23] Vella, S.J.; Beattie, P.; Cademartiri, R.; Laromaine, A.; Martinez, A.W.; Phillips, S.T.; Mirica, K.A.; Whitesides, G.M., Measuring Markers of Liver Function Using a Micropatterned Paper Device Designed for Blood from a Fingerstick. *Analytical Chemistry* **2012**, *84*, 2883-2891.

[24] Songjaroen, T.; Dungchai, W.; Chailapakul, O.; Henry, C.S.; Laiwattanapaisal, W. Blood separation on microfluidic paper-based analytical devices. *Lab on a Chip* **2012**, *12*, 3392-3398.

[25] Govindarajan, A.V.; Ramachandran, S.; Vigil, G.D.; Yager, P.; Bohringer, K.F. A low cost point-of-care viscous sample preparation device for molecular diagnosis in the developing world; an example of microfluidic origami. *Lab on a Chip* **2012**, *12*, 174-181.

[26] Apilux, A.; Siangproh, W.; Praphairaksit, N.; Chailapakul, O. Simple and rapid colorimetric detection of Hg(II) by a paper-based device using silver nanoplates. *Talanta* **2012**, *97*, 388-394.

[27] Dungchai, W.; Chailapakul, O.; Henry, C.S. A low-cost, simple, and rapid fabrication method for paper-based microfluidics using wax screen-printing. *Analyst* **2011**, *136*, 77-82.

[28] Huang, D.J.; Ou, B.X.; Prior, R.L. The chemistry behind antioxidant capacity assays. *Journal of Agricultural and Food Chemistry* **2005**, *53*, 1841-1856.

[29] Shukla, S.; Mehta, A.; John, J.; Singh, S.; Mehta, P.; Vyas, S.P. Antioxidant activity and total phenolic content of ethanolic extract of Caesalpinia bonducella seeds. *Food and Chemical Toxicology* **2009**, *47*, 1848-1851.

[30] Yu, Y.Y.; Wu, Q.S.; Wang, X.G.; Ding, Y.P. Electrochemical determination of ferulic acid in Chinese traditional medicine Xiao Yao Pills at electrode modified with carbon nanotube. *Russian Journal of Electrochemistry* **2009**, *45*, 170-174.

[31] George, S.; Brat, P.; Alter, P.; Amiot, M.J. Rapid determination of polyphenols and vitamin C in plant-derived products. *Journal of Agricultural and Food Chemistry* **2005**, *53*, 1370-1373.

[32] Sheng, Y. X.; Li, L.; Wang, Q.; Guo, H.Z.; Guo, D.A. Simultaneous determination of gallic acid, albiflorin, paeoniflorin, ferulic acid and benzoic acid in Si-Wu decoction by high-performance liquid chromatography DAD method. *Journal of Pharmaceutical and Biomedical Analysis* **2005**, *37*, 805-810.

Chapter XI

Conclusions

From the results obtained in chapter II-V, we are successful development of the new device named “lab-on-paper” by coupling with optical detection. These devices can be used to detect both organic and inorganic analytes depended on the purpose of the use. Results obtained exhibited the high potential of these proposed analytical systems for real samples detection. Chapter VI-VIII, we are also successful development of lab-on-paper coupled to electrochemical detection for the determination of organic or inorganic compounds as well. The benefit of these created systems is that can overcame the limitation of the use of quantification data by visually comparing the color intensity of the reaction spots with the developed color intensity. Matching color and color intensity by the naked eye is complicated by many factors including different visual perception of color from one person to another, lighting, and the difference between the colors of a dry printed color on label stock and the colors seen in a reacted (i.e., wetted) paper. Chapter IX-X, we are successful to combine both colorimetric and electrochemical detection onto lab-on-paper. The use of dual electrochemical and colorimetric based lab-on-paper device developed here displayed a simple and rapid quantitation of analyte using electrochemistry while screening for interference using colorimetry. Therefore, the introduction of these devices could be a new strategy for applying them to various applications in future.